

พอลิอิมิตละลายได้ที่มีพอร์ไพรีน: การสังเคราะห์และสมบัติเชิงแสง



นางสาวสุดคณิง สิงห์โต

ศูนย์วิทยทรัพยากร
จุฬาลงกรณ์มหาวิทยาลัย

วิทยานิพนธ์นี้เป็นส่วนหนึ่งของการศึกษาตามหลักสูตรปริญญาวิทยาศาสตรมหาบัณฑิต


สาขาวิชาปิโตรเคมีและวิทยาศาสตร์พอลิเมอร์

คณะวิทยาศาสตร์ จุฬาลงกรณ์มหาวิทยาลัย

ปีการศึกษา 2551

ลิขสิทธิ์ของจุฬาลงกรณ์มหาวิทยาลัย

**SOLUBLE PORPHYRIN-CONTAINING POLYIMIDE: SYNTHESIS AND
OPTICAL PROPERTIES**



Miss Sudkanueng Singto

ศูนย์วิทยทรัพยากร
จุฬาลงกรณ์มหาวิทยาลัย

A Thesis Submitted in Partial Fulfillment of the Requirements
for the Degree of Master of Science Program in Petrochemistry and Polymer Science

Faculty of Science

Chulalongkorn University


Academic Year 2008

Copyright of Chulalongkorn University

511592


Thesis Title SOLUBLE PORPHYRIN-CONTAINING POLYIMIDE:
SYNTHESIS AND OPTICAL PROPERTIES
By Miss Sudkanueng Singto
Field of Study Petrochemistry and Polymer Science
Thesis Advisor Associate Professor Supawan Tantayanon, Ph.D.
Thesis Co-Adviser Professor Robert E. Connors, Ph.D.

Accepted by the Faculty of Science, Chulalongkorn University in Partial
Fulfillment of the Requirements for the Master's Degree


.....Dean of the Faculty of Science
(Professor Supot Hannongbua, Dr. rer.nat.)

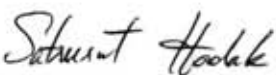
THESIS COMMITTEE


.....Chairman
(Professor Pattarapan Prasassarakich, Ph.D.)


.....Thesis Adviser
(Associate Professor Supawan Tantayanon, Ph.D.)


.....Thesis Co-adviser
(Professor Robert E. Connors, Ph.D.)


.....Member
(Assistant Professor Varawut Tangpasuthadol, Ph.D.)


.....Member
(Dr. Satreerat Hodak, Ph.D.)

ศุคหนึ่ง สิงห์โต: พอลิอิมิดละลายได้ที่มีพอร์ไฟริน: การสังเคราะห์และสมบัติเชิงแสง
(SOLUBLE PORPHYRIN-CONTAINING POLYIMIDE: SYNTHESIS AND
OPTICAL PROPERTIES) อ.ที่ปรึกษาวิทยานิพนธ์หลัก: รศ.ดร.ศุภวรรณ ดันตยานนท์,
อ.ที่ปรึกษาร่วม: ศ.ดร.โรเบิร์ต คอนเนอร์, 134 หน้า.

ได้สังเคราะห์พอลิอิมิดที่มีหน่วยพอร์ไฟรินด้วยปฏิกิริยาพอลิเมอไรเซชันแบบควบแน่น
ของไดแอมีนมอนอเมอร์ 2 ชนิดคือ 5,10-บิส(4-แอมิโนเฟนิล)-10,20-ไดเฟนิลพอร์ไฟริน(ซิส-ดีเอ
ทีพีพี) หรือ 5,15-บิส(4-แอมิโนเฟนิล)-10,20-ไดเฟนิลพอร์ไฟริน(ทรานส์-ดีเอทีพีพี)และ 2,2'-บิส
(โทรฟลูออโรเมทิล)-4,4'-ไดแอมิโนไบเฟนิล (พีเอฟเอ็มบี) กับไดแอนไฮโดรคคือ 4,4'-เฮกซะฟลูออ
โรไอโซพรอพิลไดนไคพทาสิกแอนไฮโดรค (6 เอฟดีเอ)ที่อัตราส่วน1:1 โดยแปรค่าปริมาณของซิส-
ดีเอทีพีพีหรือทรานส์-ดีเอทีพีพีในส่วนของไดแอมีนมอนอเมอร์ในช่วง 5-30%โดยโมล ได้
สังเคราะห์พอลิอิมิดที่มีโลหะซึ่งอยู่ในหน่วยพอร์ไฟรินด้วย ยืนยันโครงสร้างของพอลิอิมิดทั้ง 4
ชนิดที่มี ซิส-ดีเอทีพีพี, ทรานส์-ดีเอทีพีพี, ซิส-ซิงค์ดีเอทีพีพีและทรานส์-ซิงค์ดีเอทีพีพีด้วยเอทีอาร์-
ไออาร์และ โปรตอน-เอ็นเอ็มอาร์ พอลิอิมิดทั้งหมดละลายในตัวทำละลายโพลาร์อะโพรติก ที่เอช
เอฟ ดีเอ็มเอซีและ ไคคลอโรมีเทน และมีความหนืดสูงกว่าพอลิอิมิดที่ไม่มีหน่วยพอร์ไฟริน ได้
ศึกษาอุวิ-วิสและฟลูออเรสเซนส์สเปกโทรสโกปีของพอลิอิมิดในไคคลอโรมีเทนและดีเอ็มเอซี
ค่าคงที่อัตราเร็วสำหรับการถ่ายโอนอิเล็กตรอนของพอลิอิมิดที่มีปริมาณซิส-ดีเอทีพีพีและทรานส์-ดี
เอทีพีพีสูงสุดได้แก่ พีไอ-ซี4 และพีไอ-ที4 เป็น 1.50×10^7 และ 1.48×10^7 s^{-1} และเมทิลโพรไฟ
รินได้แก่พีไอ-ซิงค์ซี4และพีไอ-ซิงค์ที4 เป็น 9.25×10^7 และ 8.90×10^7 s^{-1} ในไคคลอโรมีเทน
ตามลำดับ ฟลูออเรสเซนส์แควนซิงค์ของพอร์ไฟรินมอนอเมอร์และพอลิอิมิดที่มีพอร์ไฟรินด้วย
แอนทราควิโนนเป็นตัวรับอิเล็กตรอน เกี่ยวข้องกับกลไกแควนซิงค์แบบสถิตและแบบพลศาสตร์
นอกจากนี้แล้วพอลิอิมิดทั้งหมดมีความเสถียรทางความร้อนตามที่พิจารณาด้วยการวิเคราะห์ทาง
เทอร์โมกราวิเมตริก.

สาขาวิชา:ปิโตรเคมีและวิทยาศาสตร์พอลิเมอร์..ลายมือนิสิต:ศุคหนึ่ง สิงห์โต.....

ปีการศึกษา:2551.....ลายมือชื่อ.ที่ปรึกษาวิทยานิพนธ์หลัก: *ศุภวรรณ ดันตยานนท์*
ลายมือชื่อ.ที่ปรึกษาวิทยานิพนธ์ร่วม: *Robert S. Connor*

4872515623: MAJOR PETROCHEMISTRY AND POLYMER SCIENCE

KEYWORD: SOLUBLE POLYIMIDES/ DIAMINOTETRAPHENYLPORPHYRIN/
PHOTOINDUCED ELECTRON TRANSFER/ FLUORESCENCE QUENCHING

SUDKANUENG SINGTO: SOLUBLE PORPHYRIN-CONTAINING
POLYIMIDE: SYNTHESIS AND OPTICAL PROPERTIES. THESIS
PRINCIPAL ADVISOR: ASSOC. PROF SUPAWAN TANTAYANON,
Ph.D., THESIS CO-ADVISOR: PROF. ROBERT E. CONNORS, Ph.D., 134
pp.

Polyimides containing porphyrin moieties were synthesized by condensation polymerization of two diamino monomers, either 5,10-*bis*(4-aminophenyl)-10,20-diphenylporphyrin(*cis*-DATPP) or 5,15-*bis*(4-aminophenyl)-10,20-diphenylporphyrin (*trans*-DATPP) and 2,2'-*bis*(trifluoromethyl)-4,4'-diaminobiphenyl (PFMB) and a dianhydride, 4,4'-hexafluoroisopropylidenediphthalic anhydride (6FDA) at 1:1 ratio. The content of *cis*-DATPP or *trans*-DATPP in diamino monomer part was varied in the range of 5-30% by mole. The incorporation of Zn metal in the porphyrin moieties of these polyimides was also carried out. The structures of these four types of polyimides, containing *cis*-DATPP, *trans*-DATPP, *cis*-ZnDATPP and *trans*-ZnDATPP, were confirmed by ATR-IR and H^1 -NMR. All polyimides were soluble in polar aprotic solvents, THF, DMAc and CH_2Cl_2 and had higher viscosity than the polyimides without porphyrin moiety. UV-vis and fluorescence spectroscopy of these polyimides in CH_2Cl_2 and DMAc were investigated. The rate constants for electron transfer of polyimides containing the highest content of *cis*-DATPP and *trans*-DATPP, PI-C4 and PI-T4, were 1.50×10^7 and 1.48×10^7 s^{-1} and the corresponding metalloporphyrins, PI-ZnC4 and PI-ZnT4, were 9.25×10^7 and 8.90×10^7 s^{-1} in CH_2Cl_2 , respectively. Fluorescence quenching of the porphyrin monomers and porphyrin polyimides by anthraquinone as an electron acceptor involved both static and dynamic quenching mechanisms. In addition, all of these polyimides displayed good thermal stability as determined by thermogravimetric analysis.

Field of study:..Petrochemistry and Polymer Science...Student's signature: *Sudkanueng Singto*

Academic year:2008.....Advisor's signature: *Supawan Tantayanon*

Co-advisor's signature: *Robert E. Connors*

ACKNOWLEDGEMENTS

I take this opportunity to place on record my deep sense of gratitude to my advisor, Associate Professor Dr. Supawan Tantayanon for introducing me to the exciting field of photochemistry polymer. I am deeply indebted for her guidance through my thesis and her valuable advice at all times.

I am sincerely grateful to my co-adviser, Professor Dr. Robert E. Connors for his suggestions, guidance, encouragement and support during my research at Worcester Polytechnic Institute (WPI) Massachusetts USA.

I am grateful to a research funding from WPI for 10 months. I would like also to thank the Department of Chemistry and Biochemistry for giving me a responsibility as a Teaching Assistant during the 2007-2008 academic years. Appreciation is also extended to National Center of Excellence for Petroleum, Petrochemicals, and Advanced Materials, NCE-PPAM in Thailand.

I would like to especially thank Christopher Zoto, a graduate student working under Dr. Connors at WPI, who has been giving all his suggestions, encouragement and good friendship over 10 months and making me feel comfortable, even during the most difficult times. In addition, I would also like to thank Tharinee Vongnakorn, a WPI graduate student, for her support and friendship, most especially her assistance with the NMR instrument.

Many thanks to the group members in Dr. Supawan's lab in Thailand for advise and support over the years.

I am at a total loss of words in expressing the depth of my emotion for my parents and brothers for their constant support and inspiration.

Finally, I am thankful to my friends, especially Chalisa Supporn for making me feel comfortable during the most difficult and trying moments of my life.

CONTENTS

	Page
ABSTRACT (THAI).....	iv
ABSTRACT (ENGLISH).....	v
ACKNOWLEDGEMENTS.....	vi
CONTENTS.....	vii
LIST OF TABLES.....	x
LIST OF FIGURES.....	xi
LIST OF SCHEMES.....	xiv
LIST OF ABBREVIATIONS.....	xv
CHEAPTER I: INTRODUCTION	
1.1 Introduction.....	1
1.2 Object of this research.....	1
1.3 Scope of Investigation.....	2
CHEAPTER II: THEORETICAL BACKGROUND	
2.1 Porphyrin.....	3
2.2 Polyimides.....	4
2.3 Absorption spectra of porphyrins.....	6
2.4 Fluorescence Spectroscopy.....	7
2.5 Fluorescence Quantum Yield and Lifetime.....	8
2.6 Fluorescence quenching and its types.....	9
2.7 Literature Reviews.....	12
CHAPTER III: EXPERIMENTAL	
3.1 Chemicals.....	16
3.1.1 Reagents.....	16
3.1.2 Solvents.....	17
3.2 Instrumentation.....	18
3.2.1 Nuclear Magnetic Resonance (NMR) Spectrometer.....	18
3.2.2 UV-visible Spectrophotometer.....	18

3.2.3 Attenuated Total Reflection Infrared (ATR-IR) Spectroscopy...	18
3.2.4 Fluorescence Spectroscopy.....	18
3.2.5 Thermogravimetric Analysis (TGA).....	18
3.2.6 Gel Permeation Chromatography (GPC).....	18
3.2.7 Viscosities Analysis.....	19
3.2.8 Fluorescence Lifetime Spectrometer.....	19
3.3 Monomer Synthesis.....	19
3.3.1 Synthesis of 5,10,15,20-tetraphenylporphyrin.....	19
3.3.2 Synthesis of 5,10,15,20-tetraphenylporphyrinatozinc(II).....	20
3.3.3 Synthesis of 5,10- <i>bis</i> (4-aminophenyl)-10,20-diphenylporphyrin and 5, 15- <i>bis</i> (4-aminophenyl)-10,20-diphenylporphyrin.....	20
3.3.4 Synthesis of zinc 5,10- <i>bis</i> (4-aminophenyl)-10,20-diphenyl porphyrin and zinc 5,15- <i>bis</i> (4-aminophenyl)-10,20-diphenyl porphyrin.....	21
3.4 Polymer syntheses.....	21
3.5 Spectrophotometric Analysis.....	23
3.5.1 Fluorescence Quantum Yield Determination.....	23
3.5.2 Fluorescence Lifetime Measurements.....	24
3.6 Fluorescence Quenching Analysis.....	24
 CHAPTER IV RESULTS AND DISCUSSION	
4.1 Monomer Syntheses.....	27
4.1.1 5,10,15,20-Tetraphenylporphyrin (TPP).....	27
4.1.2 5,10,15,20-Tetraphenylporphyrinatozinc(II) (ZnTPP).....	29
4.1.3 Synthesis of 5,10- <i>bis</i> (4-aminophenyl)-10,20-diphenylporphyrin (<i>cis</i> -DATPP) and 5,15- <i>bis</i> (4-aminophenyl)-10,20-diphenyl porphyrin (<i>trans</i> -DATPP).....	30
4.1.4 Synthesis of zinc 5, 10- <i>bis</i> (4-aminophenyl)-10,20-diphenylporphyrin and zinc 5,15- <i>bis</i> (4-aminophenyl)-10,20-diphenylporphyrin.....	36
4.2 Polymer Syntheses.....	40
4.2.1 Synthesis of polyimide.....	40
4.2.2 Identification of polyimides.....	44
4.2.2.1 Infrared spectroscopy.....	44

4.2.2.2 ¹ H-NMR spectroscopy.....	46
4.3 Determination of porphyrin content in polyimides.....	48
4.4 Polymer Properties.....	50
4.4.1 Polymer solubility.....	50
4.4.2 Viscosity of polyimides.....	52
4.4.3 Molecular weight determination.....	53
4.4.4 Thermal properties of polyimides.....	53
4.4.4.1 Decomposition temperature.....	53
4.4.5 Spectroscopic properties of polyimides.....	55
4.4.5.1 Absorption properties of polyimides.....	55
4.4.5.2 Fluorescence properties of polyimides.....	58
4.4.6 Fluorescence Quantum Yields Determination.....	60
4.4.7 Fluorescence Quenching Determination.....	64
4.5 Fluorescence quenching at high anthraquinone concentration of TPP and ZnTPP in CH ₂ Cl ₂ and DMAc.....	76
 CHAPTER V CONCLUSION AND SUGGESTIONS	
CONCLUSION.....	84
REFERENCES.....	87
APPENDICES.....	93
APPENDIX A Absorption spectra of porphyrins and polyimides.....	94
APPENDIX B Fluorescence Spectra of porphyrin and polyimides.....	97
APPENDIX C Infrared spectra of polyimides.....	100
APPENDIX D Determination of porphyrin content in polyimides.....	101
APPENDIX E Fluorescence spectra and Stern-Volmer plot of porphyrin and polyimides.....	102
APPENDIX F Fluorescence Quantum Yield Determination.....	114
APPENDIX G Fluorescence Lifetime Determination.....	120
APPENDIX H Thermogravimetric analysis (TGA).....	122
APPENDIX I Intrinsic viscosity measurement.....	125
APPENDIX J Molecular weight of polyimide determination.....	128
VITAE.....	134

LIST OF TABLES

Tables	Page
3.1 Polyimides at various ratios of monomers.....	22
3.2 The varied range of concentration of Anthraquinone.....	26
4.1 ¹ H-NMR data of 5,10,15,20-tetraphenylporphyrin(TPP).....	29
4.2 ¹ H-NMR data of 5,10,15,20-tetraphenylporphyrinaozinc(II) (ZnTPP).....	30
4.3 ¹ H-NMR data of 5,10- <i>bis</i> (4-aminophenyl)-10,20-diphenylporphyrin.....	33
4.4 ¹ H-NMR data of 5,15- <i>bis</i> (4-aminophenyl)-10,20-diphenylporphyrin.....	35
4.5 ¹ H-NMR data of zinc 5,10- <i>bis</i> (4-aminophenyl)-10,20-diphenylporphyrin (<i>cis</i> -DATPP).....	38
4.6 ¹ H-NMR data of zinc 5,15- <i>bis</i> (4-aminophenyl)-10,20-diphenylporphyrin (<i>trans</i> -DATPP).....	39
4.7 Four series of polyimides.....	43
4.8 Porphyrin content in polyimides.....	49
4.9 Solubility of polyimides in organic solvents.....	51
4.10 The physical property data of polyimides.....	54
4.11 UV-vis absorption maxima of polyimides in CH ₂ Cl ₂ and DMAc.....	57
4.12 Fluorescence maxima of polyimides in CH ₂ Cl ₂ and DMAc.....	59
4.13 Fluorescence quantum yields and lifetimes of polyimides.....	63
4.14 Summary of photophysical data of polyimides (series I and II) in CH ₂ Cl ₂ and DMAc.....	69
4.15 Summary of photophysical data of polyimides (series III and III) in CH ₂ Cl ₂ and DMAc.....	70
4.16 Lifetimes of TPP and ZnTPP (ns) with different concentration of AQ in CH ₂ Cl ₂	78
4.17 Lifetimes of TPP and ZnTPP (ns) with different concentration of AQ in DMAc.....	78

LIST OF FIGURES

Figure	Page
2.1 The chemical structure of a free base porphyrin.....	3
2.2 Jabłoński diagram.....	7
2.3 Pathway of dynamic (collisional) quenching.....	10
2.4 Pathway of static quenching.....	11
2.5 Stern-Volmer plots of (a) static quenching and (b) combination of static and dynamic quenching.....	12
2.6 Structure of polyimide prepared from 2,2'-bis(trifluoromethyl)-4,4',5,5'-biphenyl tetra-carboxylic dianhydride.....	12
2.7 Copolyimide films containing tetraphenylporphyrin (TPP) and carbazole (Cz) units.....	13
2.8 Polyimide containing biphenylporphyrin (BPP).....	13
2.8 Polyimides containing <i>trans</i> -DATPP and <i>trans</i> -ZnDATPP.....	14
4.1 IR spectrum of 5,10,15,20-tetraphenylporphyrin (TPP).....	28
4.2 ¹ H-NMR spectrum of free-base tetraphenylporphyrin(TPP).....	28
4.3 ATR-IR spectrum of 5,10,15,20-tetraphenylporphyrinatozinc (II) (ZnTPP).....	29
4.4 ¹ H-NMR spectrum of 5,10,15,20-tetraphenylporphyrinatozinc (II) (ZnTPP).....	30
4.5 Structures of 5,10- <i>bis</i> (4-aminophenyl)-10,20-diphenylporphyrin and 5,15- <i>bis</i> (4-aminophenyl)-10,20-diphenylporphyrin.....	31
4.6 IR spectrum of 5,10- <i>bis</i> (4-aminophenyl)-10,20-diphenylporphyrin.....	32
4.7 ¹ H-NMR spectrum of 5,10- <i>bis</i> (4-aminophenyl)-10,20-diphenylporphyrin.....	33
4.8 IR spectrum of 5,15- <i>bis</i> (4-aminophenyl)-10,20-diphenylporphyrin.....	34
4.9 ¹ H-NMR spectrum of 5,15- <i>bis</i> (4-aminophenyl)-10,20-diphenylporphyrin.....	34
4.10 UV-vis absorption data of TPP, <i>cis</i> - and <i>trans</i> -DATPP.....	35
4.11 IR spectrum of <i>cis</i> -ZnDATPP.....	37
4.12 ¹ H-NMR spectrum of zinc 5,10- <i>bis</i> (4-aminophenyl)-10,20-diphenylporphyrin (<i>cis</i> -ZnDATPP).....	37
4.13 IR-spectrum of <i>trans</i> -ZnDATPP.....	38
4.14 ¹ H-NMR spectrum of zinc 5,15- <i>bis</i> (4-aminophenyl)-10,20-diphenylporphyrin (<i>trans</i> -ZnDATPP).....	38
4.15 Chemical structure of ZnTPP, <i>cis</i> -DATPP and <i>trans</i> -DATPP.....	39

4.16 UV-vis absorption characteristics of ZnTPP, <i>cis</i> -DATPP and <i>trans</i> -DATPP.	40
4.17 IR spectra of polyimides.....	45
4.18 ¹ H-NMR of polyimides.....	47
4.19 Stern-Volmer plots of fluorescence quenching of TPP by AQ in CH ₂ Cl ₂ and DMAc.....	65
4.20 Stern-Volmer plots of fluorescence quenching of <i>cis</i> -DATPP by AQ in CH ₂ Cl ₂ and DMAc.....	65
4.21 Stern-Volmer plots of fluorescence quenching of <i>trans</i> -DATPP by AQ in CH ₂ Cl ₂ and DMAc.....	66
4.22 Fluorescence quenching of 5x10 ⁻⁶ mol.dm ⁻³ of TPP and Stern-Volmer plot of fluorescence quenching by Anthraquinone [2x10 ⁻⁴ -1.4x10 ⁻³ M] in CH ₂ Cl ₂	71
4.23 Fluorescence quenching of 5x10 ⁻⁶ mol.dm ⁻³ of <i>cis</i> -DATPP and Stern- Volmer plot of fluorescence quenching by Anthraquinone [2x10 ⁻⁴ - 1.4x10 ⁻³ M] in CH ₂ Cl ₂	71
4.24 Fluorescence quenching of 5x10 ⁻⁶ mol.dm ⁻³ of <i>trans</i> -DATPP and Stern-Volmer plot of fluorescence quenching by Anthraquinone [2x10 ⁻⁴ -1.4x10 ⁻³ M] in CH ₂ Cl ₂	71
4.25 A-D Fluorescence quenching of polyimide containing 5-30% <i>cis</i> -DATPP moieties and Stern-Volmer plots of fluorescence quenching by AQ [2x10 ⁻⁴ -1.4x10 ⁻³ M] in CH ₂ Cl ₂	72
4.26 A-D Fluorescence quenching of polyimide containing 5-30% <i>trans</i> -DATPP moieties and Stern-Volmer plots of fluorescence quenching by AQ [2x10 ⁻⁴ -1.4x10 ⁻³ M] in CH ₂ Cl ₂	73
4.27 Pathway of dynamic (collisional) quenching and static quenching.....	76
4.28 Fluorescence quenching (A) and Stern-Volmer plots (B) of fluorescence quenching of 5x10 ⁻⁶ mol.dm ⁻³ TPP by AQ concentration 0.002-0.016 M in CH ₂ Cl ₂	79
4.29 Plot of [(F ₀ /F) - 1]/[AQ] vs. AQ for TPP fluorescence quenching by AQ in CH ₂ Cl ₂	79
4.30 Fluorescence quenching and Stern-Volmer plots of fluorescence quenching of 5x10 ⁻⁶ mol.dm ⁻³ Zn-TPP by AQ concentration 0.002-0.016 M in CH ₂ Cl ₂	80
4.31 Plot of [(F ₀ /F) - 1]/[AQ] vs. AQ for ZnTPP fluorescence quenching by AQ in CH ₂ Cl ₂	80

4.32 Fluorescence quenching and Stern-Volmer plots of fluorescence quenching of $5 \times 10^{-6} \text{ mol.dm}^{-3}$ TPP by AQ concentration 0.002-0.016 M in DMAc.....	82
4.33 Plot of $[(F_0/F) - 1]/[AQ]$ vs. AQ for TPP fluorescence quenching by AQ in DMAc.....	82
4.34 Fluorescence quenching and Stern-Volmer plots of fluorescence quenching of $5 \times 10^{-6} \text{ mol.dm}^{-3}$ ZnTPP by AQ concentration 0.002-0.016 M in DMAc.....	83
4.35 Plot of $[(F_0/F) - 1]/[AQ]$ vs. AQ for ZnTPP fluorescence quenching by AQ in DMAc.....	83



ศูนย์วิทยทรัพยากร
จุฬาลงกรณ์มหาวิทยาลัย

LIST OF SCHEMES

Scheme	Page
2.1 A one step method to prepare aromatic polyimides.....	5
2.2 Mechanism of nucleophilic substitution.....	5
2.3 The thermal imidization pathways of polyimides.....	6
4.1 5,10,15,20-tetraphenylporphyrin (TPP).....	27
4.2 Synthesis of 5,10- <i>bis</i> (4-aminophenyl)-10,20-diphenylporphyrin and 5,15- <i>bis</i> (4-aminophenyl)-10,20-diphenylporphyrin.....	36
4.3 Synthesis of zinc 5,10- <i>bis</i> (4-aminophenyl)-10,20-diphenylporphyrin.....	36
4.4 Synthesis of zinc 5,15- <i>bis</i> (4-aminophenyl)-10,20-diphenylporphyrin.....	36
4.5 Syntheses of polyimides without porphyrin.....	40
4.6 Syntheses of polyimides in series I.....	41
4.7 Syntheses of polyimides in series II.....	41
4.8 Syntheses of polyimides in series III.....	42
4.9 Syntheses of polyimides in series IV.....	42
4.10 pi-pi interaction and metal ligation in porphyrin.....	52


 ศูนย์วิจัยทรัพยากร
 จุฬาลงกรณ์มหาวิทยาลัย

LIST OF ABBREVIATION

AQ	: Anthraquinone
ATR-IR	: Attenuated Total Reflection Infrared Spectroscopy
CH ₂ Cl ₂	: Dichloromethane
DMAc	: Dimethylacetamide
DMF	: <i>N,N'</i> -Dimethylformamide
DMSO	: Dimethylsulfoxide
6FDA	: 4,4'-Hexafluoroisopropylidenediphthalic dianhydride
NMP	: <i>N</i> -methyl-2-pyrrolidone
PFMB	: 2,2'- <i>Bis</i> (trifluoromethyl)-4,4'-diaminobiphenyl
TFA	: Trifluoroacetic acid
TGA	: Thermal gravimetric analysis
THF	: Tetrahydrofuran
TPP	: Tetraphenylporphyrin
<i>Cis</i> -DATPP	: 5,10- <i>Bis</i> (4-aminophenyl)-10,20-diphenylporphyrin
<i>Cis</i> -ZnDATPP	: Zinc 5,10- <i>bis</i> (4-aminophenyl)-10,20-diphenylporphyrin
<i>Trans</i> -DATPP	: 5,15- <i>Bis</i> (4-aminophenyl)-10,20-diphenylporphyrin
<i>Trans</i> -ZnDATPP	: Zinc 5,15- <i>bis</i> (4-aminophenyl)-10,20-diphenylporphyrin
ZnTPP	: Zinc tetraphenylporphyrin
K_Q	: Stern-Volmer quenching constant
K_q	: The bimolecular quenching rate constant
K_{diff}	: The limiting diffusion rate constants
k_f	: The first-order radiative rate of decay
k_{nr}	: The first-order nonradiative rate of decay
F_0	: The fluorescence intensities in the absence of quencher
F	: The fluorescence intensities in the presence of quencher
τ_0	: The fluorescence lifetime in the absence of quencher
τ	: The fluorescence lifetime in the presence of quencher
δ	: Chemical Shifts
Φ	: Quantum yield

$[\eta]$: Intrinsic Viscosity
η_{sp}	: Specific Viscosity
\bar{M}_n	: Number average molar mass
\bar{M}_w	: Weight average molar mass
PDI	: Polydispersity index



ศูนย์วิทยทรัพยากร
จุฬาลงกรณ์มหาวิทยาลัย

CHAPTER I

INTRODUCTION

1.1 Introduction

Porphyrins have attracted interest in recent years due to their potential use in photochemical processes of photodynamic therapy (PDT) [1,2,3] and light harvesting [4]. The interaction of porphyrin base with various metal ions has been extensively studied [5,6]. They also have important applications in photocatalysis, photochemical conversion, and storage of solar energy as well as photosynthesis, photobiology and photomedicine [7,8].

Aromatic polyimides are best known for their mechanical and electrical properties [9], as well as for their outstanding thermal stability [10,11]. These class of compounds also display high softening temperatures and excellent chemical resistance. Currently, much attention to a related class of aromatic polyimides containing-porphyrin moieties are of considerable interest, due to their potential properties as photoconductive and charge-transporting materials [12-15].

This report discusses the synthesis, spectroscopic and photophysical examination of polyimide-containing porphyrins with differing concentrations containing unsubstituted tetraphenylporphyrin, diaminotetraphenylporphyrin and their corresponding zinc analogues. Spectroscopic data will involve measuring both the absorption and fluorescence properties of these compounds in two solvents. Photophysical properties of these classes of compounds involve determining both the fluorescence quantum yield (Φ_f) and fluorescence lifetime (τ_f) parameters in both solvents. Fluorescence quenching of the porphyrin monomers and porphyrin polyimides by an electron acceptor (anthraquinone) has been studied in detail.

1.2 Objective of this research

- To synthesize organo-soluble polyimides containing tetraphenylporphyrin moieties.
- To examine the behavior of fluorescent porphyrin and polyimides in the presence of an external electron acceptor.

1.3 Scope of Investigation

The stepwise investigation was carried out as follows:

1. Literature survey for related research work
2. To synthesize 5,10-*bis*(4-aminophenyl)-10,20-diphenylporphyrin(*cis*-DATPP) and 5,15-*bis*(4-aminophenyl)-10,20-diphenylporphyrin(*trans*-DATPP)
3. To synthesize zinc 5,10-*bis*(4-aminophenyl)-10,20-diphenylporphyrin(*cis*-Zn DATPP) and zinc 5,15-*bis*(4-aminophenyl)-10,20-diphenylporphyrin(*trans*-ZnDATPP)
4. To prepare polyimide containing porphyrin by polymerization at various mole ratios of porphyrins in the polymer
5. To characterize polyimide by ATR-IR spectroscopy, UV-vis spectroscopy, fluorescence spectroscopy, gel permeation chromatography, viscosity of polyimides
6. To measurement thermal properties of polyimides by TGA
7. To study photophysical properties of polyimides involve determining both the fluorescence quantum yield and fluorescence lifetime parameters in organic solvents
8. To study the behavior of fluorescence quenching porphyrin and polyimides in the presence of external quencher by fluorescence lifetime spectrometer

CHAPTER II

THEORETICAL BACKGROUND

2.1 Porphyrin

Porphyrins are aromatic tetrapyrrolic macrocycles largely used in electrophilic substitution reactions. This class of organic compounds contain 22 conjugated π -electrons, 18 of which are included in a cyclic delocalized conjugation pathway as shown in Figure 2.1. The numbering system is adopted for the porphyrin nucleus. The 2, 3, 7, 8, 12, 13, 17 and 18 positions have commonly been referred to generically as the “beta”-positions. Similarly, positions 1, 4, 6, 9, 11, 14, 16 and 19 have been referred to generically as the “alpha”-positions, while those at 5, 10, 15 and 20 are termed the “meso” positions. The vast majorities of porphyrins are structurally planar. These conditions fulfill the requirements for aromaticity according to Hückel’s rules of π electrons ($4n+2$; $n=4$).

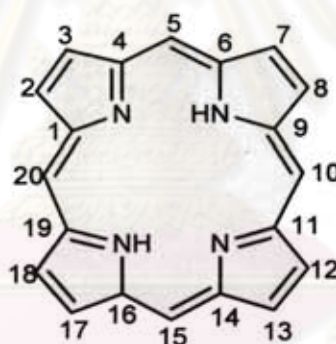


Figure 2.1 The chemical structure of a free base porphyrin.

Porphyrins are highly colored, showing a characteristically intense Soret band at around 400 nm in the absorption spectrum with very high extinction coefficients at this region. In addition, porphyrins have four bands between 450-700 nm, which are referred to as Q bands. The Soret band is a major characteristic of the optical absorption spectrum of the porphyrin macrocycle as it disappears with the disruption of the macrocycle. The intensity and wavelength of the absorption bands change with variations on the peripheral positions of the macrocycle. Protonation of two of the inner nitrogen atoms or insertion of a metal into the porphyrin cavity also changes the visible absorption spectrum. The large diamagnetic ring current observed in porphyrins is expressed by their $^1\text{H-NMR}$ spectra. The ring current generated by the

applied external field induces a local magnetic field similar to that in benzene. The inner N-H protons inside the porphyrin ring system are shifted upfield to as high as $\delta = -5$ ppm whereas the deshielded meso-protons are $\delta = 8-10$ ppm [16]. These compounds are conjugated, planar ligands ubiquitous in living systems and widely available in nature, also acting as sensitizers in the photosynthesis of plants, light harvesting and electron transfer [17]. In addition, porphyrins play a number of critical biological roles such as molecular binding and reaction catalysis [4, 17]. They also have been proven to be efficient sensitizers and catalysts in a number of chemical and photochemical processes, most especially photodynamic therapy (PDT) [1, 2, 3].

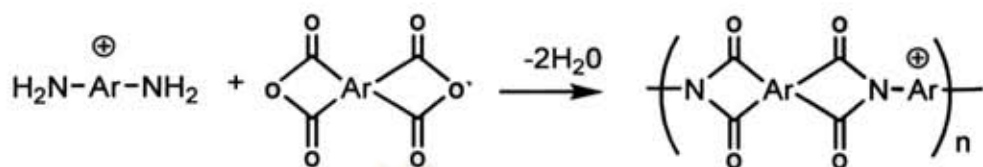
A porphyrin in which a metal is coordinated to the inner four nitrogens of the macrocycle is termed a metalloporphyrin. Metalloporphyrins are embedded within the active site of numerous protein environments, whose functions range from oxygen transfer and storage (hemoglobin and myoglobin) to electron transfer (cytochrome c, cytochrome oxidase) and energy conversion [18-21].

2.2 Polyimides

Aromatic polyimides are known for their excellent thermal and oxidative stability, as well as their exceptional mechanical properties [22-27]. They also display heat and excellent chemical resistance [28]. They are used in place of metals and glass in many high performance applications within the electronics, automotive and aerospace industries. The present work on porphyrin-containing polyimides mainly involved studying fundamental spectroscopic and photophysical properties necessary for the understanding of the incorporation of artificial solar energy conversion systems [29, 30], catalytic effects [31], photoresponsive materials [32], molecular wires [33] and photoinduced intramolecular electron transfer properties [12-15].

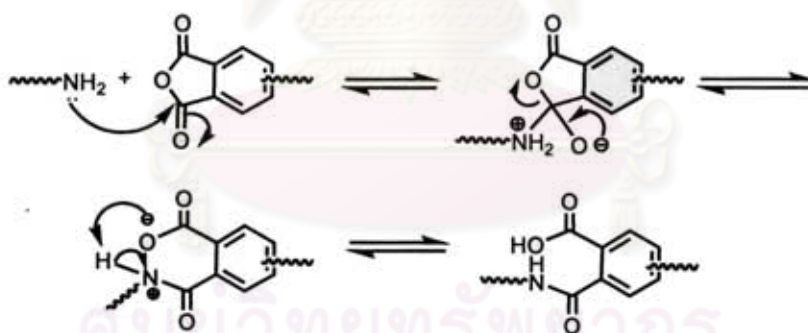
In general, aromatic polyimides are insoluble in common organic solvents. Thus, they must be processed in the form of their soluble poly(amic acid) (PAA) precursors. However, there are several drawbacks to the PAA approach, such as the release of water during imidization, which can create weakening voids in thick parts of the material [34]. Therefore, the synthesis of soluble porphyrin-containing aromatic polyimides represents a considerable part of this research.

A one step method to prepare soluble aromatic polyimides was reported in [35]. In this method, diamines and dianhydrides are polymerized at elevated temperatures to form the polyimides and imidization occurs without isolation of the poly(amic acid) intermediate as shown in scheme 2.1.

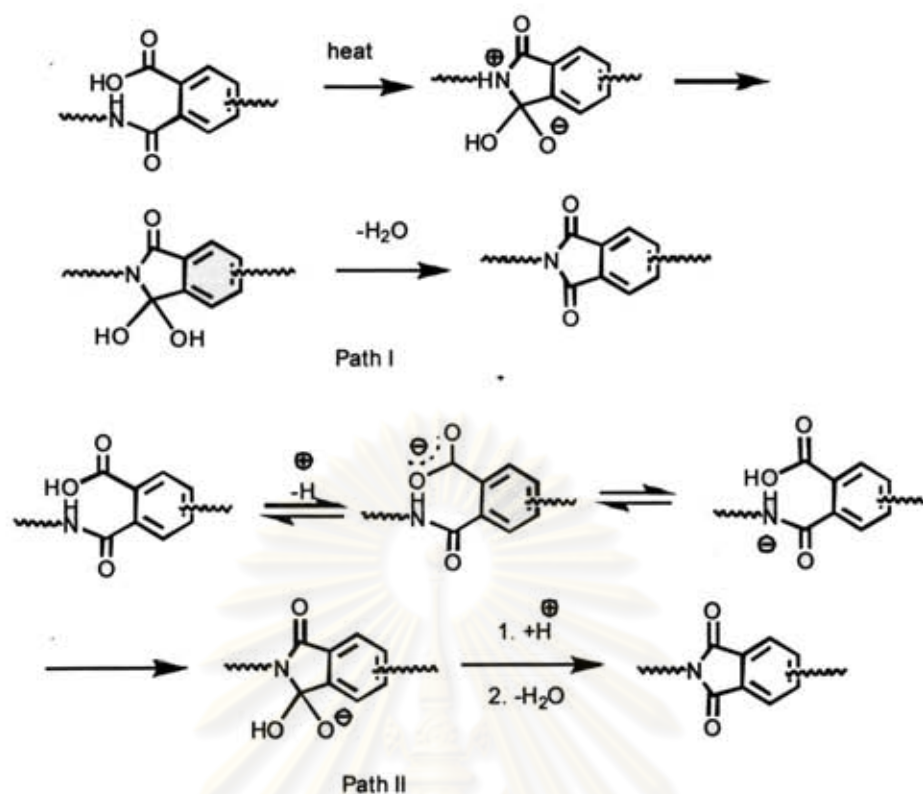


Scheme 2.1 A one step method to prepare aromatic polyimides.

This method is suitable for synthesizing polyimides that can be soluble in organic solvents. The water generated by imidization is usually allowed to distill from the reaction mixture to drive the imidization reaction to completion. With this method, unreactive or sterically hindered monomers can be successfully polymerized due to the high temperature used. In this study, porphyrin-containing polyimides have been synthesized by using this one-step approach. The mechanism is illustrated in the scheme 2.2 and 2.3.



Scheme 2.2 Mechanism of nucleophilic substitution



Scheme 2.3 The thermal imidization pathways of polyimides

The imidization can occur via two different pathways as shown in Scheme 2.3. In the first path, the amine proton is lost after cyclization. In the second pathway, the proton is lost prior or during ring closure. Ring closure is faster in the second pathway because the nucleophilicity of the conjugate base of the amide is much stronger than that of amide. In addition, the imidization processes give off water as by product [35].

2.3 Absorption spectra of porphyrins

The heterocyclic nucleus is fully conjugated with a characteristic absorption spectrum. The absorption spectra of aromatic tetrapyrrolic macrocycles display an intense band in the region of 400 nm. This absorption is called the Soret band and has a strong absorption with a high molar extinction coefficient. Porphyrins are highly colored and they show a characteristic intense Soret band at around 417 nm and also display four accompanying bands, commonly referred to as the Q-bands, of lower intensity between 450-650 nm. The Soret band is a major characteristic of the optical absorption spectrum of the porphyrin macrocycle as it disappears with the disruption of the macrocycle. The Soret band of TPP at 418 nm in CH₂Cl₂ may be assigned to a $\pi \rightarrow \pi^*$ transition to the second electronic excited state, S₂, while the four Q-bands can

be assigned to a $\pi \rightarrow \pi^*$ transition to the first electronic excited state S_1 [51]. The intensity and wavelength of the absorption band changes with variations in the peripheral positions of the porphyrin macrocycle. Protonation of two of the inner nitrogen atoms or insertion of a metal ion into the porphyrin cavity also changes the absorption characteristics. A red shift of λ_{\max} of the Soret band from 417 nm to 426 nm is observed upon insertion of a metal ion into the porphyrin cavity of TPP corresponding to the transition to the second excited singlet state S_2 . While four Q bands are observed in the free-base porphyrins, only two peaks are present in the Zn complex, corresponding to a vibronic sequence of the transition of lower excited singlet S_1 .

2.4 Fluorescence spectroscopy

Fluorescence occurs when an excited singlet state molecule or atom relaxes to the ground singlet state, emitting light. In the excited singlet state, the electron in the excited orbital is paired (of opposite spin) with the electron in the ground-state orbital. Consequently, return to the ground state is spin-allowed and occurs rapidly by emission of a photon. The emission rates of fluorescence are typically 10^8 s^{-1} . Figure 2.2 illustrates a Jabłoński diagram for the different types of radiative and nonradiative transitions that occur in photoexcited state systems.

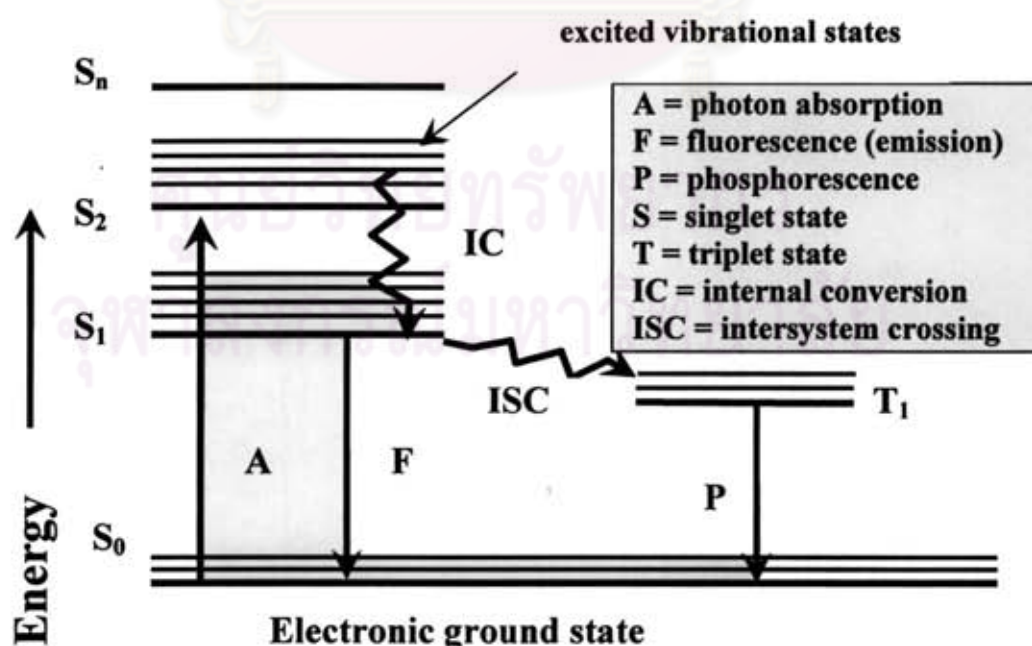


Figure 2.2 Jabłoński diagram [49]

As depicted in Figure 2.2, the ground, first-excited and second-excited singlet states are denoted as S_0 , S_1 and S_2 , respectively. A fluorophore is usually excited to some higher vibrational level of either S_1 or S_2 . With a few rare exceptions, molecules in condensed phases rapidly relax to the lowest vibrational level of S_1 . This process is termed internal conversion, which is a nonradiative transition between two states of same-spin multiplicities. Molecules in the S_1 state can also undergo a spin conversion to the corresponding triplet excited state, in which all but two electrons are spin paired. Emission of light from the first-excited triplet state (T_1) is termed phosphorescence and is generally shifted to longer wavelengths (smaller energies) relative to that of fluorescence. Nonradiative conversion between two states of different spin multiplicities (e.g. S_1 to T_1) is called intersystem crossing.

2.5 Fluorescence quantum yield and lifetime

Both the fluorescence quantum yield (Φ_f) and fluorescence lifetime (τ_f) are two photophysical parameters. The fluorescence quantum yield is defined as the ratio of number of photons emitted to the number of photons absorbed. Mathematically, the fluorescence quantum yield is related to the first-order radiative and non-radiative rate constant by the following relationship:

$$\Phi_f = \frac{k_f}{(k_f + k_{IC} + k_{ISC})} = \frac{k_f}{k_f + k_{nr}} \quad \text{Eq 2.1}$$

where k_f is the first-order radiative decay constant and k_{nr} is the first-order nonradiative decay rate constant ($k_{nr} = k_{IC} + k_{ISC}$). Nonradiative decay is any decay that does not involve the emission of a photon. The quantum yield can be close to unity if the radiationless decay rate is much smaller than the rate of radiative decay, $k_{nr} \ll k_f$.

The fluorescence lifetime (τ_f) is the inverse of the sum of the first-order radiative and nonradiative rates of decay:

$$\tau_f = \frac{1}{(k_f + k_{IC} + k_{ISC})} = \frac{1}{k_f + k_{nr}} \quad \text{Eq 2.2}$$

Combining the above two equations leads to the following equation:

$$\Phi_f = k_f \tau_f \quad \text{Eq 2.3}$$

The lifetime of the excited state is a measure of the average time the molecule spends in the excited state prior to returning to the ground state. Generally, fluorescence lifetimes are on the order of nanoseconds.

2.6 Fluorescence quenching and its types

Fluorescence quenching has been widely studied both as a fundamental phenomenon, and as a source of information about biochemical systems. These biochemical applications of quenching are due to the molecular interactions that result in quenching. The fluorescence quenching by the molecules besides fluorophores has been used extensively to study the permeability of the quenchers into the macromolecules, the environment around the fluorophore as well as the location of the fluorophores in the micelles, reverse micelles and other types of macromolecules [49, 56].

Fluorescence quenching refers to any process which decreases the fluorescence intensity of a sample. Generally speaking, in fluorescence quenching, an excited-singlet state molecule may lose its energy in the form of heat through collisions with other molecules. A variety of molecular interactions can result in quenching. These include excited-state reactions, molecular rearrangements, energy transfer, ground-state complex formation and collisional quenching [49]. Fluorescence quenching has been widely studied both as a fundamental phenomenon and as a source of information about biochemical systems [50].

Both dynamic and static quenching, which will be discussed shortly, require molecular contact between the excited-state fluorophore and quencher. In the case of collisional quenching, the quencher must diffuse to the fluorophore during the lifetime of the excited state. Upon contact, the fluorophore returns back to the ground state, without emission of a photon. In general, quenching occurs without any permanent change to the molecules, that is, without a photochemical reaction. In the case of static quenching, a complex is formed between the fluorophore and the quencher, and this complex is non-fluorescent. For either static or dynamic quenching to occur, the fluorophore and quencher must be in contact with each other. The requirement of

molecular contact results in the numerous applications of quenching. For example, quenching measurements can reveal the accessibility of fluorophores to quenchers.

Generally, there are two types of fluorescence quenching processes, first of which is collisional (or dynamic) quenching. As previously mentioned, in fluorescence quenching, an excited singlet state molecule loses its electronic energy in the form of heat through collisions with other molecules termed quenchers. Quenching can occur by different mechanisms. Collisional quenching occurs when the excited-state fluorophore is deactivated upon contact with some other molecule in solution, called the quencher. Collisional quenching is illustrated in the pathway of dynamic quenching (Figure 2.3) and described by the well-known Stern-Volmer equation Eq 2.4.

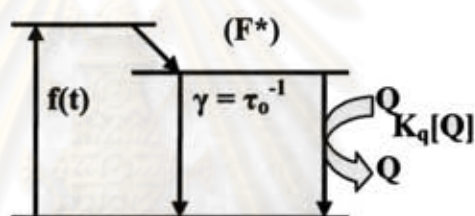


Figure 2.3 Pathway of dynamic (collisional) quenching

The rate constant for fluorescence quenching is used to determine the bimolecular rate constant of quenching (k_q) by the Stern-Volmer method as shown in equation (2.4).

$$\frac{F_0}{F} = 1 + K_Q[Q] = 1 + k_q\tau_0[Q] \quad \text{Eq 2.4}$$

In this expression, F_0 and F are the fluorescence intensities in the absence and presence of quencher, respectively, K_Q is the Stern-Volmer quenching constant, k_q is the bimolecular quenching rate constant, which is a measure of the accessibility of free diffusion of the fluorophore in the external medium, and $[Q]$ is the concentration of the external quencher. The bimolecular quenching rate, k_q , is calculated using equation (2.5).

$$K_Q = \tau_0 k_q \quad \text{Eq 2.5}$$

where τ_0 represents the fluorescence lifetime of the fluorophore in the absence of a quencher.

A linear Stern-Volmer plot is generally indicative for a single class of fluorophores, all equally accessible to quencher. If two fluorophore populations are present, and one class is not accessible to quencher, then the Stern-Volmer plots deviate from linearity toward the x-axis [49].

Static (or complex formation) quenching is the second type of fluorescence quenching. In this process, quenching can also occur as a result of the formation of a nonfluorescent complex between the fluorophore and quencher. When this complex absorbs light, it immediately returns back to the ground state in the absence of photon; in other words, nonradiatively [49].

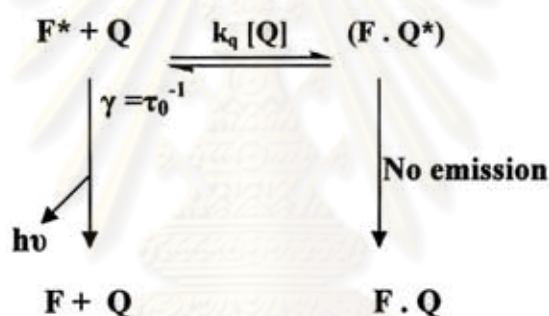


Figure 2.4 Pathway of static quenching

where F = fluorophore, Q = quencher, F* = excited fluorophore

In this case of static quenching, the lifetime of the sample will not be reduced since those fluorophores which are not complexed are able to emit after excitation. The fluorescence of the sample is reduced since the quencher is essentially reducing the number of fluorophores which can emit.

If both static and dynamic quenching are occurring in the sample, the following relation is true:

$$\frac{F_0}{F} = (1 + K_D [Q])(1 + K_S [Q]) \quad \text{Eq. 2.6}$$

In such a case, the plot of F_0/F versus $[Q]$ (Figure 2.5A) will give an upward curving plot. The upward curvature occurs because of $[Q]^2$ term in the equation.

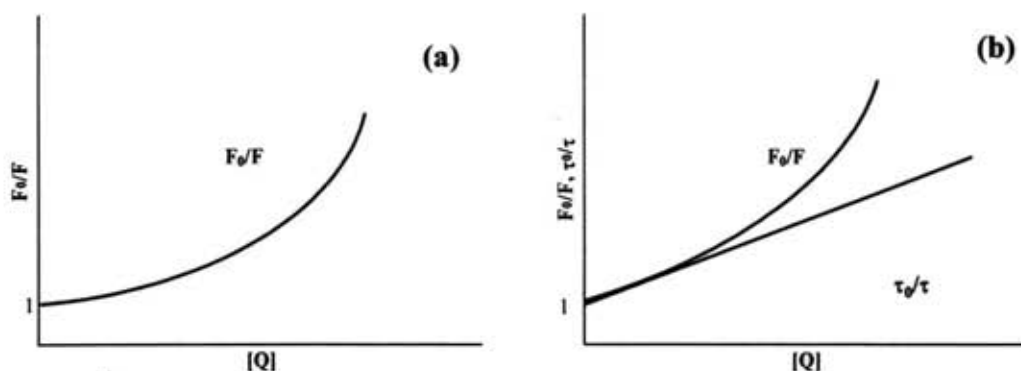


Figure 2.5 Stern-Volmer plots of (a) static quenching and (b) combination of static and dynamic quenching

However, since the lifetime is unaffected by the presence of quencher in cases of pure static quenching, a plot of τ_0/τ versus $[Q]$ would give a straight line (Figure 2.5B).

2.7 Literature Reviews

Harris, *et al* [11] synthesized polyimides from 2,2'-bis(trifluoromethyl)-4,4',5,5'-biphenyltetracarboxylic dianhydride and various type of diamines. It was determined that the polymer prepared from this dianhydride and 2,2'-bis(trifluoromethyl)-4,4'-diaminobiphenyl (PFMB) was soluble in most organic solvents, i.e., acetone, THF, DMF, DMAc and NMP. It also gave higher thermal stabilities than the polymers, which were prepared by this dianhydride and other diamines.

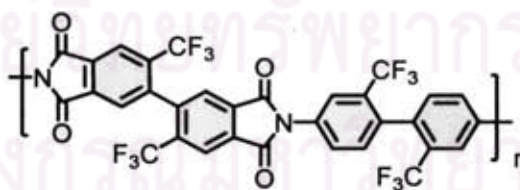


Figure 2.6 Structure of polyimide prepared from 2,2'-bis(trifluoromethyl)-4,4',5,5'-biphenyltetra-carboxylic dianhydride

Xu, *et al* [13] prepared the copolyimide film containing tetraphenylporphyrin (TPP) and carbazole (Cz) units. These copolyimides were fabricated into bilayer photoreceptors as a charge-generating layer to investigate their photoconductivity. It was determined that the photoconductivity of the copolyimides increased with the

incorporation of TPP into polymer chains (Figure 2.7). The formation of charge transfer complexes (CTCs) in these polyimides appeared to increase the photosensitivity of polymers.

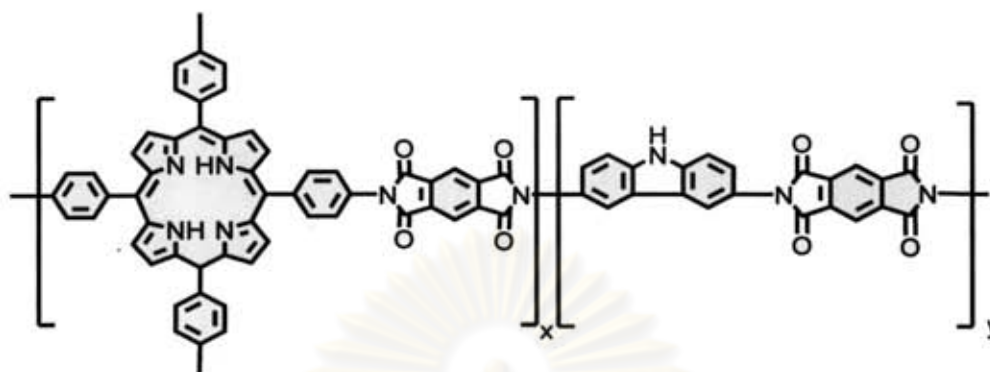


Figure 2.7 Copolyimide films containing tetraphenylporphyrin (TPP) and carbazole (Cz) units

Zhu, *et al* [15] synthesized polyimide containing biphenylporphyrin (BPP) by two-step method. It was found that the photoconductive sensitivities of polyimide increased with increasing BPP content. These results were attributed to the formation of CTCs of BPP units and imide group (BPP-imide) which could significantly improve the photosensitivity of polyimide systems.

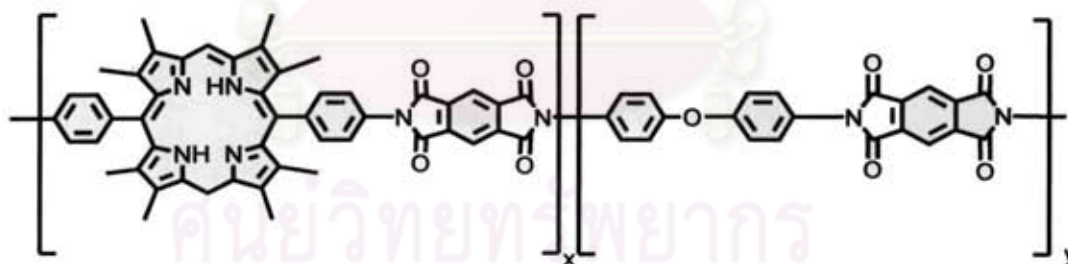


Figure 2.8 Polyimide containing biphenylporphyrin (BPP)

Anannarukan, *et al* [35] synthesized several soluble polyimides containing *trans*-diaminotetraphenylporphyrin by various amounts of 5,15-*bis*(4-aminophenyl)-10,20-diphenylporphyrin or *trans*-DATPP and zinc 5,15-*bis*(4-aminophenyl)-10,20-diphenylporphyrin or *trans*-ZnDATPP (5-15%), which was prepared from 2,2'-*bis*(trifluoromethyl)-4,4'-diaminobiphenyl (PFMB) and 4,4'-hexafluoroisopropylidene dipthalic anhydride (6FDA) at various ratios. It was determined that the polyimides were soluble in most common organic solvents. Every polyimide-containing

porphyrins exhibited significantly higher viscosities than the polyimides without porphyrin units. Furthermore, the polyimides with *trans*-ZnDATPP showed lower viscosity than *trans*-DATPP with the same porphyrin content. Steady state and time-resolved fluorescence measurements on these polymers in both solvents (CH_2Cl_2 and DMAc) revealed moderated quenching of the fluorescence that was attributed to photoinduced electron transfer from excited porphyrin units within the polymer to diimide acceptor groups.

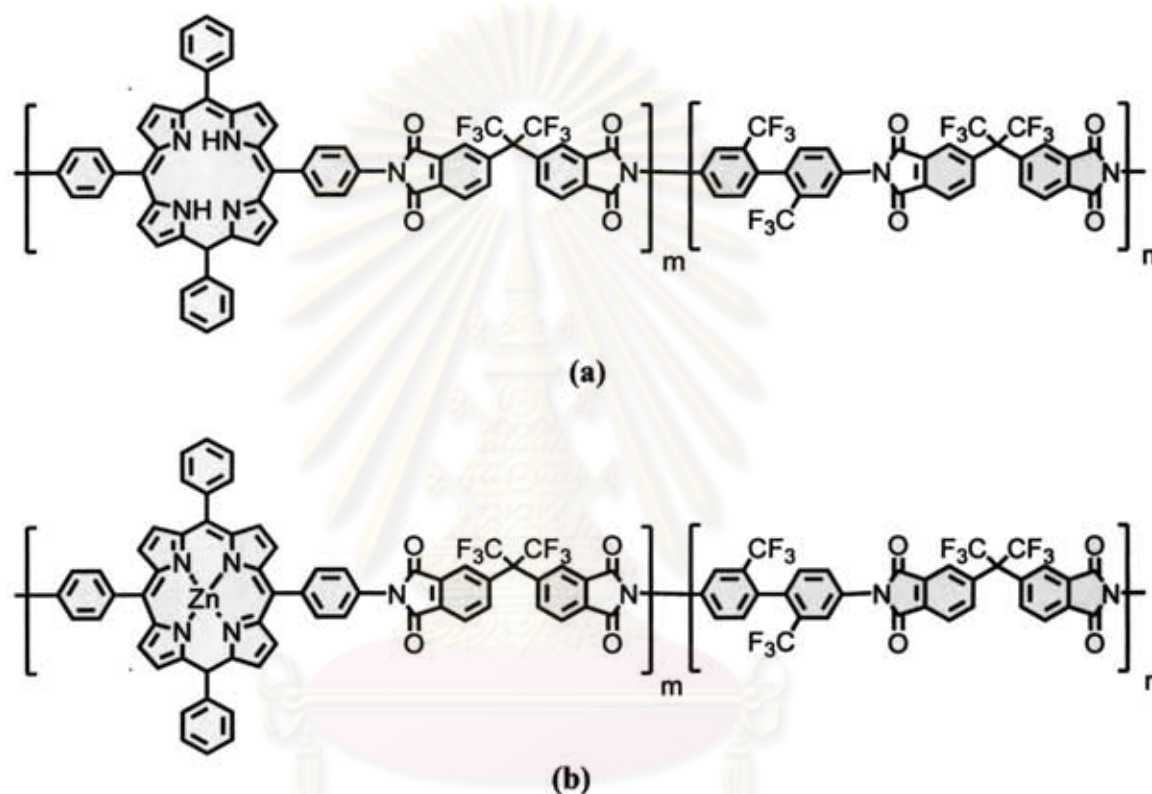


Figure 2.9 Polyimide containing *trans*-DATPP (a) and *trans*-ZnDATPP (b)

Danuta, *et al* [52] determined the optical and electron spin resonance (ESR) properties of metal-free porphyrin (TPP) and metal complex tetraphenylporphyrin such as Zn-TPP, Mg-TPP, Pt-TPP and Pb-TPP in the presence of anthraquinone [AQ] in isotropic solution of dimethylsulfoxide (DMSO). The fluorescence quenching data obtained with AQ as the external quencher of the porphyrin dye's fluorescence were analyzed using the Stern-Volmer equation. The observed decrease in the fluorescence intensity is due to quenching of the excited singlet state of TPP and metal-TPP donor due to electron transfer to AQ acceptor. The bimolecular quenching rate (k_q) values indicated faster quenching of TPP, Pb-TPP and Pt-TPP than those of Mg-TPP and Zn-TPP in the presence of AQ. Mg-TPP and Zn-TPP were characterized by longest

lifetimes compared to the remaining dyes. The slow charge recombination processes for Zn-TPP and Mg-TPP compounds could explain their high ability for photocurrent generation. In contrast because of high k_q and low ESR signals in the presence of AQ and its poor ability for conversion of photon energy to electric energy could indicate its fast charge recombination occurring in the electron donor-acceptor chain.

Sunao, *et al* [55] determined the mechanism for the fluorescence quenching of 5, 10,15,20-tetra(*p*-totyl)porphine (H_2TPP) and zinc complex (ZnTPP) in acetone by various kinds of quinones. It was determined that the transient effect for the collisional quenching caused an upward deviation in the plot of the inversed fluorescence intensities of porphyrins vs quinone concentrations and the relationship between k_q and the electron affinities of the quenchers are important for fluorescence quenching.



ศูนย์วิทยทรัพยากร
จุฬาลงกรณ์มหาวิทยาลัย

CHAPTER III

EXPERIMENTAL

3.1 Chemicals

3.1.1 Reagents

1. Activated charcoal (Acros) was used as received.
2. 9,10-Anthraquinone (Aldrich) was sublimed before use.
3. Ammonium hydroxide (Aldrich) was used as received.
4. Benzaldehyde (Aldrich) was distilled under reduced pressure prior to use.
5. 2,2'-bis(trifluoromethyl)-4,4'-diaminobiphenyl, PFMB was received by Harris's lab
6. Calcium hydride (Acros) was used as received.
7. Celite (Aldrich) was used as received.
8. 4,4'-Hexafluoroisopropylidenediphthalic anhydride, 6FDA (Fluka) was used as received.
9. Hydrochloric acid (Fisher) was used as received.
10. Isoquinoline (Aldrich) was used as received.
11. Magnesium sulfate anhydrous (EMD) was used as received.
12. Propionic acid (Fluka) was used as received.
13. Pyrrole (Acros) was distilled over calcium hydride under reduce pressure prior to use.
14. Sodium hydroxide (Fisher) was used as received.
16. Silica gel, 230-400 mesh, 60 A° (Merck) was used as received.
17. Sodium nitrite (Fluka) was used as received.
18. Sodium sulfate anhydrous (Fluka) was used as received.
19. Stannous chloride dihydrate (Aldrich) was used as received.
20. Toluene (Acros) was used as received.
21. Trifluoroacetic acid, TFA (Acros) was used as received.
22. Tin (II) chloride was used as received.
23. Zinc acetate dihydrate (Alfa Aesar) was used as received.

3.1.2 Solvents

1. Chloroform (Fisher) was used as received.
2. Chloroform-d, CDCl_3 (Aldrich) was used as received.
3. Dichloromethane (Aldrich) was distilled over calcium hydride before use.
4. Dichloromethane, spectral grade (Acros) was used as received.
5. Dimethylacetamide, DMAc (Alfa Aesar) was used as received.
6. N, N'-Dimethylformamide, DMF (Aldrich) was used as received.
7. Dimethylsulfoxide, DMSO (Aldrich) was used as received.
8. Dimethylsulfoxide-d₆, DMSO-d₆, (Aldrich) was used as received.
9. Ethanol, absolute (Fisher) was used as received.
10. Ethyl acetate (Fisher) was used as received.
11. Hexane (EMD) was used as received.
12. N-methyl-2-pyrrolidone, NMP (Aldrich) was distilled over calcium hydride under reduced pressure prior to use.
13. Tetrahydrofuran (Fisher) was used as received.

3.2 Instrumentation

3.2.1 Nuclear Magnetic Resonance (NMR) Spectrometer

Proton nuclear magnetic resonance ($^1\text{H-NMR}$) spectra were obtained in deuterated chloroform (CDCl_3) or deuterated sulfoxide ($\text{DMSO-}d_6$) using a Bruker[®] AVANCE 400 MHz NMR spectrometer. Chemical shifts (δ) are reported in parts per million (ppm) relative to the residual protonated solvent signal as a reference.

3.2.2 UV-visible Spectrophotometer

UV-visible absorption was recorded on a Perkin Elmer Lambda 35 UV/Vis spectrophotometer.

3.2.3 Attenuated Total Reflection Infrared (ATR-IR) Spectroscopy

Attenuated total reflectance infrared (ATR-IR) spectra were performed on a Perkin Elmer[®] Spectrum One. ATR-IR spectroscopy technique is used to analyze material surface. It is also suitable for characterization of materials which are either too thick or too strong absorbing to be analyzed by transmission spectroscopy.

3.2.4 Fluorescence Spectroscopy

Fluorescence spectra were collected using Perkin Elmer[®] LS50B Luminescence Spectrometer.

3.2.5 Thermogravimetric Analysis (TGA)

The combustion stage and melting point were investigated by a Mettler Toledo thermo gravimetric analyzer model NETZSCH STA 409 using a heating rate of 10 °C/min heating rate under ambient atmosphere.

3.2.6 Gel Permeation Chromatograph (GPC)

Molecular weight of polyimides were determined by gel permeation chromatography (GPC). GPC chromatogram of Polyimides was obtained from waters 150-CV chromatography equipped with PL-gel 10 μm mixed B 2 columns (MW resolving range = 500-10,000,000) at 35°C. Tetrahydrofuran (THF) was used as a solvent and the mobile phase with an injection rate of 1.0 mL/min. Degassed THF mobile phase was passed through the column for 20 minutes before sample with

injected. The sample volume 100 μL was injected and run for 40 minutes. A standard Polystyrenes (MW = 5,460-1,290,000) mixed column served as a stationary phase. The molecular weight was determined by a reflection index detector.

3.2.7 Viscosities Analysis

Intrinsic viscosities were determined with SCHOTT-Ostwald viscometer. Flow times were recorded for Dimethylacetamide (DMAc) with polymer concentration of approximately 0.2-1.0 g/dL at $35 \pm 0.1^\circ\text{C}$

3.2.8 Fluorescence Lifetime Spectrometer

Fluorescence lifetimes of both the monomers and the series of polyimides were measured using a Photon Technology International® the fluorescence decay of an instrument response function (IRF) was measured to be at about the same maximum intensity as that of the sample decay. The IRF used was a non-dairy creamer solution.

3.3 Monomer syntheses

3.3.1 Synthesis of 5,10,15,20-tetraphenylporphyrin (TPP)

Benzaldehyde (1.62 mL, 16 mmol) and pyrrole (1.11 mL, 16 mmol) were added simultaneously to refluxing with propionic acid 100 mL and the mixture was refluxed for 1 hour before set aside stirred for 30 min at room temperature. The mixture was added with cold methanol 20 mL and continuously stirred in the ice bath. The product was filtered off, then washed with hot water and methanol until the filtrate was colorless, giving purple glistering crystals (0.21g, 27 % yield) : m.p. $> 400^\circ\text{C}$, ATR-IR (cm^{-1}): 3314 (NH), 3050 and 3017 (ArH), 1470 and 1440 (NH bending), 698 (out-of-plane bending deformation, monosubstituted benzene); $^1\text{H-NMR}$ (CDCl_3) δ : -2.73 (s, 2H, internal NH), 7.28 (s, 4H p-phenyl), 7.79 (m, 12H, m-, p-phenyl), 8.24-8.21 (m, 8H, o-phenyl), 8.88 (s, 8H, β -pyrrole); UV/Visible (CH_2Cl_2 , nm): λ_{max} 417 (soret), 514, 549, 590 and 644 (DMAc, nm): λ_{max} 417 (soret), 514, 546, 589 and 646.

3.3.2 Synthesis of 5,10,15,20-tetraphenylporphyrinatozinc(II) (ZnTPP) [37]

To a boiling solution of 5,10,15,20-tetraphenylporphyrin (0.76 g, 1.24 mmol) in chloroform (150 mL) was added a saturated solution of zinc acetate dehydrate (0.40 g, 1.86 mmole) in methanol (3mL) mixture refluxed for ½ hour, cooled down, and extracted twice with distilled water. The organic solution was dried over anhydrous sodium sulfate and the drying agent was filtered off. Purple crystals of ZnTPP (0.83 g, 99.0%) were collected on filter and washed with cold methanol [37]. ¹H-NMR(CDCl₃ 400 MHz)δ: 7.23 (s, 4H, *p*-phenyl), 7.69-7.64 (m, 12H, *m*-, *p*-phenyl), 8.16-8.09 (m, 8H, *o*-phenyl), 8.84 (s, 8H, β -pyrrole); UV/Visible (CH₂Cl₂, nm): λ_{max} 419 (soret), 548 and 587 (DMAc, nm): λ_{max} 426 (soret), 560 and 600.

3.3.3 Synthesis of 5,10-bis(4-aminophenyl)-10,20-diphenylporphyrin (*cis*-DATPP) and 5,15-bis(4-aminophenyl)-10,20-diphenylporphyrin (*trans*-DATPP) [38]

To a solution of 5,10,15,20-tetraphenylporphyrin (200 mg, 0.326 mmol) in trifluoroacetic acid (10 mL) was add sodium nitrite (183 mg, 2.65 mmol). After 90 seconds stirring at room temperature, the reaction was poured into water (100 mL) and extracted with dichloromethane (6x25 mL). The residue obtained was purified as described above and then reduced using 0.8 g (3.55 mmol) of tin(II)chloride dihydrate and 50 mL of HCl. The reaction was heat to 65°C for 90 min. The porphyrin solution was cooled to room temperature and poured into ice water and was adjusted to pH 8 with concentrated ammonium hydroxide. The aqueous phase was extracted with 5x100 mL portion of CH₂Cl₂, which were combined and dried over anhydrous magnesium sulfate. The organic phase was concentrated on a rotary evaporator to 40 mL and this solution was pre-absorbed on silica gel, flash chromatography. The two regioisomers were eluted with dichloromethane and ethyl acetate gradient (5,15-*bis*(4-aminophenyl)-10,20-diphenylporphyrin eluted first) and were recrystallized from methanol, yielding 32% of 5,10-isomer and 28% of 5,15-isomer. For *cis*-DATPP; ATR-IR: 3325 (NH), 1510 (NH), 800 cm⁻¹ (1,4-substituted. benzene). ¹H-NMR (DMSO-d₆) δ: -2.83 (s, 2H, internal NH), 5.48 (s, 4H, NH₂), 6.93 (d, 4H, aminophenyl), 7.80-7.69 (m, 10H, phenyl), 8.08 (d, 4H, aminophenyl), 8.69 (s, 4H, β-

H), 8.86 (s, 4H, β -H). UV/Visible (CH_2Cl_2 , nm): λ_{max} 422 (soret), 519, 555, 593 and 650 (DMAc, nm): λ_{max} 424 (soret), 520, 566, 599 and 657.

For *trans*-DATPP; ATR-IR: 3328 (NH), 1504 (NH), 800 cm^{-1} (1,4-substituted benzene). $^1\text{H-NMR}$ (DMSO- d_6) δ : -2.81 (s, 2H, internal NH), 5.52 (s, 4H, NH_2), 6.92 (d, 4H, amimophenyl), 7.78-7.73 (m, 10H, phenyl), 8.22 (d, 4H, aminophenyl), 8.7 (d, 4H, β -H), 8.87 (d, 4H, β -H) UV/Visible (CH_2Cl_2 , nm): λ_{max} 422 (soret), 519, 555, 593 and 650 (DMAc, nm): λ_{max} 424 (soret), 520, 566, 599 and 657.

3.3.4 Synthesis of zinc 5,10-bis(4-aminophenyl)-10,20-diphenylporphyrin (Cis-ZnDATPP) and zinc 5,15-bis(4-aminophenyl)-10,20-diphenylporphyrin trans-ZnDATPP [35]

To a solution of 190 mL of THF was added compound (*cis*-DATPP or *trans*-DATPP) (638 mg, 0.99 mmol) and zinc acetylacetonate dihydrate (1.276 g, 4.53 mmol). The solution was refluxed for 4 h, cooled to room temperature, and evaporating out the solvent. The precipitate was partially dissolved in methanol solution by heating and left overnight at 0°C . The resulting violet crystal was collected, washed with methanol, and then dried to afford compound m.p. $> 300^\circ\text{C}$, For *cis*-ZnDATPP; yield (0.56g, 80%). $^1\text{H-NMR}$ (DMSO- d_6) δ : 5.53 (s, 4H, NH_2), 6.93 (d, 4H, amimophenyl), 7.85-7.68 (m, 10H, phenyl), 8.13 (d, 4H, aminophenyl), 8.69 (s, 4H, β -H), 8.86 (s, 4H, β -H). UV/Visible (CH_2Cl_2 , nm): λ_{max} 424 (soret), 551 and 592 (DMAc, nm): λ_{max} 423 (soret), 564 and 609.

For *trans*-ZnDATPP; yield (0.66g, 85%). $^1\text{H-NMR}$ (DMSO- d_6) δ : 5.52 (s, 4H, NH_2), 6.93 (d, 4H, amimophenyl), 7.79-7.68 (m, 10H, phenyl), 8.17 (d, 4H, aminophenyl), 8.70 (d, 4H, β -H), 8.87 (d, 4H, β -H). UV/Visible (CH_2Cl_2 , nm): λ_{max} 424 (soret), 551 and 591 (DMAc, nm): λ_{max} 434 (soret), 564 and 610.

3.4 Polymer syntheses

The dianhydride monomer, 4,4'-hexafluoroisopropylidenediphthalic anhydride (6FDA) (0.93 mmol) was added to the diamine monomer (0.93 mmol) 2,2'-bis(trifluoromethyl)-4,4'-diaminobiphenyl (PFMB), PFMB/*cis*-DATPP/*cis*-ZnDATPP/*trans*-DATPP/*trans*-ZnDATPP, at various mole ratios (Table 3.1) in dry NMP containing a small catalytic amount of isoquinoline under nitrogen at ambient temperature. After the solution was stirred for 8 h, it was heated under reflux and maintained at 220°C for 12 h. After the solution was allowed to cool to ambient

temperature, it was slowly added to vigorously stirred methanol. The precipitated polymer was collected by filtration, washed with methanol, and dried under reduced pressure at 200°C for 24 h. The polymer was obtained in 90-95% yield.

Table 3.1 Polyimides at various ratios of monomers

PI	Mole in feed (%)			
	6FDA	PFMB*	DATPP	ZnDATPP
Series I				
<i>cis</i> -DATPP				
PI-C1	100	95	5	-
PI-C2	100	90	10	-
PI-C3	100	85	15	-
PI-C4	100	70	30	-
Series II				
<i>trans</i> -DATPP				
PI-T1	100	95	5	-
PI-T2	100	90	10	-
PI-T3	100	85	15	-
PI-T4	100	70	30	-
Series III				
<i>cis</i> -ZnDATPP				
PI-ZnC1	100	95	-	5
PI-ZnC2	100	90	-	10
PI-ZnC3	100	85	-	15
PI-ZnC4	100	70	-	30
Series IV				
<i>trans</i> -ZnDATPP				
PI-ZnT1	100	95	-	5
PI-ZnT2	100	90	-	10
PI-ZnT3	100	85	-	15
PI-ZnT4	100	70	-	30

3.5 Spectrophotometric Analysis

3.5.1 Fluorescence Quantum Yield Determination

The fluorescence quantum yield (Φ_f) is defined as the ratio of the number of photons emitted through fluorescence to the number of photons absorbed and calculated by using equation 3.1

$$\Phi_f = \Phi_s \frac{A_s D_c n_c^2}{A_c D_s n_s^2} \quad \text{Eq 3.1}$$

where Φ_s = The fluorescence quantum yield of known standard (from literature)

A_s = Absorbance at $\lambda(\text{ex})$ of standard

A_c = Absorbance at $\lambda(\text{ex})$ of sample

n_s = Index of refraction of standard solvent

n_c = Index of refraction of sample solvent

D_s = Computed area under corrected fluorescence emission spectrum standard

D_c = Computed area under corrected fluorescence emission spectrum sample

Stock solutions of tetraphenylporphyrin (TPP), *cis*- and *trans*-DATPP in CH_2Cl_2 and DMAc were prepared (maximum absorbance of approximately 0.5). The stock solution was accurately diluted tenfold to give an absorbance maximum of approximately 0.05. Optical absorption spectra were generated for both the stock and diluted solutions. A fluorescence emission spectrum of the diluted standard solution was obtained, fixing the excitation wavelength, which produced an emission spectrum that started and ended at baseline. Experimental fluorescence emission data was imported into Microsoft Excel to convert the data from wavelength to wavenumbers. Data was imported into Mathcad, which corrected the fluorescence emission spectra of both the standard and the analyte and computed the fluorescence quantum yields. Appendix F provides a sample calculation for the fluorescence quantum yield of tetraphenylporphyrin (TPP). The fluorescence quantum yields of the standard (Φ_s) were tetraphenylporphyrin (TPP) in toluene ($\Phi_f = 0.1 \pm 0.001$) [45], TPP in CH_2Cl_2 ($\Phi_f = 0.116$) and TPP in DMAc ($\Phi_f = 0.15$). The same procedures were utilized for

polyimide-containing metallic porphyrin; ZnTPP in toluene ($\Phi_f = 0.033$) [46], $\Phi_f = 0.02$ in CH_2Cl_2 and $\Phi_f = 0.024$ in DMAc) as a standard.

3.5.2 Fluorescence Lifetime Measurements

The fluorescence lifetime (τ_f) is the inverse of the sum of the first-order radiative and nonradiative rates of decay ($\tau_f = 1/(k_f + k_{nr})$). Fluorescence lifetimes of both the monomers and the series of polyimides were measured using a Photon Technology International® fluorescence lifetime spectrometer equipped with both nitrogen and dye lasers. FeliX 32 analysis module was the computer software program employed for generating the time-dependent fluorescence decay spectra. Data analysis involved using a curve-fitting procedure, measuring fluorescence lifetimes. Best-fit curves were chosen on how well the field-fit curve fits to the sample decay by statistical analysis. In addition, the fluorescence decay of an instrument response function (IRF) was measured to be at about the same maximum intensity as that of the sample decay. The IRF used was a non-dairy creamer solution. Appendix G shows a sample Mathcad calculation for fluorescence lifetime determination.

3.6 Fluorescence Quenching Analysis

The rate constant for fluorescence quenching was used to determine the bimolecular rate constant of quenching (k_q) by the Stern-Volmer method as shown in equation (3.2).

$$\frac{F_0}{F} = 1 + K_Q [Q] \quad \text{Eq 3.2}$$

where F_0 and F represents the fluorescence intensities in the absence and presence of quencher, K_Q is the Stern-Volmer quenching constant. The bimolecular quenching rate k_q was calculated using equation (3.3).

$$K_Q = \tau_0 k_q \quad \text{Eq 3.3}$$

where τ_0 represent the fluorescence lifetime of the porphyrin in the absence of a quencher. In addition, k_q values of the TPP-AQ system are approximately equivalent as the limiting diffusion rate constants (k_{diff}), which generally shows that the rate with

reactant A and B diffuse together in solution and collide. The k_{diff} values for CH_2Cl_2 and DMAc are 1.57×10^{10} and $3.32 \times 10^9 \text{ M}^{-1}\text{s}^{-1}$ respectively, as calculated by Eq. 3.4

$$k_d = \frac{8000RT}{3\eta} \quad \text{Eq.3.4}$$

where k_d has units of $\text{dm}^3\text{mol}^{-1}\text{s}^{-1}$, R is the gas constant ($8.314 \text{ JK}^{-1}\text{mol}^{-1}$), T is the absolute temperature, and η is the viscosity of the solvent ($\eta = 4.13 \times 10^{-4} \text{ kgm}^{-1}\text{s}^{-1}$ for CH_2Cl_2 at 25°C and $1.956 \times 10^{-3} \text{ kgm}^{-1}\text{s}^{-1}$ for DMAc) [47]. Electron-transfer rate constants were calculated using Equation 3.5 where

$$k_{ET} = \frac{1}{\tau_{PI}} - \frac{1}{\tau_{ref}} \quad \text{Eq. 3.5}$$

τ_{PI} represents the fluorescence lifetime of polyimides and τ_{ref} represents the fluorescence lifetime of reference (TPP).

9,10-Anthraquinone behaved as the fluorescence quencher for all quenching studies. Stock solutions of tetraphenylporphyrin, *cis*- and *trans*-DATPP and Zn-complexed TPP, (*cis*- and *trans*-ZnDATPP) concentrations were kept constant ($C = 5 \times 10^{-6} \text{ M}$). For low anthraquinone (AQ) concentration varied in the range of 2×10^{-4} to $1.4 \times 10^{-3} \text{ M}$ and high Anthraquinone concentration varied in the range of 2×10^{-3} to $1.4 \times 10^{-2} \text{ M}$. The set of porphyrins and AQ were dissolved in dichloromethane (CH_2Cl_2) and N, N-dimethylacetamide (DMAc). For polyimides containing *cis*-, *trans*-DATPP and metallic *cis*-, *trans*-ZnDATPP weighting polymers, 25 mL concentrations were the same in every portions. Exactly 2.5 mL of each stock solution were transferred to separate 5 mL volumetric flasks, along with the appropriate volume of AQ, as listed in Table 3.2.

Table 3.2 The varied range of concentration of anthraquinone (AQ)

Flask	mL of anthraquinone (AQ)	Low concentration of [AQ] M	High concentration of [AQ] M
1	0	0	0
2	0.2	2.0×10^{-4}	2.0×10^{-3}
3	0.4	4.0×10^{-4}	4.0×10^{-3}
4	0.6	6.0×10^{-4}	6.0×10^{-3}
5	0.8	8.0×10^{-4}	8.0×10^{-3}
6	1.0	1.0×10^{-3}	1.0×10^{-2}
7	1.2	1.2×10^{-3}	1.2×10^{-2}
8	1.4	1.4×10^{-3}	1.4×10^{-2}
9	1.6		1.6×10^{-2}



ศูนย์วิทยทรัพยากร
จุฬาลงกรณ์มหาวิทยาลัย

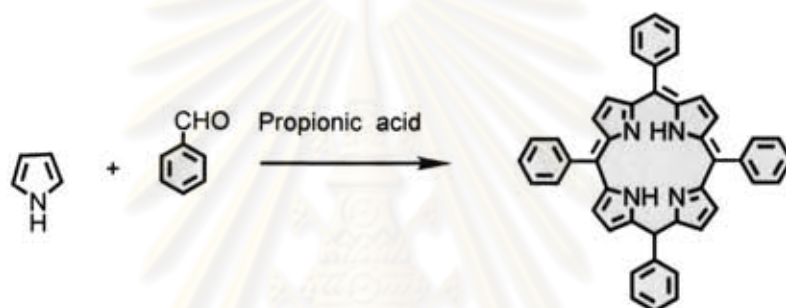
CHAPTER IV

RESULTS AND DISCUSSION

4.1 Monomer Syntheses

4.1.1 5,10,15,20-Tetraphenylporphyrin (TPP)

The synthesis of 5,10,15,20-tetraphenylporphyrin (TPP) was attempted by starting at the condensation of pyrrole and benzaldehyde according to Adler and Longo's method [36]. After a workup, the compound was obtained as purple crystals in 27% yield as shown in Scheme 4.1.



Scheme 4.1 5,10,15,20-tetraphenylporphyrin (TPP)

The compound was then characterized by ATR-IR, ¹H-NMR and UV-visible absorption spectroscopy. According to the infrared spectrum, TPP usually has doublets at 1440 and 1470 cm⁻¹ (NH) bending, which is the characteristic for the free metal porphyrin. The absorptions at 798 and 698 cm⁻¹ were also found, which indicated the presence of 1, 4-substituted benzene in the structure (Figure 4.1).

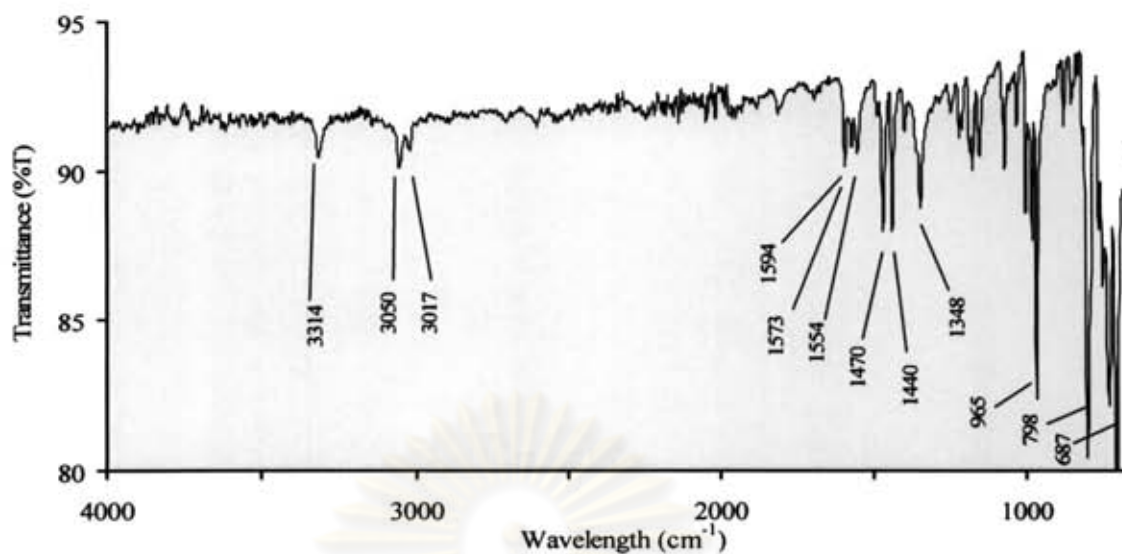


Figure 4.1 IR spectrum of 5,10,15,20-tetraphenylporphyrin (TPP)

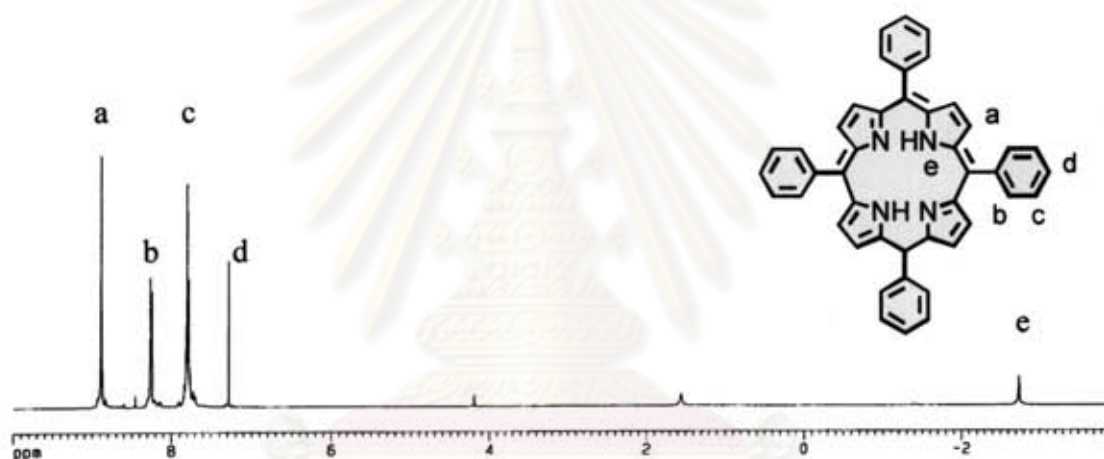


Figure 4.2 $^1\text{H-NMR}$ (400 MHz, CDCl_3) spectrum of free-base tetraphenylporphyrin

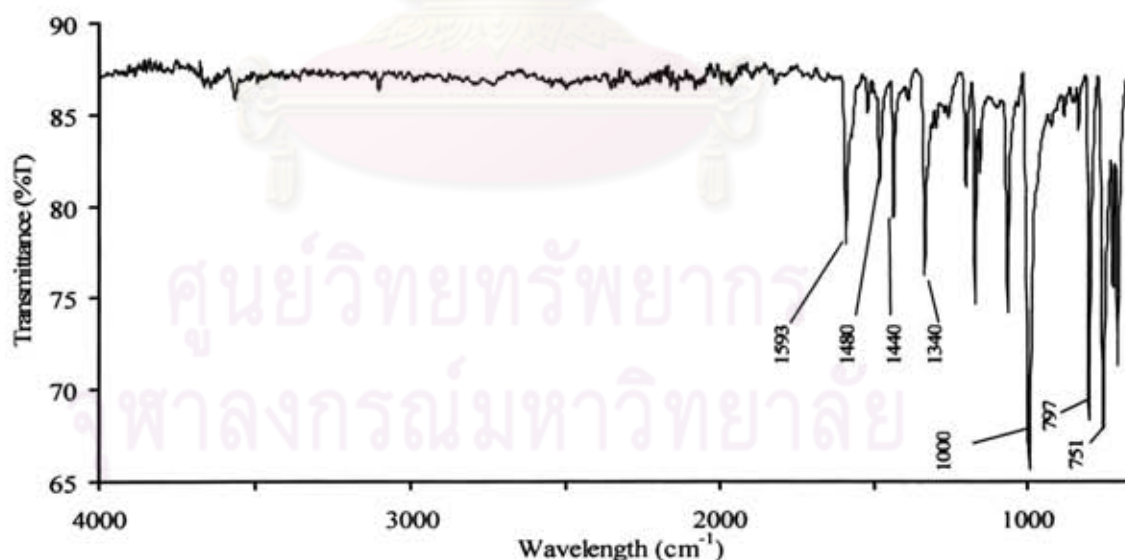
The $^1\text{H-NMR}$ spectrum of free-base tetraphenylporphyrin showed three multiplet series in the aromatic region at δ 7.78-7.79, 8.24-8.21 and 8.88 ppm. The upfield singlet signal at -2.73 ppm refers corresponds to internal NH of porphyrin. NMR signals appearing other chemical shifts were assigned for the corresponding protons as presented in Table 4.1.

Table 4.1 $^1\text{H-NMR}$ data of 5,10,15,20-tetraphenylporphyrin (TPP)

δ (ppm)	number of proton (s), type of proton
8.88	s, 8H, β -pyrrole (a)
8.24-8.21	m, 8H, <i>o</i> -phenyl (b)
7.79	m, 12H, <i>m</i> -, <i>p</i> -phenyl (c)
7.28	s, 4H, <i>p</i> -phenyl (d)
-2.73	s, 2H, internal NH (e)

4.1.2 5,10,15,20-Tetraphenylporphyrinatozinc(II) (ZnTPP)

5,10,15,20-Tetraphenylporphyrinatozinc(II) (ZnTPP) was reacted between a saturated zinc acetate dehydrate solution and chloroform solution of TPP. Zinc ion was easily inserted into the core of the free-base TPP as indicated by a change in the color of the solution from deep to bright purple. The product was characterized by ATR-IR and $^1\text{H-NMR}$ spectroscopy. The disappearance of the absorption band at 3314 cm^{-1} , which was due to the internal NH stretching for TPP. The infrared spectrum of ZnTPP is shown in Figure 4.3.

**Figure 4.3** ATR-IR spectrum of 5,10,15,20-tetraphenylporphyrinatozinc(II) (ZnTPP)

The chemical structure of ZnTPP was also identified by $^1\text{H-NMR}$ (Figure 4.4). Table 4.2 lists the chemical shifts for the corresponding hydrogen atoms.

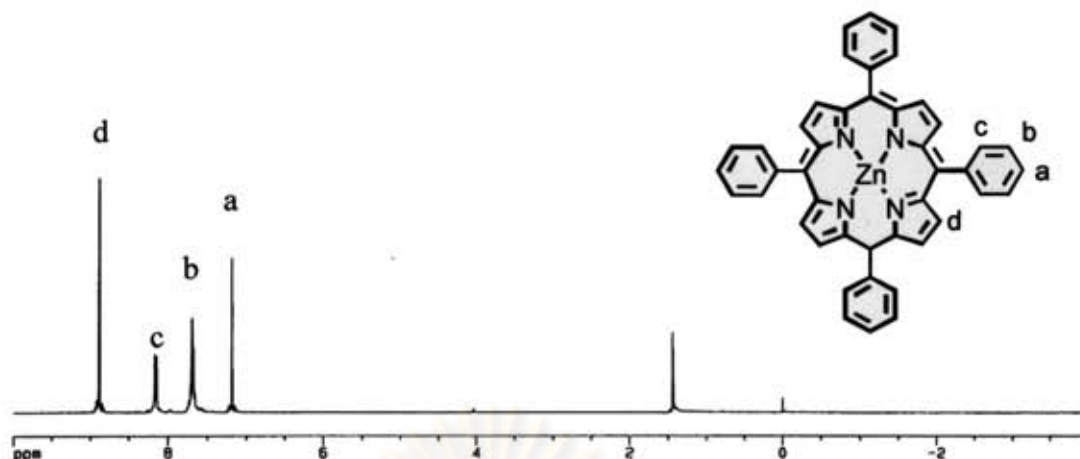


Figure 4.4 $^1\text{H-NMR}$ (400 MHz, CDCl_3) spectrum of 5,10,15,20-tetraphenylporphyrinatozinc(II) (ZnTPP)

The $^1\text{H-NMR}$ spectrum of ZnTPP similarly resembled the proton signals for the free base 5,10,15,20-tetraphenylporphyrin. The signal of internal N-H protons in the spectrum of the free base at -2.81 ppm disappears.

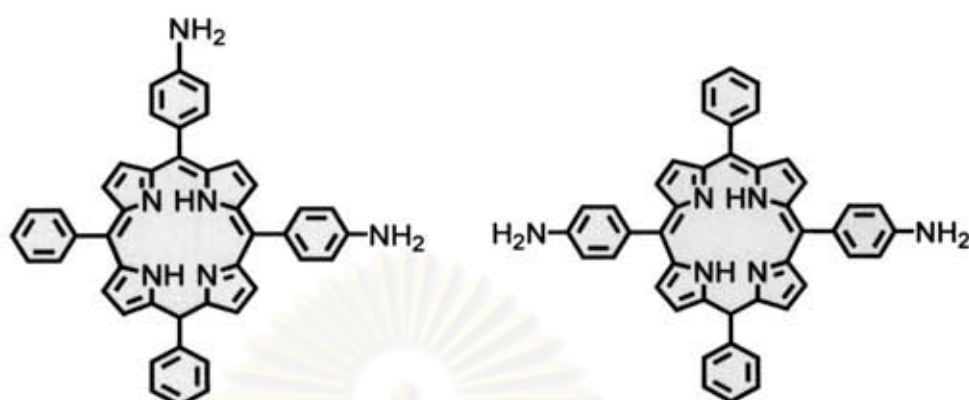
Table 4.2 $^1\text{H-NMR}$ data (400 MHz, CDCl_3) of 5,10,15,20-tetraphenylporphyrinatozinc (II) (ZnTPP)

δ (ppm)	number of proton (s), type of proton
8.84	s, 8H, β -pyrrole (d)
8.16-8.09	m, 8H, <i>o</i> -phenyl (c)
7.69-7.64	m, 12H, <i>m</i> -, <i>p</i> -phenyl (b)
7.23	s, 4H, <i>p</i> -phenyl (a)

4.1.3 Synthesis of 5,10-bis(4-aminophenyl)-10,20-diphenylporphyrin (*cis*-DATPP) and 5,15-bis(4-aminophenyl)-10,20-diphenylporphyrin (*trans*-DATPP)

Normally, 5,10-bis(4-aminophenyl)-10,20-diphenylporphyrin, the *cis*-isomer of diaminotetraphenylporphyrin abbreviated as *cis*-DATPP (2) and 5,15-bis(4-aminophenyl)-10,20-diphenylporphyrin, the *trans*-isomer of diaminotetraphenylporphyrin, abbreviated as *trans*-DATPP (3) can be synthesized by two steps, which involve the formation and the subsequent reduction of 5,10-bis(4-nitrophenyl)-10,20-diphenylporphyrin and 5,15-bis(4-nitrophenyl)-10,20-diphenylporphyrin. This section

describes and illustrates the synthesis and structural identification of both *cis*-DATPP(2) and *trans*-DATPP(3). Whose chemical structures are shown in Figure 4.5.



5,10-*bis*(4-aminophenyl)-10,20-diphenylporphyrin 5,15-*bis*(4-aminophenyl)-10,20diphenylporphyrin

cis-DATPP

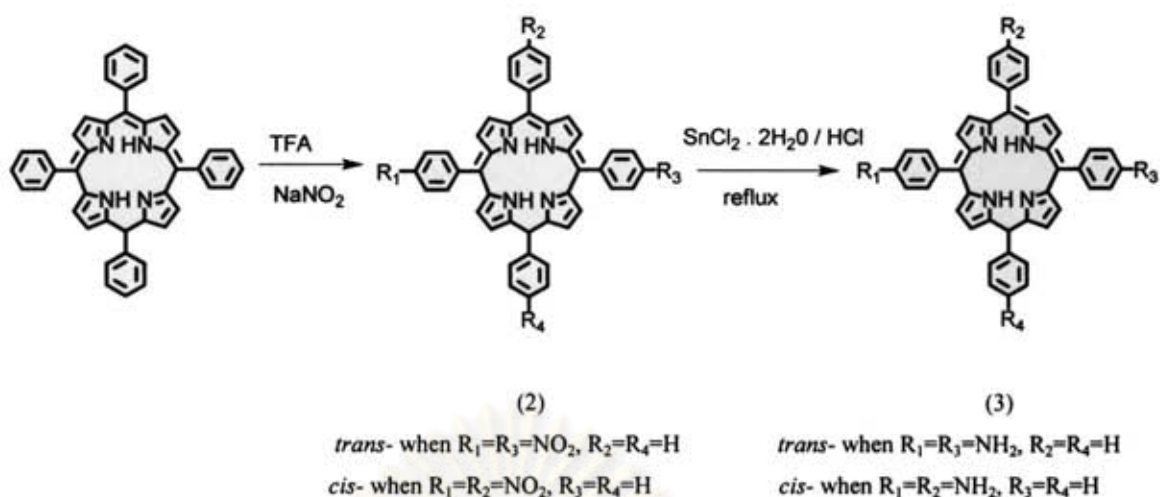
trans-DATPP

(2)

(3)

Figure 4.5 Structures of 5,10-*bis*(4-aminophenyl)-10,20-diphenylporphyrin (2) and 5,15-*bis*(4-aminophenyl)-10,20-diphenylporphyrin (3)

The synthesis of 5,10-*bis*(4-aminophenyl)-10,20-diphenylporphyrin (2) or 5,15-*bis*(4-aminophenyl)-10,20-diphenylporphyrin (3) (Scheme 4.2) was attempted by starting with tetraphenylporphyrin and a catalytic amount of trifluoroacetic acid (TFA) at room temperature. Sodium nitrite (NaNO_2) was also added to the reaction mixture. *Cis*-DATPP and *trans*-DATPP were reduced in accordance with the method employed by [38] in using stannous (II) chloride dihydrate and concentrated hydrochloric acid (HCl). The complete reaction was obtained when both regioisomers were separated by flash column chromatography on silica gel using dichloromethane as the eluting solvent. 5,15-*bis*(4-aminophenyl)-10,20-diphenylporphyrin (*trans*-DATPP) eluted out first and recrystallized from methanol, yielding 32% of (2) and 28% yield of (3).



Scheme 4.2 Synthesis of 5,10-*bis*(4-aminophenyl)-10,20-diphenylporphyrin (2) and 5,15-*bis*(4-aminophenyl)-10,20-diphenylporphyrin (3)

The chemical structures of both *cis*- and *trans*-DATPP were identified by ATR-IR and ¹H-NMR spectroscopy. The absorption bands for the IR spectrum of *cis*-DATPP (2) were at 3325 (NH), 1510(NH), and 800 cm⁻¹ (monosubstituted benzene) (Figure 4.6).

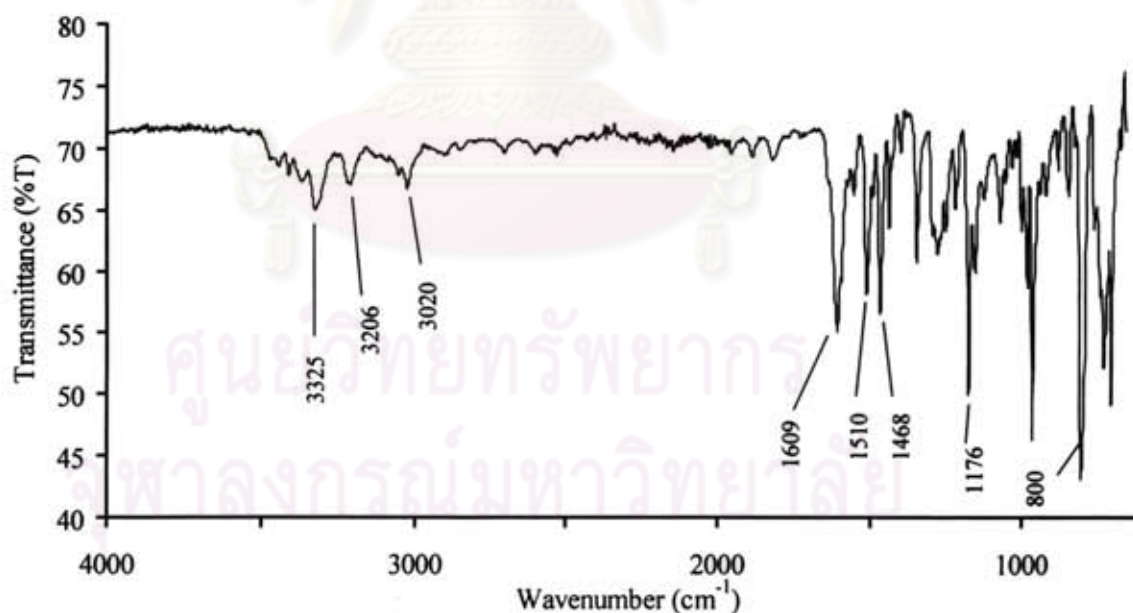


Figure 4.6 IR spectrum of 5,10-*bis*(4-aminophenyl)-10,20-diphenylporphyrin (2)

Figure 4.7 shows the $^1\text{H-NMR}$ spectrum of 5,10-*bis*(4-aminophenyl)-10,20-diphenylporphyrin (2). The proton NMR signals for (2) are presented in Table 4.3.

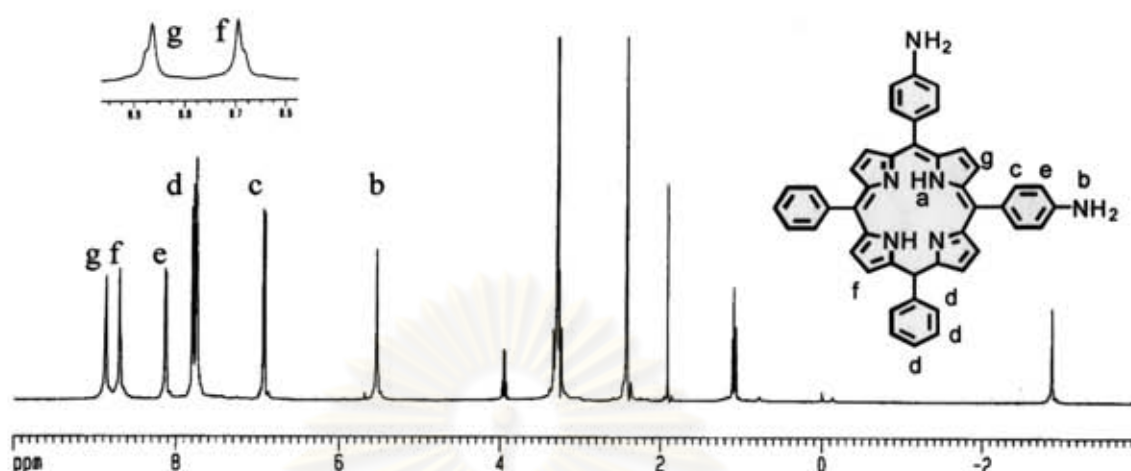


Figure 4.7 $^1\text{H-NMR}$ (400 MHz, DMSO-d_6) spectrum of 5,10-*bis*(4-aminophenyl)-10,20-diphenylporphyrin (2)

Table 4.3 $^1\text{H-NMR}$ data of 5,10-*bis*(4-aminophenyl)-10,20-diphenylporphyrin (2)

δ (ppm)	number of proton (s), type of proton
8.86	s, 4H (g)
8.69	s, 4H (f)
8.08	d, 4H, aminophenyl (e)
7.80-7.69	m, 10H, phenyl (d)
6.93	d, 4H, aminophenyl (c)
5.48	s, 4H, NH_2 (b)
-2.83	s, 2H, internal NH (a)

In addition, the structure of 5,15-*bis*(4-aminophenyl)-10,20-diphenylporphyrin (3) was also identified by ATR-IR and $^1\text{H-NMR}$ spectroscopy. The IR spectrum of *trans*-DATPP (3) showed the absorption bands at 3325 (NH), 1504 (NH), and 800 cm^{-1} (1,4 disubstituted benzene) (Figure 4.8).

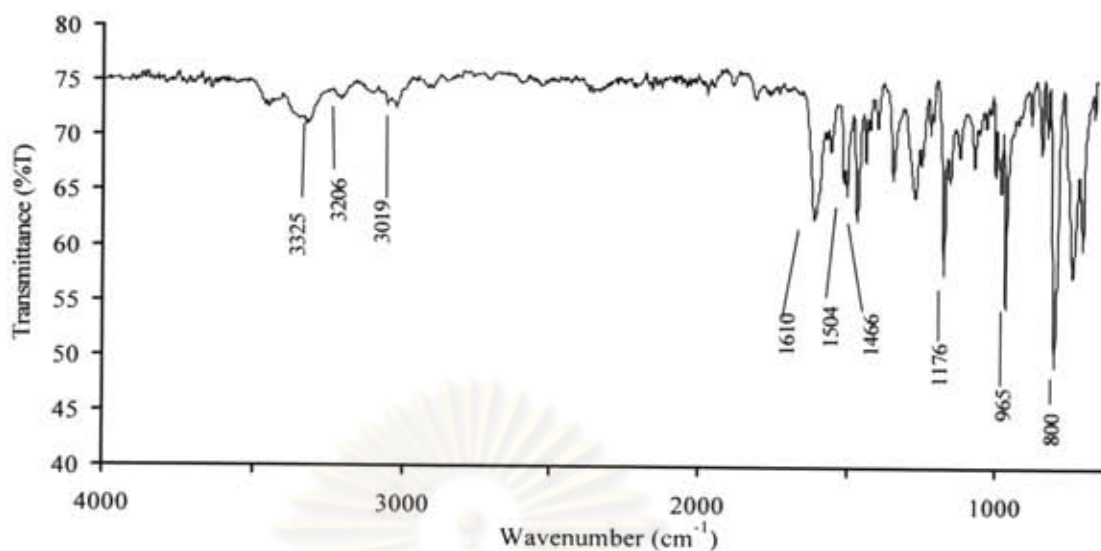


Figure 4.8 IR spectrum of 5,15-bis(4-aminophenyl)-10,20-diphenylporphyrin (3)

Figure 4.9 shows the $^1\text{H-NMR}$ spectrum of *trans*-DATPP, along with interpreted data presented in Table 4.4.

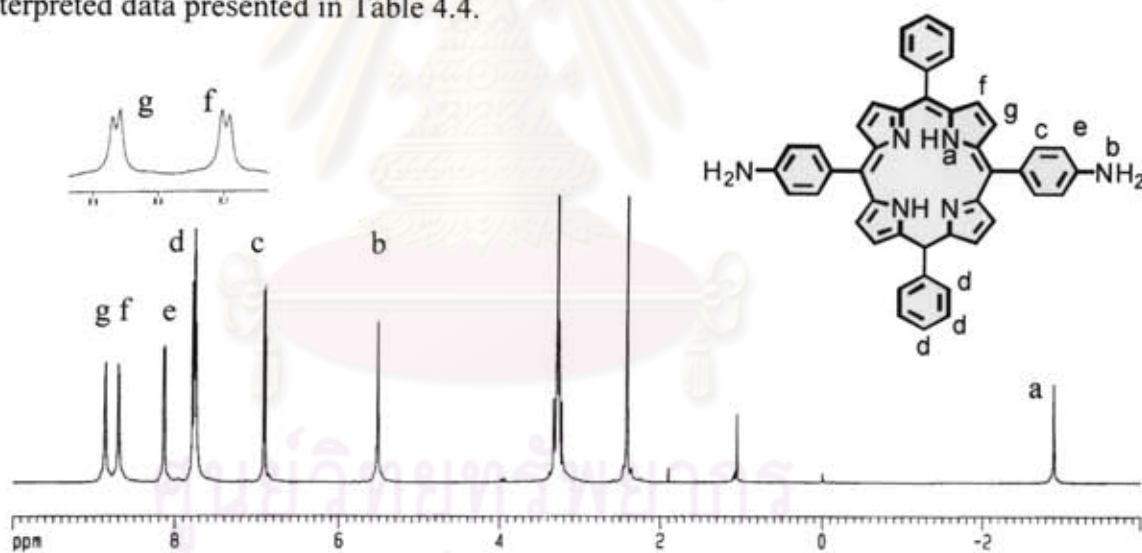
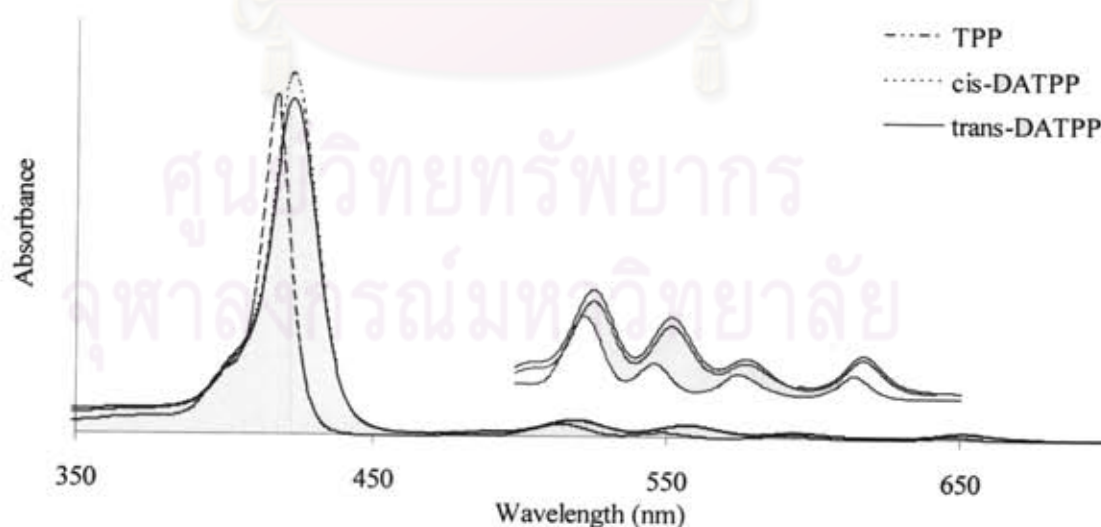


Figure 4.9 $^1\text{H-NMR}$ (400 MHz, DMSO-d_6) spectrum of 5,15-bis(4-aminophenyl)-10,20-diphenylporphyrin (3)

Table 4.4 $^1\text{H-NMR}$ data of 5,15-bis(4-aminophenyl)-10,20-diphenylporphyrin (3)

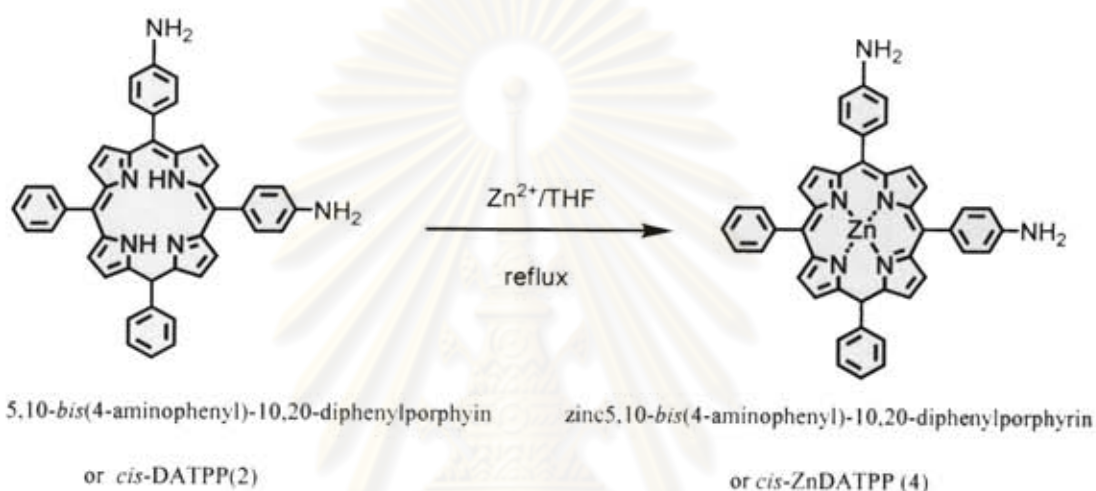
δ (ppm)	number of proton (s), type of proton (position)
8.87	d, 4H, β -H (g)
8.70	d, 4H, β -H (f)
8.22	d, 4H, aminophenyl (e)
7.78-7.73	m, 10H, phenyl (d)
6.92	d, 4H, aminophenyl (c)
5.52	s, 4H, NH_2 (b)
-2.81	s, 2H, internal NH (a)

UV-vis absorption spectra of *cis*-DATPP (2) and *trans*-DATPP (3) compared to tetraphenylporphyrin (TPP) in CH_2Cl_2 and DMAc are shown in Figure 4.10. Five absorption bands were found for each compound. The UV-vis absorption spectrum of *cis*- and *trans*-DATPP exhibits a typical pattern of free base porphyrin, and is similar to that of TPP. In CH_2Cl_2 , the Soret band and the four Q-bands of both *cis*- and *trans*-DATPP were observed at slightly lower wavelength than in DMAc solvent. The cause of the small red-shift of *cis*- and *trans*-DATPP compared to TPP is due to the presence of donating amino groups substituted on the benzene rings.

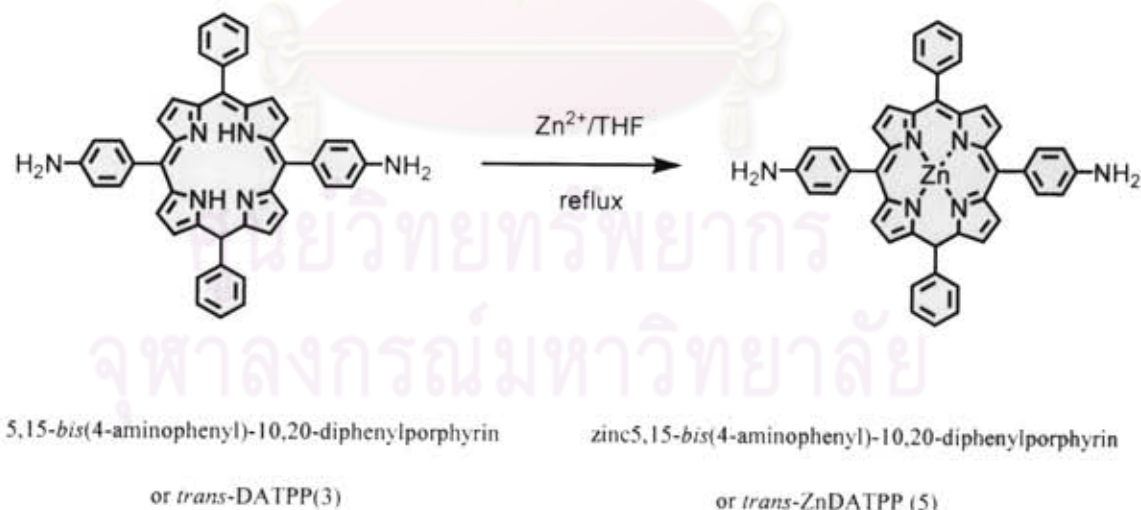
**Figure 4.10** UV-vis absorption data of TPP, *cis*- and *trans*-DATPP

4.1.4 Synthesis of zinc 5,10-*bis*(4-aminophenyl)-10,20-diphenylporphyrin (4) and zinc 5,15-*bis*(4-aminophenyl)-10,20-diphenylporphyrin (5)

The incorporation of zinc into the structure of *cis*-DATPP and *trans*-DATPP was performed by first reacting *cis*- and *trans*-DATPP with zinc acetylacetonate dihydrate, then inserting the zinc ion into the core of *cis*- and *trans*-DATPP as indicated by a change in the color of the solution from deep to bright purple yielding 80% of (4) and 85% yield of (5). (Scheme 4.3) [35].



Scheme 4.3 Synthesis of zinc 5,10-*bis*(4-aminophenyl)-10,20-diphenylporphyrin (4)



Scheme 4.4 Synthesis of zinc 5,15-*bis*(4-aminophenyl)-10,20-diphenylporphyrin (5)

The formation of zinc 5,10-*bis*(4-aminophenyl)-10,20-diphenylporphyrin (4), or *cis*-ZnDATPP, and zinc 5,15-*bis*(4-aminophenyl)-10,20-diphenylporphyrin (5), or *trans*-ZnDATPP, was confirmed by infrared spectroscopy. The disappearance of the

absorption band at 3325 cm^{-1} , due to the internal NH stretching for *cis*- and *trans*-DATPP, was observed in Figure 4.11 and 4.13. In addition, the $^1\text{H-NMR}$ spectrum of *cis*- and *trans*-DATPP are shown in Figures 4.12 and 4.14, respectively. The spectrum showed the characteristic internal NH at δ -2.81 ppm, while the signal disappeared in the $^1\text{H-NMR}$ spectrum of *cis*- and *trans*-ZnDATPP. This observation clearly indicates that zinc had bound with *cis*- and *trans*-DATPP. Other signals at various chemical shifts were assigned for the corresponding protons of *cis*- and *trans*-ZnDATPP, as shown in Table 4.5 and 4.6.

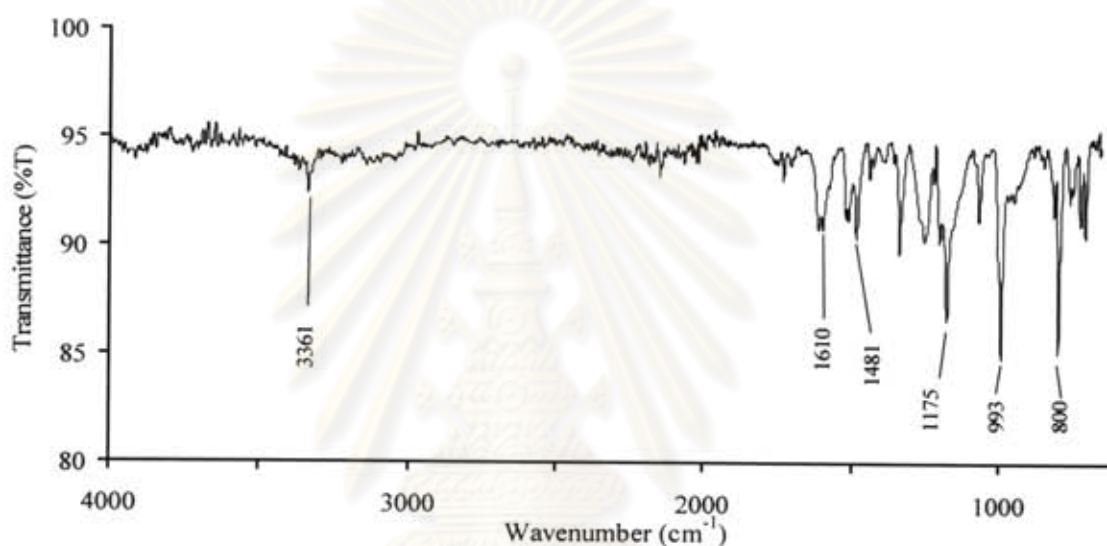


Figure 4.11 IR spectrum of *cis*-ZnDATPP

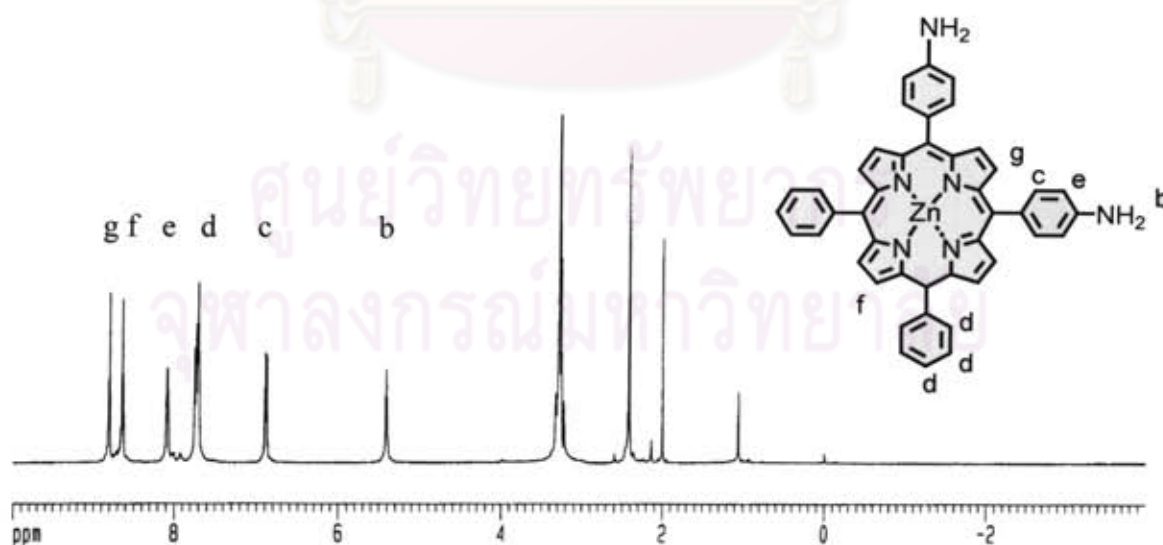


Figure 4.12 $^1\text{H-NMR}$ (400 Hz, DMSO-d_6) spectrum of zinc 5,10-*bis*(4-amino phenyl)-10,20-diphenylporphyrin (*cis*-ZnDATPP)

Table 4.5 $^1\text{H-NMR}$ data of zinc 5,10-*bis*(4-aminophenyl)-10,20-diphenylporphyrin (*cis*-ZnDATPP)

δ (ppm)	number of proton (s), type of proton (position)
8.86	s, 4H, β -H (g)
8.69	s, 4H, β -H (f)
8.13	d, 4H, aminophenyl (e)
7.85-7.68	m, 10H, phenyl (d)
6.93	d, 4H, aminophenyl (c)
5.53	s, 4H, NH_2 (b)

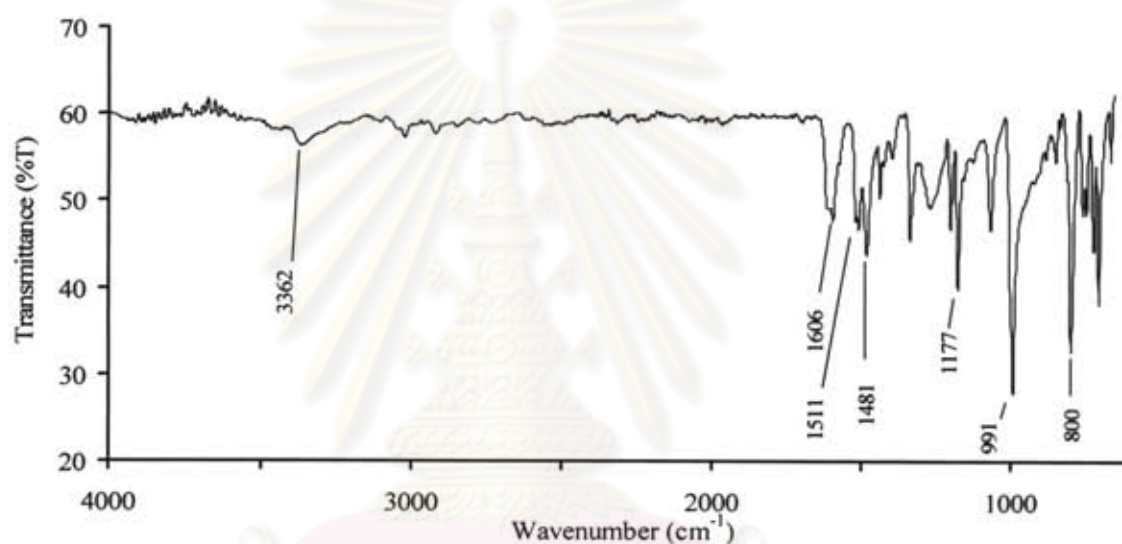


Figure 4.13 IR spectrum of *trans*-ZnDATPP

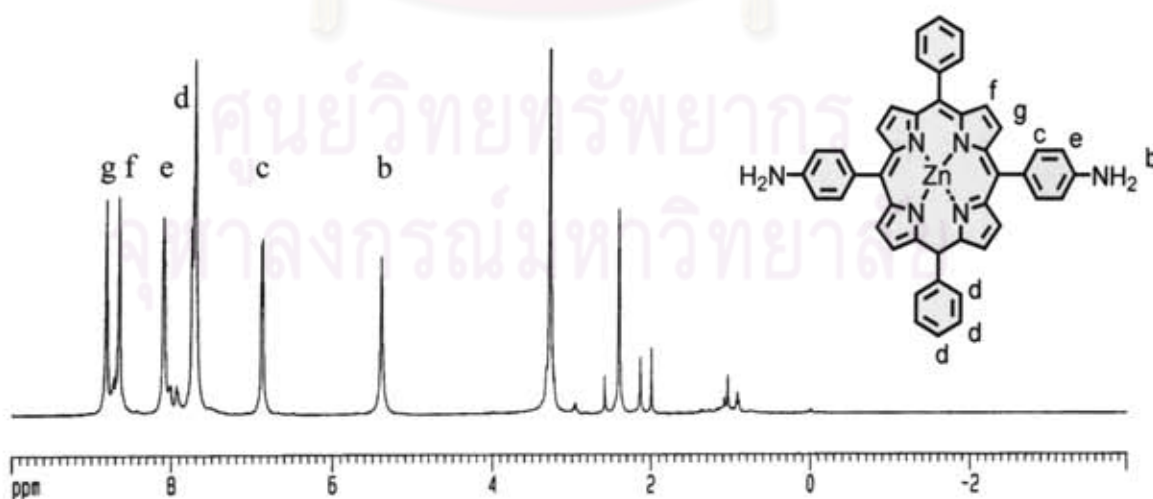


Figure 4.14 $^1\text{H-NMR}$ (400 Hz, DMSO-d_6) spectrum of zinc 5,15-*bis*(4-aminophenyl)-10,20-diphenylporphyrin (*trans*-ZnDATPP)

Table 4.6 $^1\text{H-NMR}$ data of zinc 5,15-bis(4-aminophenyl)-10,20-diphenylporphyrin (*trans*-ZnDATPP)

δ (ppm)	number of proton (s), type of proton (position)
8.87	d, 4H, β -H (g)
8.70	d, 4H, β -H (f)
8.17	d, 4H, aminophenyl (d)
7.79-7.68	m, 10H, phenyl (e)
6.93	d, 4H, aminophenyl (c)
5.52	s, 4H, NH_2 (b)

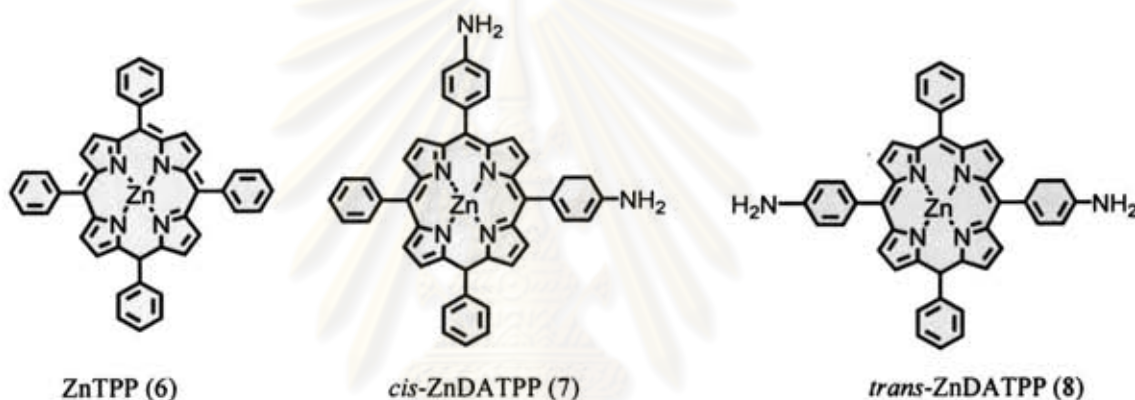


Figure 4.15 Chemical structure of ZnTPP, *cis*-ZnDATPP and *trans*-ZnDATPP

UV-vis absorption spectra of *cis*-ZnDATPP (7) and *trans*-ZnDATPP (8) compared to zinc tetraphenylporphyrin (ZnTPP) (6) in CH_2Cl_2 and DMAc, are shown in Appendix A. There were 3 absorption bands for each compound as detailed in Figure 4.16. The absorption spectrum of *cis*-ZnDATPP and *trans*-ZnDATPP showed a typical pattern for porphyrin with metallation, which was similar to that of ZnTPP. In CH_2Cl_2 , the Soret bands for *cis*- and *trans*-ZnDATPP were observed at 423 nm, while ZnTPP absorbs at 418 nm. The cause of this small red-shift is dependent upon both the nature of the end group and the solvent. Upon metallation of *cis*- and *trans*-ZnDATPP, the four Q-bands collapse to two bands. This simplification of the spectrum is known to be a direct result of the increase in symmetry as the system approaches square planar symmetry.

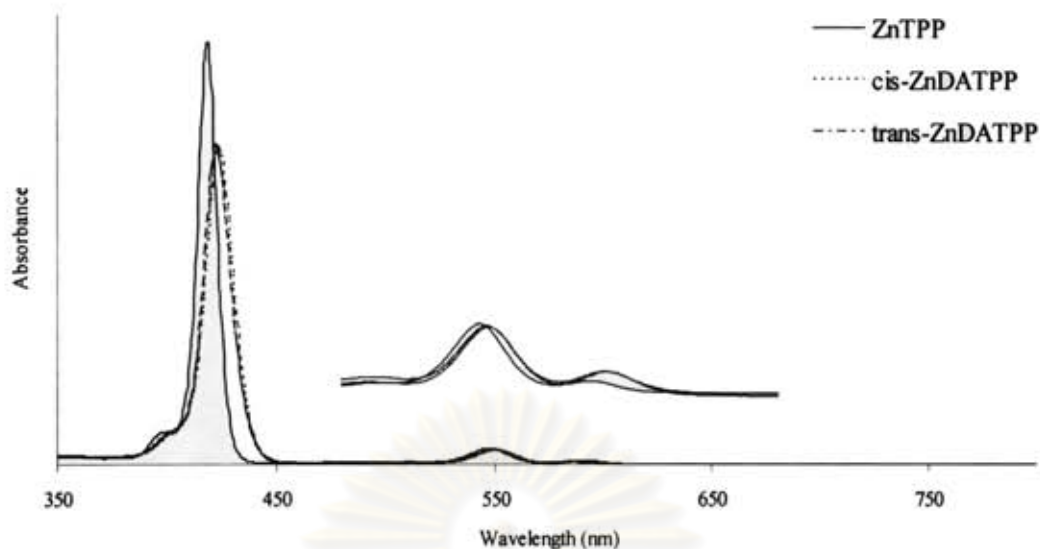


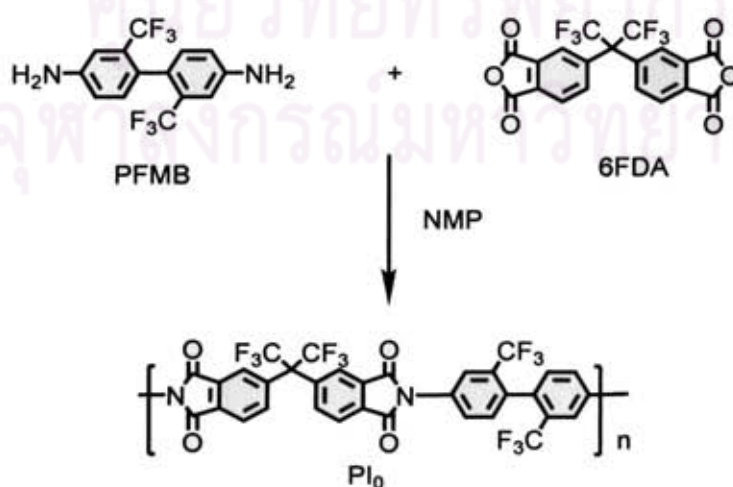
Figure 4.16 UV-vis absorption characteristics of ZnTPP, *cis*-ZnDATPP and *trans*-ZnDATPP.

4.2 Polymer Syntheses

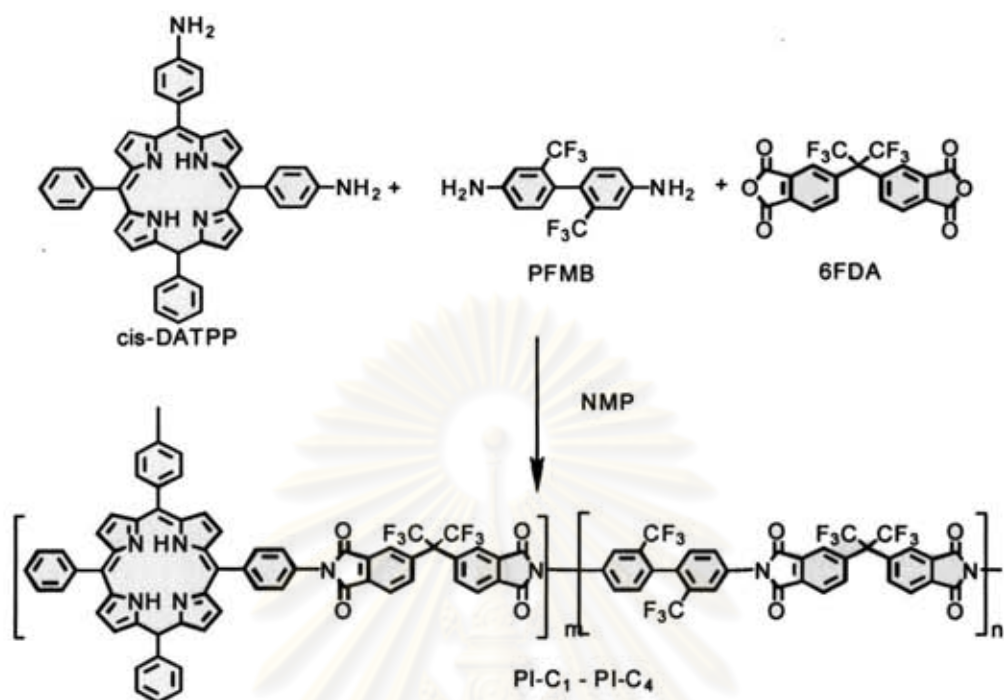
4.2.1 Synthesis of polyimide

Four series of polyimides were prepared from dianhydride and diamine compounds at various mole percents. The first series of polyimides (PI-C1- PI-C4) was synthesized by the condensation reaction between 6FDA, the dianhydride, and two diamines, PFMB and *cis*-, *trans*-DATPP, *cis*-ZnDATPP or *trans*-ZnDATPP, as shown in Scheme 4.6-4.8.

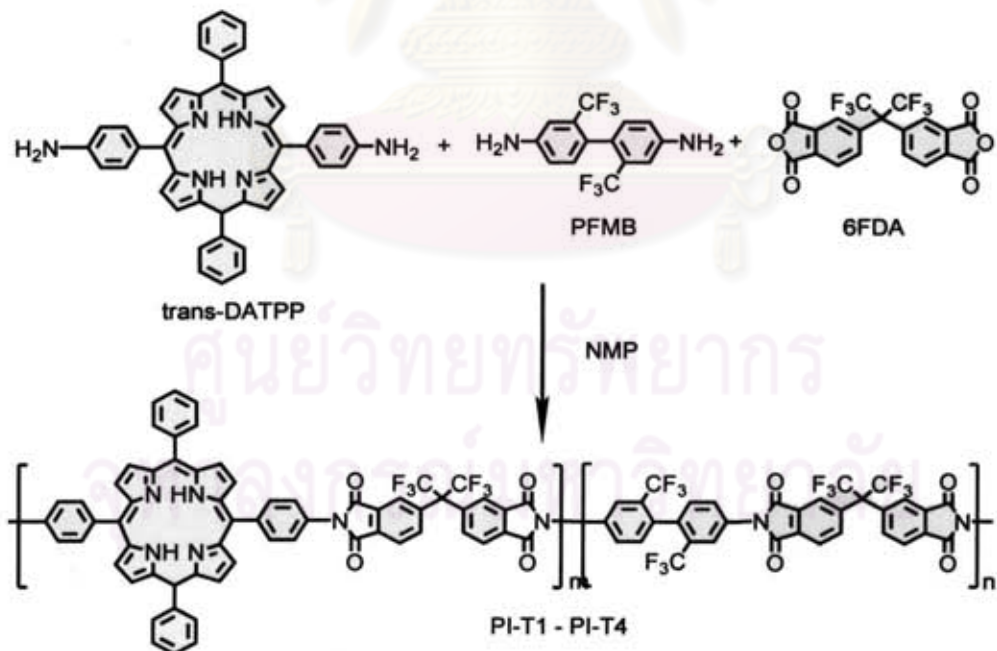
The polyimide without porphyrin moiety (PI0) was also prepared from 6FDA and PFMB as shown in Scheme 4.5.



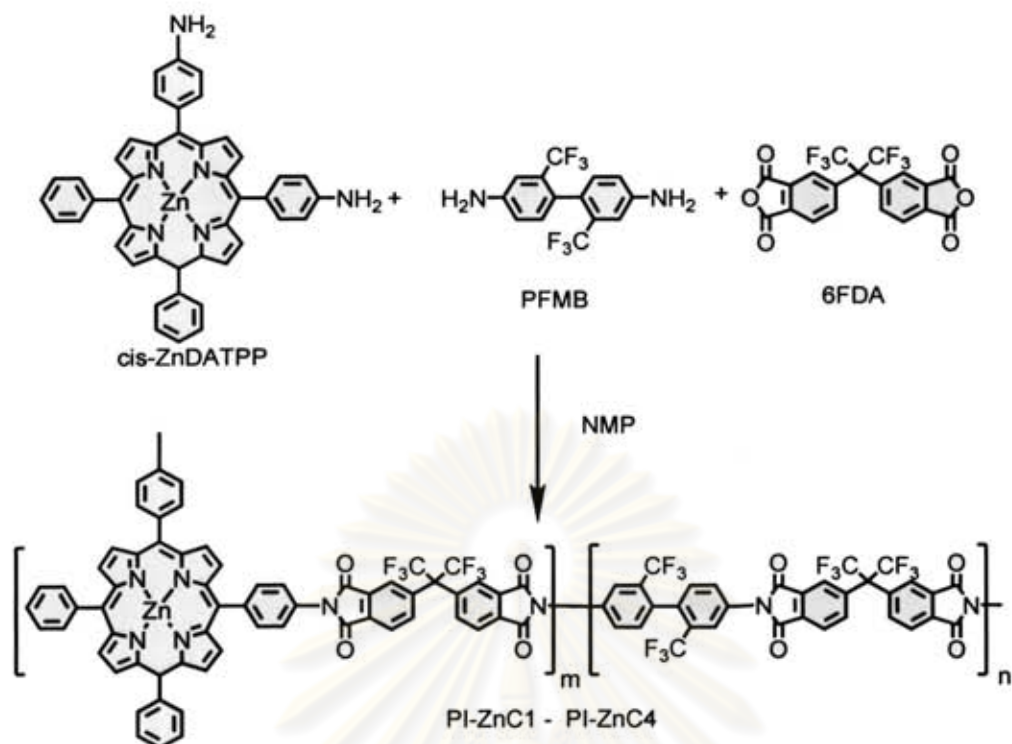
Scheme 4.5 Syntheses of polyimide without porphyrin



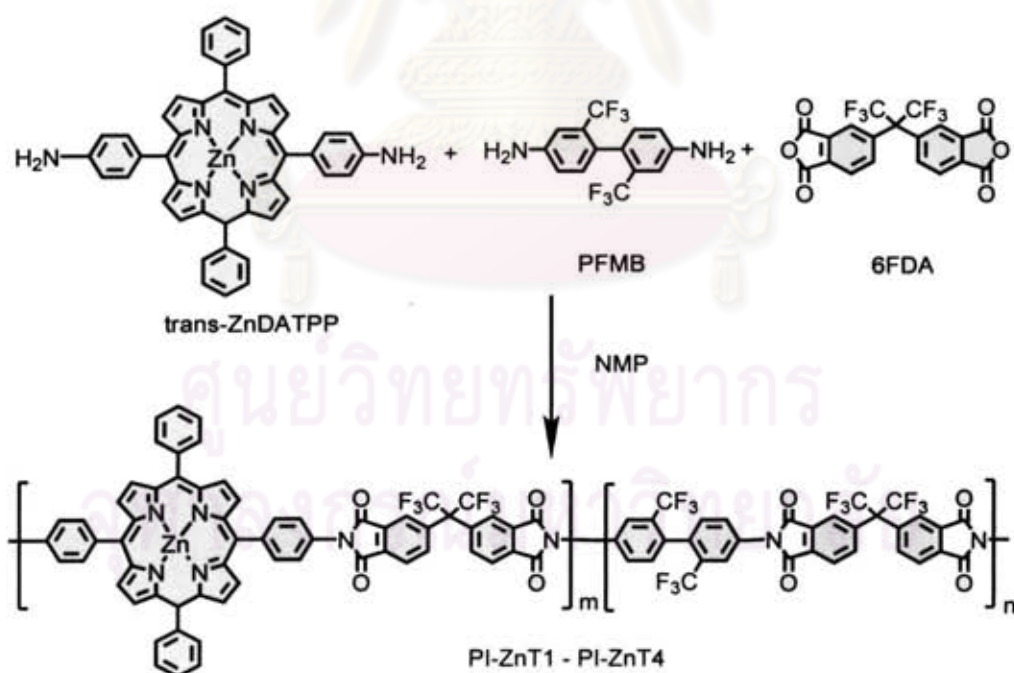
Scheme 4.6 Syntheses of polyimides in series I



Scheme 4.7 Syntheses of polyimide in series II



Scheme 4.8 Syntheses of polyimide in series III



Scheme 4.9 Syntheses of polyimides in series IV

The mole percent of monomers in the feed used for preparing all polyimides and percent yield of these polyimides were shown in Table 4.7.

Table 4.7 Four series of polyimides

PI	Mole in feed (%)				Yield (%)
	6FDA	PFMB	DATPP	ZnDATPP	
Series I					
<i>cis</i> -DATPP					
PI-C1	100	95	5	-	94.88
PI-C2	100	90	10	-	93.53
PI-C3	100	85	15	-	92.22
PI-C4	100	70	30	-	91.17
Series II					
<i>trans</i> -DATPP					
PI-T1	100	5	-	-	92.75
PI-T2	100	90	10	-	92.70
PI-T3	100	85	15	-	91.74
PI-T4	100	70	30	-	89.63
Series III					
<i>cis</i> -ZnDATPP					
PI-ZnC1	100	95	-	5	94.59
PI-ZnC2	100	90	-	10	91.59
PI-ZnC3	100	85	-	15	91.48
PI-ZnC4	100	70	-	30	93.15
Series IV					
<i>trans</i> -ZnDATPP					
PI-ZnT1	100	95	-	5	93.72
PI-ZnT2	100	90	-	10	91.78
PI-ZnT3	100	85	-	15	90.40
PI-ZnT4	100	70	-	30	92.15

จุฬาลงกรณ์มหาวิทยาลัย

4.2.2 Identification of polyimides

4.2.2.1 Infrared spectroscopy

The IR spectra of all polyimides are shown in Appendix C. Figure 4.17 exhibits the representative IR spectra of the polyimides (PI-C4, PI-T4, PI-ZnC4, PI-ZnT4). It clearly reveals that there are no characteristic absorption bands of amines indicating that no amine monomers are left in the resulting products. In addition, no absorption bands of amide as well as carboxylic acid of poly(amic acid) intermediate appeared in the spectra, indicating that the poly(amic acid) had been converted completely to the corresponding polyimides during refluxing. This was proved by the appearance of the absorption bands at 1784 (asymmetric stretching C=O), 1728 (symmetric stretching C=O), 1365 (stretching C-N) and 721 cm^{-1} (bending C=O) which were the characteristic absorption bands of polyimide. Polyimides in series I and II, containing *cis*- and *trans*-DATPP or free-base porphyrin, had the internal NH in the structure. However, the characteristic internal NH absorption band was not observed in these spectra. This may be attributed to the rigid structure of the polymer chain which made it difficult for NH vibration [35].

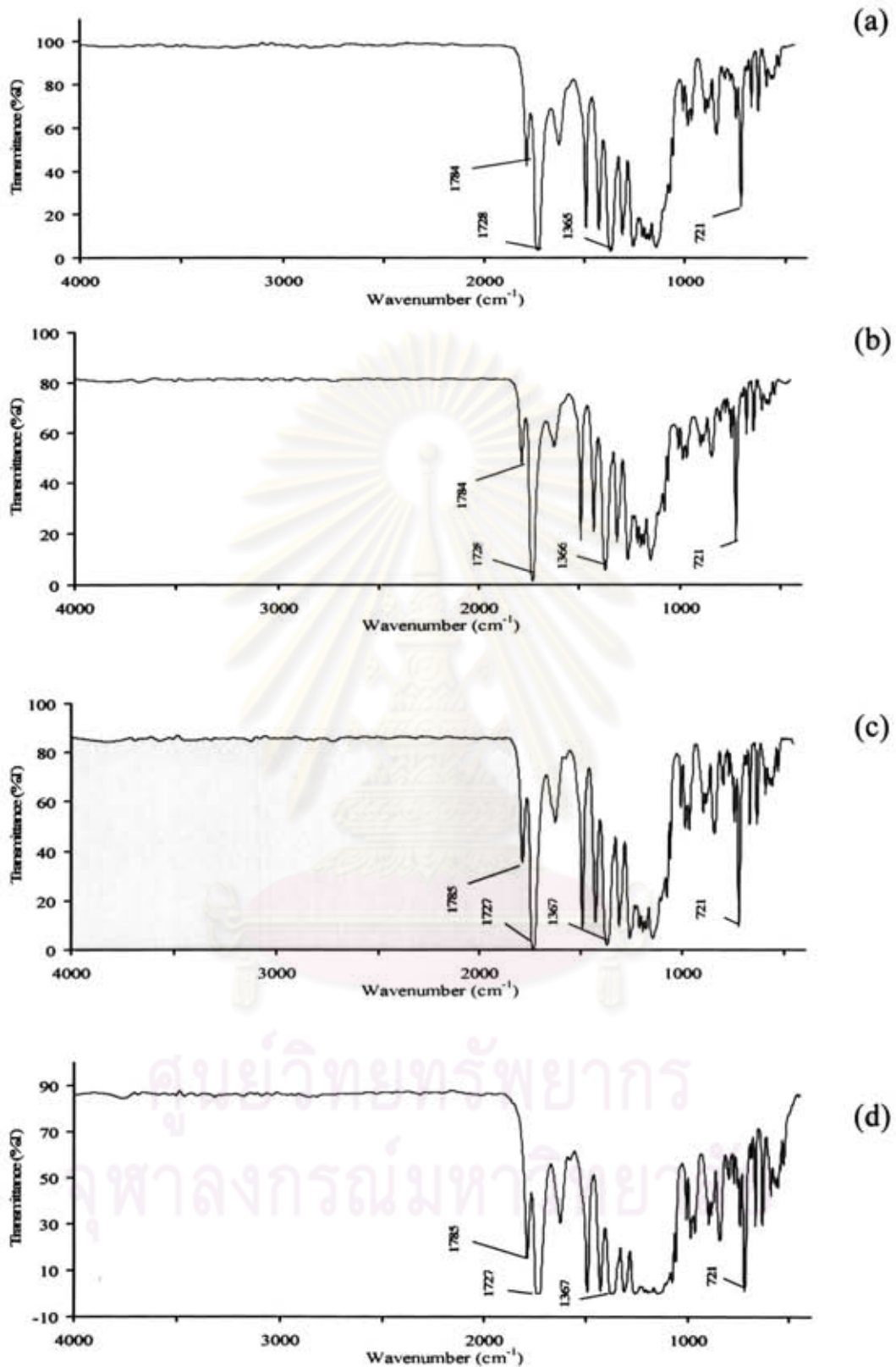


Figure 4.17 IR spectra of polyimide; (a) PI-C4, (b) PI-T4,(c) PI-ZnC4 and (d)PI-ZnT4

4.2.2.2 $^1\text{H-NMR}$ spectroscopy

$^1\text{H-NMR}$ spectroscopic technique was employed to differentiate the polyimides containing *cis*-, *trans*-DATPP and *cis*-, *trans*-ZnDATPP. $^1\text{H-NMR}$ spectra of polyimides PI-C4, PI-T4, PI-ZnC4 and PI-ZnT4 were shown in Figure 4.18. All spectra of polyimides showed the signal at δ 8.90 ppm, due to protons located at the β positions on pyrrole rings of the porphyrin moiety. It was also observed that only polyimides PI-C4 and PI-T4, which contained *cis*- and *trans*-DATPP or free-base porphyrin, showed the signal of internal NH at δ -2.80 ppm. In case of polyimides containing both *cis*- and *trans*-ZnDATPP (PI-ZnC4 and PI-ZnT4), no appearance of this characteristic internal NH signal was observed and the rest of the signals were similar to polyimides PI-C4 and PI-T4. Therefore, these $^1\text{H-NMR}$ results confirmed the incorporation of porphyrin into the polymer structure.



ศูนย์วิทยทรัพยากร
จุฬาลงกรณ์มหาวิทยาลัย

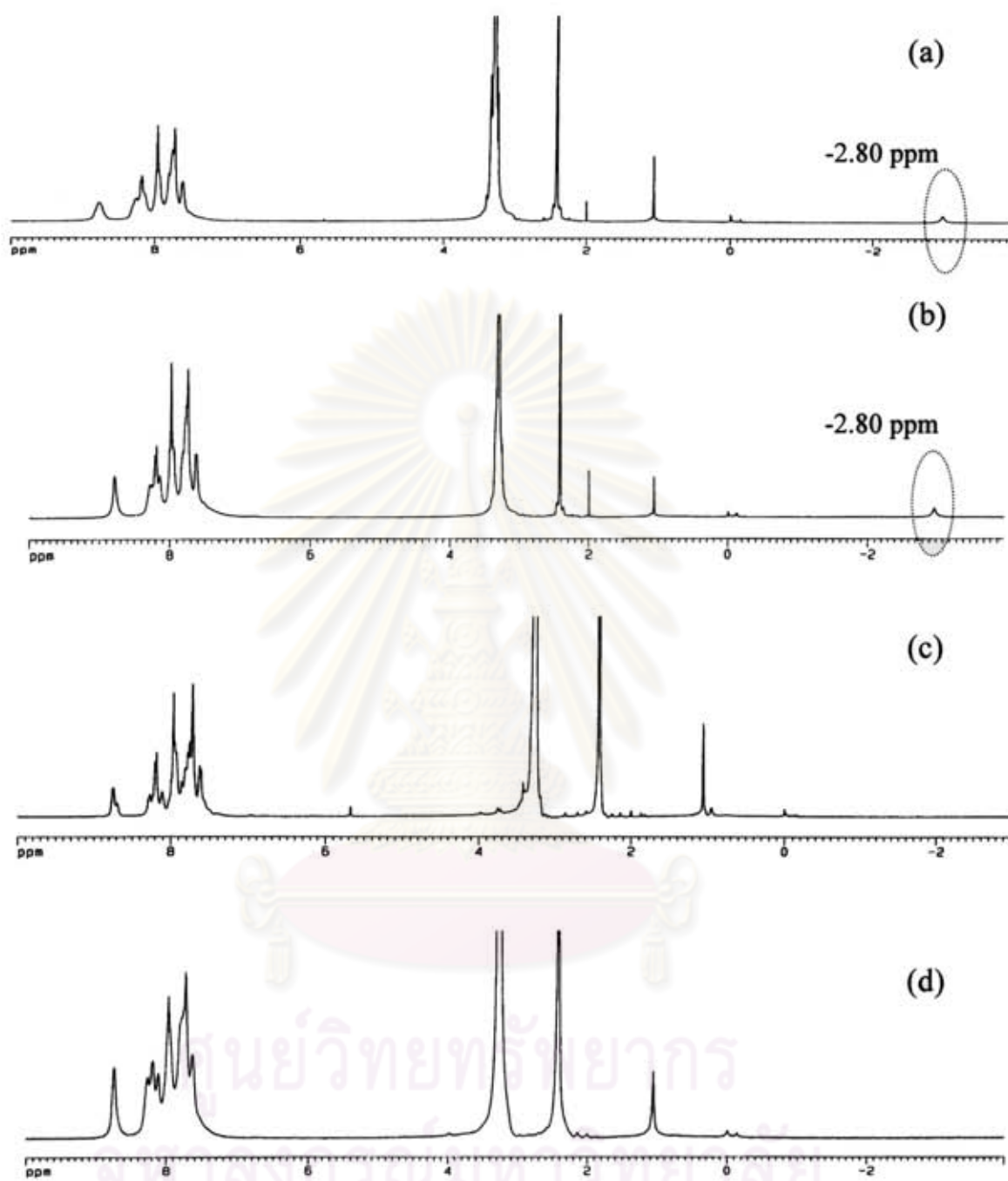


Figure 4.18 $^1\text{H-NMR}$ (400 MHz, DMSO-d_6) of polyimides; (a) PI-C4, (b) PI-T4, (c) PI-ZnC4 and (d) PI-ZnT4.

4.3 Determination of porphyrin content in polyimides

Cis-DATPP, *trans*-DATPP and *cis*-, *trans*-ZnDATPP content in the polymer structure can be determined by UV-visible spectroscopy (Appendix D). Table 4.8 showed the calculated results of porphyrin content in polyimides as the weight percent. The determination was performed by measuring the optical density of the polyimides in CH₂Cl₂ at the Soret band, $\lambda_{\max} = 417$ nm for series I and II and $\lambda_{\max} = 419$ nm for series III and IV. These were the characteristic absorption band of porphyrin moieties which were not interfered by the absorption of other parts of the polyimides.

The results demonstrated that *cis*-, *trans*-DATPP and *cis*-, *trans*-ZnDATPP were incorporated into the polymer backbones as expected. In the calculation, it was assumed that all the other monomers were completely incorporated into polymer structure. However, it was postulated that some monomers must be lost during the experiment. Therefore, porphyrin content in polyimides should be slightly higher than the calculated amounts.



ศูนย์วิทยทรัพยากร
จุฬาลงกรณ์มหาวิทยาลัย

Table 4.8 Porphyrin content in polyimides

PI	Weight of porphyrin (%)	
	in feed	in polymer
Series I <i>cis</i> -DATPP		
PI-C1	5	3.43
PI-C2	10	6.65
PI-C3	15	12.16
PI-C4	30	25.79
Series II <i>trans</i> -DATPP		
PI-T1	5	3.61
PI-T2	10	7.03
PI-T3	15	12.44
PI-T4	30	24.69
Series III <i>cis</i> -ZnDATPP		
PI-ZnC1	5	3.61
PI-ZnC2	10	8.51
PI-ZnC3	15	13.62
PI-ZnC4	30	25.94
Series IV <i>trans</i> -ZnDATPP		
PI-ZnT1	5	3.51
PI-ZnT2	10	8.66
PI-ZnT3	15	13.31
PI-ZnT4	30	25.94

ศูนย์วิจัยทอพอยีกร
จุฬาลงกรณ์มหาวิทยาลัย

4.4 Polymer Properties

4.4.1 Polymer solubility

To determine the solubility of these porphyrin-containing polyimides, they were dissolved in seven organic solvents. The solubility behavior of the polyimides is summarized in Table 4.9. All four series of polyimides were apparently soluble in the polar aprotic solvents DMAc, DMF, DMSO, NMP, THF, acetone and CH_2Cl_2 . However, the polyimides seemed not readily soluble in CH_2Cl_2 , and took longer time for dissolving than in the THF or acetone. The excellent solubility of these polyimides compared to normal aromatic polyimides due to the presence of hexafluoro isopropylidene group in 6FDA in their polymer structures. This flexible group interrupts chain packing. The decrease in chain packing leads to an increase in free volume, which allows solvent molecules to penetrate the polymer chain. Furthermore, the increase in solubility can also be attributed to the twisted biphenyl structure of the PFMB unit. As previously stated, this type of structure hinders chain packing because of the non-coplanarity of the two phenyl rings. The decrease in chain packing leads to an increase in free volume. A similar phenomenon has already been reported by other research groups [10, 11, 35, 42, 43 and 44].

Table 4.9 Solubility of polyimides in organic solvents

PI	Solubility of polyimides						
	NMP	DMAc	DMSO	DMF	THF	Acetone	CH ₂ Cl ₂
Series I							
<i>cis</i> -DATPP							
PI-C1	++	++	++	++	++	++	+
PI-C2	++	++	++	++	++	++	+
PI-C3	++	++	++	++	++	++	+
PI-C4	++	++	++	++	++	++	+
Series II							
<i>trans</i> -DATPP							
PI-T1	++	++	++	++	++	++	+
PI-T2	++	++	++	++	++	++	+
PI-T3	++	++	++	++	++	++	+
PI-T4	++	++	++	++	++	++	+
Series III							
<i>cis</i> -ZnDATPP							
PI-ZnC1	+++	+++	+++	+++	++	++	+
PI-ZnC2	+++	+++	+++	+++	++	++	+
PI-ZnC3	+++	+++	+++	+++	++	++	+
PI-ZnC4	+++	+++	+++	+++	++	++	+
Series IV							
<i>trans</i> -ZnDATPP							
PI-ZnT1	+++	+++	+++	+++	++	++	+
PI-ZnT2	+++	+++	+++	+++	++	++	+
PI-ZnT3	+++	+++	+++	+++	++	++	+
PI-ZnT4	+++	+++	+++	+++	++	++	+

Solubility was performed at the concentration 5% (W/V) at room temperature

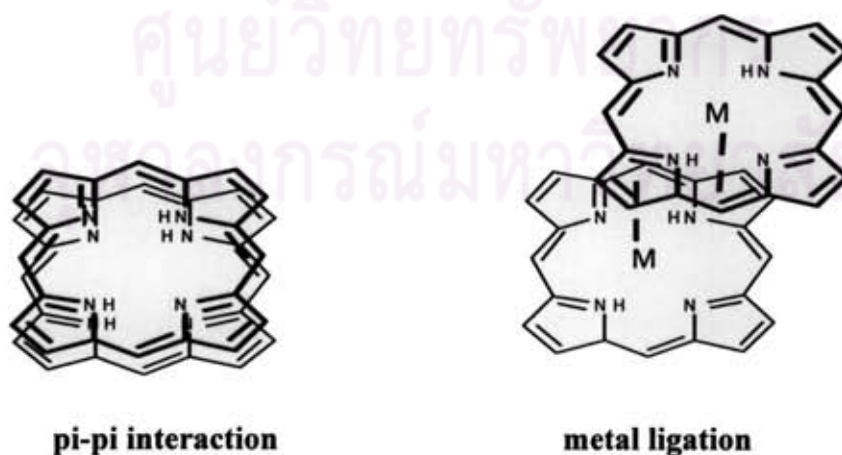
+++ : completely soluble in 1 hour

++ : completely soluble in 6 hours

+ : completely soluble overnight

4.4.2 Viscosity of polyimides

The soluble polyimides-containing porphyrins were successfully prepared and the intrinsic viscosity $[\eta]$ of these polyimides measured in DMAc at 35 ± 0.1 °C Table 4.10 and appendix I. All polyimides in Series I-IV had higher viscosity than the polyimide without porphyrin (PI0). These results indicated that the incorporated porphyrin play a role for the significant increase in viscosity. It is possible that much higher molecular weight of polymers were obtained when porphyrins were incorporated into polyimide chains. It has been reported that strong attractive interactions between porphyrins can lead to aggregation in solution [48]. Intrachain aggregation within the polyimide *via* pi-pi interactions of porphyrins on the same chain is expected to result in a decrease in viscosity with increasing porphyrin moiety (greater coiling), while interchain aggregation is expected to result in an increase in viscosity through increased chain entanglement (Scheme 4.10). A decrease in viscosity with increasing porphyrin content in all polyimides series I-IV indicating probably intrachain interaction. It is noted that solution viscosities are dependent in part on the size of polymer molecules that expanded in solvent. In addition, both intra- and inter- interactions of polyimide chains would attribute to the higher viscosity compared to the polyimide without porphyrin content. The polyimides in series III and IV had lower viscosity than polyimides in series I and II at the same level of porphyrin content. A possible for explanation the low viscosity in series III and IV could be due to the ligation of the zinc porphyrin with either the polymer or the solvent (Scheme 4.10) [35].



Scheme 4.10 pi-pi interaction and metal ligation in porphyrin

4.4.3 Molecular weight determination

Molecular weight polyimides were synthesized using dianhydride and diamine compounds at various mole percents. The number average molecular weight (M_n) and weight average molecular weight (M_w) by GPC technique are shown in Table 4.10 and in appendix J. The small amount of porphyrin in the polymer chain (PI-C1 and PI-T1) had number average molecular weight (M_n) 79920 and 77226 g/mol and weight average molecular weight (M_w) 124151 and 105549 g/mol. When the presence of a greater number of porphyrin molecules in the polymer (PI-C4 and PI-T4) had low number average molecular weight (M_n) 34853 and 28760 g/mol and weight average molecular weight (M_w) 49294 and 48093 g/mol were resulted. Similar to the series III and IV in case of metalloporphyrins, the small amount of porphyrin in the polymer chain (PI-ZnC1 and PI-ZnT1) had number average molecular weight (M_n) 96074 and 99069 g/mol and weight average molecular weight (M_w) 152367 and 176702 g/mol. For polyimides-containing 30% of porphyrin (PI-ZnC4 and PI-ZnT4), lower number average molecular weight (M_n) 28496 and 22198 g/mol and weight average molecular weight (M_w) 42532 and 48300 g/mol were resulted.

These results were consistent with their corresponding viscosities. It thus agreed with the previously mentioned assumption that the more amount of porphyrin in the molecule more intra- and inter- pi-pi interactions and the additional metal ligation, in case of the presence of Zn, would result which caused the aggregation of the polymers. Accordingly the sizes of the agglomerates were smaller.

4.4.4 Thermal properties of polyimides

4.4.4.1 Decomposition temperature

According to the literature, these porphyrin-containing polyimides showed good thermal and thermooxidative stabilities [10, 11]. The decomposition temperatures of the polyimides were determined by TGA (appendix H) in air and were taken as the temperature at which 5% weight loss occurred (Table 4.10). The polyimides in series I and II, which contained *cis*- and *trans*-DATPP, appear slightly more stable than polyimides in series III and IV, which contained *cis*- and *trans*-ZnDATPP, at the same level of porphyrin content. From the TGA data, it was found that the existence of *cis*- and *trans*-DATPP and *cis*- and *trans*-ZnDATPP in the

polymer did not significantly affect the thermal stabilities of these polyimides as compared to the polyimides in the absence of porphyrin.

Table 4.10 The physical property data of polyimides

PI	Viscosity [η] ^a (dL/g)	Molecular weight			Decomposition temperature ^b (°C)
		\overline{M}_n	\overline{M}_w	PDI	
PI0	0.64	23313	37986	1.882	530
Series I <i>cis</i> -DATPP					
PI-C1	1.25	79920	124151	1.553	532
PI-C2	1.12	48782	99710	2.044	538
PI-C3	0.94	38894	55103	1.417	522
PI-C4	0.67	34853	49294	1.444	527
Series II <i>trans</i> -DATPP					
PI-T1	1.23	77226	105549	1.664	534
PI-T2	1.00	51914	74916	1.443	528
PI-T3	0.91	34335	67960	1.407	530
PI-T4	0.71	28760	48093	2.360	531
Series III <i>cis</i> -ZnDATPP					
PI-ZnC1	1.10	96074	152367	1.586	521
PI-ZnC2	0.89	63382	101080	1.594	518
PI-ZnC3	0.77	43696	66426	1.520	513
PI-ZnC4	0.67	28496	42532	1.493	520
Series IV <i>trans</i> -ZnDATPP					
PI-ZnT1	1.19	99069	176702	1.784	510
PI-ZnT2	0.96	62262	103219	1.657	519
PI-ZnT3	0.83	48180	67258	1.708	516
PI-ZnT4	0.77	22198	48300	2.170	522

^a Viscosity determined in DMAc at 35±0.1 °C

^b Temperature at 5% weight loss occurred when polymers were subjected to TGA with a heating rate of 10 °C/min.

4.4.5 Spectroscopic properties of polyimides

The good solubility of these polymers enables us to investigate the photophysical processes of these polymers (*i.e.* absorption, fluorescence quenching, fluorescence lifetime and photoinduced electron transfer processes).

4.4.5.1 Absorption properties of polyimides

The heterocyclic nucleus is fully conjugated with a characteristic absorption spectrum. The absorption spectra of these aromatic tetrapyrrolic macrocycles display an intense band in the region of 400 nm. This absorption is called the Soret band and has a strong absorption with a high molar extinction coefficient. Porphyrins also display four accompanying bands, commonly referred to as the Q-bands, of lower intensity between 450-650 nm. Upon the metallation of the porphyrin, the four Q-bands collapse to two peaks as seen in the Zn complex.

Absorption spectra of both *cis*- and *trans*-DATPP compared to tetraphenylporphyrin (TPP) in CH₂Cl₂ and DMAc are shown in appendix A, Table 4.11. In both CH₂Cl₂ and DMAc, the absorption spectra of the Soret and Q bands for TPP are essentially the same in their absorption maxima and band profiles. On the other hand, the absorption spectra of both *cis*- and *trans*-DATPP compared to TPP were slightly lower in wavelength due to the presence of electron donating amino groups covalently substituted on the benzene rings.

In CH₂Cl₂, the Soret and Q bands due to π - π^* electronic transitions of *cis*- and *trans*-DATPP were observed at slightly lower wavelengths when compared to DMAc. Both absorption bands may undergo a blue shift in less polar media (e.g. CH₂Cl₂). This description can be used to describe the absorption spectra of ZnTPP, *cis*- and *trans*-ZnDATPP.

Absorption spectra obtained from polyimides containing *cis*- and *trans*-DATPP (series I and II) and metallic porphyrin, *cis*- and *trans*-ZnDATPP (series III and IV) are similar to tetraphenylporphyrin (TPP) and zinc tetraphenylporphyrin (ZnTPP) in both CH₂Cl₂ and DMAc. However, they are slightly different from the corresponding porphyrin monomers (*cis*-DATPP, *trans*-DATPP, *cis*-ZnDATPP and *trans*-ZnDATPP). In CH₂Cl₂, the absorption spectra obtained from polyimides in series I, II, III and IV showed Soret transitions that were substantially blue-shifted from *cis*-DATPP, *trans*-DATPP, *cis*-ZnDATPP and *trans*-ZnDATPP monomers, respectively. The shift of the absorption bands to higher energy was also observed in

the Q-band region. The source of this blue-shift is surely related to the nature of the structure of porphyrin incorporated into the polymer chain. Thus, *cis*-DATPP, *trans*-DATPP, *cis*-ZnDATPP and *trans*-ZnDATPP, after incorporation into polyimides, exhibited the absorption that is similar to TPP and ZnTPP, respectively.

The Soret bands for polyimides in series I and II are observed at 418 nm in CH₂Cl₂ and 419 nm in DMAc, while TPP absorbs at 417 nm in both CH₂Cl₂ and DMAc. In the case of polyimides in series III and IV, the Soret bands are observed at 420 nm in CH₂Cl₂ and 428 nm in DMAc, while ZnTPP is observed at 419 nm in CH₂Cl₂ and 426 nm in DMAc.

In the case of the polymer, there is no such effect of solvent polarity on the Soret and Q band maxima in CH₂Cl₂ and DMAc. This suggests that TPP and ZnTPP moieties in the polymer are confined in the microdomains of polyimide stacks and protected from solvent.



ศูนย์วิจัยทรัพยากร
จุฬาลงกรณ์มหาวิทยาลัย

Table 4.11 UV-vis absorption maxima of polyimides in CH₂Cl₂ and DMAc.

UV-vis absorption maxima of porphyrin monomers and polyimides										
Compound	CH ₂ Cl ₂					DMAc				
	Soret band (nm)	Q-band (nm)				Soret band (nm)	Q-band (nm)			
TPP	417	514	549	590	644	417	514	546	589	646
<i>cis</i> -DATPP	422	519	555	593	650	424	520	566	599	657
<i>trans</i> -DATPP	422	519	555	593	650	424	520	566	598	658
ZnTPP	419		548	587		426		560	600	
<i>cis</i> -ZnDATPP	424		551	592		434		564	609	
<i>trans</i> -ZnDATPP	424		551	591		434		564	610	
Series I										
<i>cis</i> -DATPP										
PI-C1	418	514	550	590	646	419	515	548	590	645
PI-C2	418	514	550	590	645	419	515	550	591	646
PI-C3	418	514	550	590	645	419	515	550	590	646
PI-C4	418	514	550	590	646	419	514	550	591	646
Series II										
<i>trans</i> -DATPP										
PI-T1	418	515	550	590	646	419	515	550	591	646
PI-T2	418	515	550	590	645	419	515	550	591	646
PI-T3	418	515	550	590	646	419	515	550	591	646
PI-T4	418	515	550	590	646	419	515	550	591	646
Series III										
<i>cis</i> -ZnDATPP										
PI-ZnC1	420		549	588		428		560	600	
PI-ZnC2	420		549	588		429		560	600	
PI-ZnC3	421		549	588		429		560	600	
PI-ZnC4	421		549	588		429		560	600	
Series IV										
<i>trans</i> -ZnDATPP										
PI-ZnT1	421		549	590		428		560	600	
PI-ZnT2	420		549	590		428		560	600	
PI-ZnT3	421		549	589		429		560	600	
PI-ZnT4	421		549	588		429		560	600	

4.4.5.2 Fluorescence properties of polyimides

The steady-state fluorescence measurements of polyimides containing *cis*-, *trans*-DATPP and metallic porphyrin, *cis*- and *trans*-ZnDATPP, are given in Table 4.12, in both CH₂Cl₂ and DMAc. The fluorescence spectra of polyimides (series I and II), which have emission bands at 653 and 718 nm in both solvents, are shown in appendix B. These emission spectra are essentially the same as TPP in both solvents, which have emission bands at 654 and 718 nm in CH₂Cl₂, 654 and 718 nm in DMAc. For the fluorescence spectrum of *cis*- and *trans*-DATPP, the wavelengths of maximum emission are the same (663 and 724 nm in CH₂Cl₂ and 680 and 750 nm in DMAc).

The fluorescence spectra of the polyimides containing *cis*- and *trans*-ZnDATPP (series III and IV) are given in appendix B. In CH₂Cl₂, the fluorescence spectra of polyimides (series III and IV), which have emission bands at 599-600 nm and 647 nm, while in DMAc, emission bands are at 609-610 nm and 661 nm. These spectrums are essentially the same in ZnTPP in the same solvents, which have emission bands at 600 and 647 nm in CH₂Cl₂, 609 and 660 nm in DMAc. These spectral shifts are unlike those observed for polyimides in series I and II, which showed very little change in fluorescence maxima.

Red-shifts in the fluorescence maxima of ZnTPP from CH₂Cl₂ (599 and 647 nm) to DMAc (609 and 660 nm) were observed. Likewise, the fluorescence maxima of *cis*- and *trans*-ZnDATPP were observed from CH₂Cl₂ (604 and 650 nm) to DMAc (628 and 673 nm). The red shift shows the solvatochromic properties in different aprotic solvent systems.

จุฬาลงกรณ์มหาวิทยาลัย

Table 4.12 Fluorescence maxima of polyimides in CH₂Cl₂ and DMAc

Fluorescence maxima of porphyrin monomers and polyimides				
Compound	CH ₂ Cl ₂		DMAc	
TPP	654	718	654	718
<i>cis</i> -DATPP	663	724	680	750
<i>trans</i> -DATPP	663	725	680	751
ZnTPP	600	647	609	660
<i>cis</i> -ZnDATPP	604	650	628	677
<i>trans</i> -ZnDATPP	604	650	628	677
Series I				
<i>cis</i> -DATPP				
PI-C1	653	718	653	719
PI-C2	653	718	653	718
PI-C3	653	718	653	718
PI-C4	653	718	653	718
Series II				
<i>trans</i> -DATPP				
PI-T1	654	718	653	719
PI-T2	654	718	653	718
PI-T3	653	718	653	719
PI-T4	653	718	653	719
Series III				
<i>cis</i> -ZnDATPP				
PI-ZnC1	599	647	609	661
PI-ZnC2	600	647	609	661
PI-ZnC3	600	647	610	661
PI-ZnC4	599	647	610	661
Series IV				
<i>trans</i> -ZnDATPP				
PI-ZnT1	600	647	609	660
PI-ZnT2	599	647	609	661
PI-ZnT3	599	647	610	661
PI-ZnT4	600	647	610	661

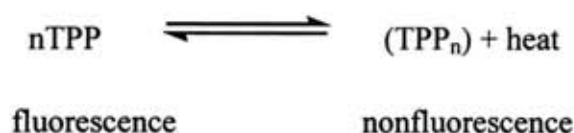
4.4.6 Fluorescence Quantum Yields Determination

The fluorescence quantum yields (Φ_f) of these polyimides in the absence of quencher in solvents of different polarity (CH_2Cl_2 and DMAc) are presented in Table 4.13. Quantum yields were determined by using Eq. 3.1. The fluorescence quantum yield of the TPP monomer is lower than that of *cis*- and *trans*-DATPP in both CH_2Cl_2 and DMAc due to the presence of electron donating diamino groups covalently bonded on the porphyrin molecule. Moreover, the fluorescence quantum yields (Φ_f) of TPP, *cis*- and *trans*-DATPP in DMAc are slightly higher than those in CH_2Cl_2 due to the influence of solvent polarity. The fluorescence quantum yield (Φ_f) is defined in Equation 2.1.

$$\Phi_f = \frac{k_F}{(k_F + k_{IC} + k_{ISC})} = \frac{k_F}{k_F + k_{NR}} \quad \text{Eq.2.1}$$

where k_{NR} is the total nonradiative decay rate constant ($k_{NR} = k_{IC} + k_{ISC}$) and k_F is the first-order radiative decay constant. A gradual increase in solvent polarity results in an increase in Φ_f , due to a decrease in the nonradiative decay rate, most likely k_{ISC} (Jablonski state energy-level diagram).

In case of increasing the amount of porphyrin in polyimides from 5% to 30%, it is possible that higher porphyrin units were incorporated into the polyimide chains. In fact, it has been reported that strong attractive interactions between porphyrins can lead to aggregation in solution [48]. Intrachain aggregation within the polyimide *via* π - π interactions of porphyrins on the same chain is expected to result in a decrease in viscosity with increasing porphyrin content (greater coiling). A decrease in viscosity with increasing porphyrin content in all of series I, II, III and IV was observed, indicating probable intrachain interaction (i.e., coiling). Polymer aggregation could be due to greater porphyrin content within the polyimide (30%). Neighboring porphyrin molecules within the polymer have strong π - π interactions with each other. It may be that self-quenching of an excited-state porphyrin molecule by interaction with another porphyrin molecule in the ground state can occur as described below.



In this case, the fluorescence quantum yields for polyimides in all series (I–IV) decrease when increasing the porphyrin content due to self quenching. The rate of electron transfer (k_{ET}) (Eq.3.5) from excited-state porphyrin units within the polymer to diimide acceptor groups in both CH_2Cl_2 and DMAc are very fast when increasing the porphyrin moiety. For series III and IV in the case of metalloporphyrins, k_{ET} is significantly larger than the corresponding free-base porphyrins (Series I and II). The k_{ET} values of PI-ZnC4 and PI-ZnT4 were calculated as 9.25×10^7 and $8.90 \times 10^7 \text{ s}^{-1}$ compared to that of PI-C4 and PI-T4, calculated as 1.50×10^7 and $1.48 \times 10^7 \text{ s}^{-1}$ in CH_2Cl_2 , respectively. Similarly, in DMAc, the k_{ET} values of PI-ZnC4 and PI-ZnT4 were calculated as 4.54×10^7 and $5.05 \times 10^7 \text{ s}^{-1}$ compared to the values of PI-C4 and PI-T4, calculated to be 4.74×10^6 and $5.77 \times 10^6 \text{ s}^{-1}$. The larger k_{ET} values in the zinc porphyrins could perhaps be due to the easy distribution of electronic charge through the conjugated system from the pi donor to the pi acceptor.

The fluorescence quantum yields for polyimides (Φ_{PI}) in series I and II show substantial electron transfer when decreased slightly with an increase of both *cis*- and *trans*-DATPP in both CH_2Cl_2 and DMAc. In CH_2Cl_2 , the quantum yields are decreased substantially relative to TPP in both *cis*-DATPP (32-53%) and *trans*-DATPP (34-58%). In DMAc, the fluorescence quantum yield data indicates a small effect of electron transfer of *cis*-DATPP (1-35%) and (15-44%) in *trans*-DATPP, when compared to the starting porphyrin (TPP). As expected, *trans*-DATPP is slightly more efficient in transferring electronic charge along the conjugated molecule than *cis*-DATPP in both CH_2Cl_2 and DMAc.

For ZnTPP, the quantum yields of polyimides in series III show substantial electron transfer in both CH_2Cl_2 and DMAc, decreasing with the increase of *cis*-ZnDATPP content. In CH_2Cl_2 , the electron transfer is 5-50%, and in DMAc, electron transfer is 25-58% when compared both with ZnTPP.

The quantum yields of polyimides in series IV decrease with the increase in *trans*-ZnDATPP content both of CH_2Cl_2 and DMAc. The electron transfer is 10-60% in CH_2Cl_2 and 29-58% in DMAc, when compared both with ZnTPP. In case of polyimides in series III and IV, the effect of solvent polarity is insignificant. A reasonable explanation as to why the metallic porphyrins have lower fluorescence

quantum yields than the free-base porphyrins can be due to the rapid rate of intersystem crossing (k_{NR}) (Eq.2.1).

From this data indicated that the rate of electron transfer (k_{ET}) for polyimides-containing porphyrin units within the polymer to diimide acceptor groups in both CH_2Cl_2 and DMAc are very fast when increasing the porphyrin moiety. A possible explanation for these values is that influence of self quenching within the polymer chain.



ศูนย์วิทยทรัพยากร
จุฬาลงกรณ์มหาวิทยาลัย

Table 4.13 Fluorescence quantum yields and lifetimes of polyimides

Compound	CH ₂ Cl ₂			DMAc		
	Φ_{PI}	τ_0 (ns)	$K_{ET}(s^{-1})$	Φ_{PI}	τ_0 (ns)	$K_{ET}(s^{-1})$
TPP	0.116	9.21	-	0.150	11.94	-
<i>cis</i> -DATPP	0.181	8.02	-	0.196	4.43	-
<i>trans</i> -DATPP	0.171	8.06	-	0.198	4.93	-
ZnTPP	0.025	1.97	-	0.024	1.94	-
<i>cis</i> -ZnDATPP	0.029	1.55	-	0.044	1.90	-
<i>trans</i> -ZnDATPP	0.027	1.50	-	0.042	1.86	-
Series I						
<i>cis</i> -DATPP						
PI-C1	0.079	8.83	4.73x10 ⁶	0.148	11.67	1.94x10 ⁶
PI-C2	0.070	8.47	9.45x10 ⁶	0.128	11.50	3.20x10 ⁶
PI-C3	0.068	8.38	1.07x10 ⁷	0.108	11.32	4.59x10 ⁶
PI-C4	0.054	8.09	1.50x10 ⁷	0.098	11.30	4.74x10 ⁶
Series II						
<i>trans</i> -DATPP						
PI-T1	0.076	8.65	7.02x10 ⁶	0.160	11.56	2.75x10 ⁶
PI-T2	0.063	8.51	8.96x10 ⁶	0.129	11.40	3.97x10 ⁶
PI-T3	0.057	8.27	1.24x10 ⁷	0.112	11.30	4.74x10 ⁶
PI-T4	0.049	8.11	1.48x10 ⁷	0.084	11.17	5.77x10 ⁶
Series III						
<i>cis</i> -ZnDATPP						
PI-ZnC1	0.019	1.73	7.20x10 ⁷	0.018	1.80	4.13x10 ⁷
PI-ZnC2	0.013	1.67	9.18x10 ⁷	0.013	1.78	4.54x10 ⁷
PI-ZnC3	0.012	1.65	9.72x10 ⁷	0.011	1.78	4.73x10 ⁷
PI-ZnC4	0.010	1.67	9.25x10 ⁷	0.010	1.78	4.54x10 ⁷
Series IV						
<i>trans</i> -ZnDATPP						
PI-ZnT1	0.018	1.75	6.54x10 ⁷	0.017	1.78	4.63x10 ⁷
PI-ZnT2	0.012	1.66	9.43x10 ⁷	0.012	1.77	4.95x10 ⁷
PI-ZnT3	0.011	1.67	9.11x10 ⁷	0.011	1.78	4.60x10 ⁷
PI-ZnT4	0.009	1.68	8.90x10 ⁷	0.010	1.77	5.05x10 ⁷

4.4.7 Fluorescence Quenching Determination

The rate constant for fluorescence quenching of free base porphyrin, metallic porphyrin and all polyimides (series I, II, III and IV) were determined by using the Stern-Volmer mechanism (SV) (Eq. 3.2), which was obtained with AQ as the external quencher. It is known that anthraquinone is an electron acceptor for singlet excited TPP and ZnTPP. The fluorescence spectra of polyimides exhibited two bands in the range of 600-730 nm due to emission of the porphyrin unit. The fluorescence intensity decreases upon successive addition of AQ (Figures 4.22-4.26). The observed decrease in the fluorescence intensity is due to quenching of the excited singlet state of the porphyrin in the presence of AQ.

$$\frac{F_0}{F} = 1 + K_Q[Q] \quad \text{Eq 3.2}$$

where F_0 and F are the relative fluorescence intensities in the absence and presence of quencher concentration $[AQ]$ and K_Q is the Stern-Volmer constant and may refer to static quenching if a complex between fluorophore and quencher is formed and does not undergo diffusion or to dynamic quenching if diffusion occurs during the excited-state lifetime. The second-order quenching rate constant, k_q was calculated using equation 3.3.

$$k_q = \frac{K_Q}{\tau_0} \quad \text{Eq. 3.3}$$

where τ_0 is the fluorescence lifetime of the fluorophore in the absence of the quencher. The measured lifetime values for TPP are 9.21 and 11.94 ns in CH_2Cl_2 and DMAc, while the lifetimes of *cis*- and *trans*-DATPP are 8.02 and 8.06 ns in CH_2Cl_2 and both 4.93 ns in DMAc, respectively.

Typical Stern-Volmer plots are linear in the relatively low concentration range investigated for TPP, *cis*- and *trans*-DATPP by AQ (Table 3.2). The K_Q values were determined from the slopes of the Stern-Volmer plots and found to range from 170 to 146 M^{-1} in CH_2Cl_2 and 126 to 96 M^{-1} in DMAc (Tables 4.14-4.15 and Figures 4.19-4.21).

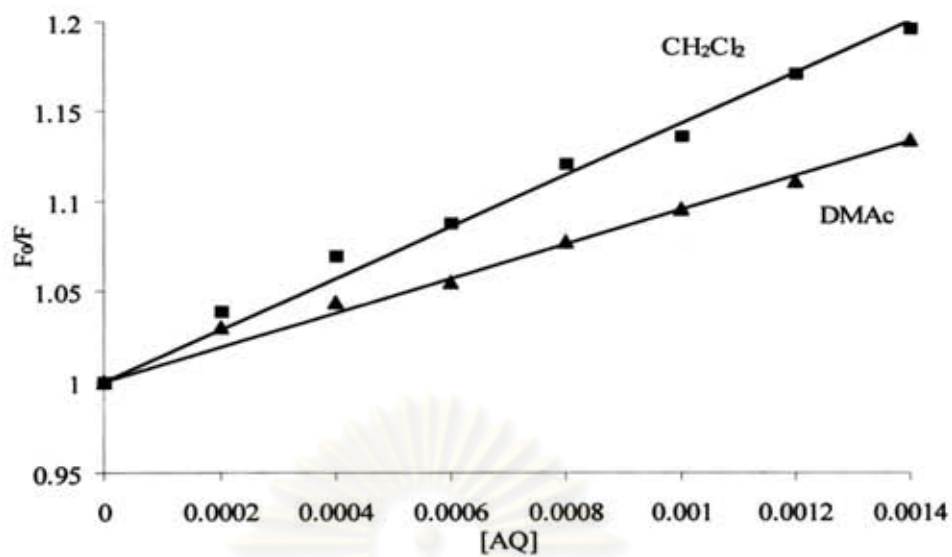


Figure 4.19 Stern-Volmer plots of fluorescence quenching of TPP by AQ in CH_2Cl_2 and DMAc

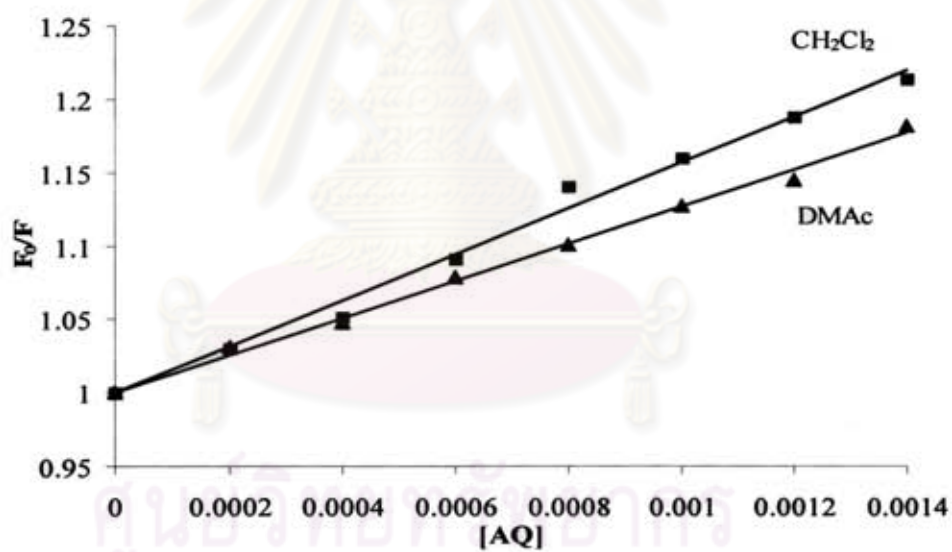


Figure 4.20 Stern-Volmer plots of fluorescence quenching of *cis*-DATPP by AQ in CH_2Cl_2 and DMAc

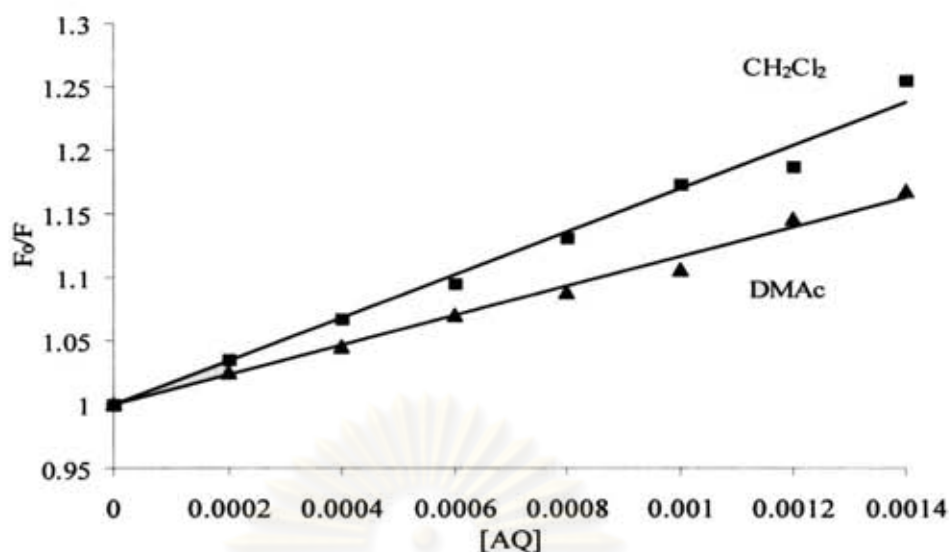


Figure 4.21 Stern-Volmer plots of fluorescence quenching of *trans*-DATPP by AQ in CH₂Cl₂ and DMAc.

Figures 4.19-4.21 show the linear SV plots for the fluorescence quenching of TPP, *cis*-DATPP and *trans*-DATPP at 654 nm by AQ in CH₂Cl₂ and DMAc, which are two organic solvents of different polarity. It is apparent that the calculated K_Q and k_q values decrease with an increase in solvent polarity. The k_q values of TPP in CH₂Cl₂ were found to be 1.59×10^{10} and 8.00×10^9 M⁻¹s⁻¹ in DMAc, indicating that the fluorescence quenching of TPP by AQ is perhaps due to the electron transfer processes leading to the generation or disappearance of the polar species [53]. Quenching by energy transfer does not normally involve nor generate highly polar intermediates; therefore, solvent effects should be minor for this pathway. In addition, k_q values of the TPP-AQ system in different solvents are close to the limiting diffusion rate constant (k_{diff}). The k_{diff} values for CH₂Cl₂ and DMAc are 1.57×10^{10} and 3.32×10^9 M⁻¹s⁻¹ respectively, as calculated by equation 3.4. This indicates that diffusion is involved in the quenching mechanism.

The bimolecular quenching rate constant k_q was calculated upon knowledge of both K_Q and τ_0 for the samples, as defined in equation 3.3. The k_q values in CH₂Cl₂ were found to be 1.59×10^{10} , 1.99×10^{10} and 2.11×10^{10} M⁻¹s⁻¹ for TPP, *cis*- and *trans*-DATPP. Similarly, the k_q value in DMAc was calculated to be 8.00×10^9 , 2.56×10^{10} and 2.36×10^{10} M⁻¹s⁻¹ for TPP, *cis*- and *trans*-DATPP, respectively (Table 4.14). Results suggest that the relative magnitudes of k_q increase from TPP to both *cis*- and

trans-DATPP due to the presence of electron donating diamino groups covalently bonded on the porphyrin moiety. Similarly, the k_q values for the metalloporphyrins, ZnTPP, *cis*- and *trans*-ZnDATPP (Table.4.15) in CH_2Cl_2 were found to be 4.72×10^{10} , 7.62×10^{10} and $8.25 \times 10^{10} \text{ M}^{-1}\text{s}^{-1}$, and those in DMAc were calculated to be 3.19×10^{10} , 4.94×10^{10} and $5.39 \times 10^{10} \text{ M}^{-1}\text{s}^{-1}$. A possible explanation for the high k_q values of the set of metalloprophyrins could be due to rapid fluorescence quenching by AQ [57].

Figures 4.22-4.26 display the set of fluorescence emission spectra along with their corresponding SV plots for TPP, *cis*-, *trans*-DATPP and polyimide-containing *cis*- and *trans*-DATPP (series I and II) by low range concentration of AQ external quencher in CH_2Cl_2 .

Fluorescence quenching of the excited singlet states of porphyrin-containing polyimides (series I, II, III and IV) in the presence of AQ were also observed. The data are shown in Tables 4.14 and 4.15. TPP ($\tau_0=9.21$ ns in CH_2Cl_2 and 11.94 ns in DMAc) was characterized by longest lifetimes compared to ZnTPP ($\tau_0=1.97$ ns in CH_2Cl_2 and 1.94 ns in DMAc). This result implies that TPP could interact with the anthraquinone quencher for a longer period of time in the nanosecond time range. Their fluorescence was quenched more slowly ($k_q = 1.59 \times 10^{10}$ in CH_2Cl_2 and $k_q = 8.00 \times 10^9 \text{ M}^{-1}\text{s}^{-1}$ in DMAc) when the estimated parameters are compared with ZnTPP ($k_q = 4.72 \times 10^{10}$ in CH_2Cl_2 and $k_q = 3.19 \times 10^{10} \text{ M}^{-1}\text{s}^{-1}$ in DMAc).

The values for τ_0 of polymers in series I and II in CH_2Cl_2 and DMAc were uniformly smaller than those of standard porphyrin (TPP and ZnTPP). The major component for PI-C4 and PI-T4 were found to be 8.09 and 8.11 ns in CH_2Cl_2 and 11.30 and 11.17 ns in DMAc. These values are smaller than those of TPP (9.21 ns in CH_2Cl_2 and 11.94 ns in DMAc) (Table 4.14), while the major component in polymer PI-ZnC4 and PI-ZnT4 (Table 4.15) were found to be 1.67 and 1.68 ns in CH_2Cl_2 and 1.78 and 1.77 ns in DMAc. These values are smaller than those of the metallic porphyrin ZnTPP, with lifetimes measured as 1.97 ns in CH_2Cl_2 and 1.94 ns in DMAc (Table 4.15).

Moreover, the lifetime in the absence of AQ quencher (τ_0) in polyimides containing *cis*- and *trans*-DATPP (series I and II) slightly decrease from 5-30% (8.83 to 8.09 ns for PI-C1 to PI-C4 and 8.65 to 8.11 ns for PI-T1 to PI-T4 in CH_2Cl_2). In DMAc, the lifetime in the absence of AQ (τ_0) for polyimide series I and II were larger

than those in CH_2Cl_2 (11.67 to 11.30 ns for PI-C1 to PI-C4 and 11.56 to 11.17 ns for PI-T1 to PI-T4). The fluorescence lifetimes in the presence of AQ quencher (τ_F) in polyimides containing both *cis*- and *trans*-DATPP are smaller than the fluorescence lifetimes in the absence of quencher. For instance, in series I, the τ_F values for polyimides PI-C1 to PI-C4 are slightly less than those in the absence of quencher (e.g. for PI-C1 in CH_2Cl_2 , $\tau_F = 7.68$ ns and $\tau_0 = 8.83$ ns; for PI-C4, $\tau_F = 7.94$ ns and $\tau_0 = 8.09$ ns, for PI-C1 in DMAc, $\tau_F = 10.95$ ns and $\tau_0 = 11.67$ ns; for PI-C4, $\tau_F = 11.17$ ns and $\tau_0 = 11.30$ ns). Results indicated that the decrease in the fluorescence lifetimes in both CH_2Cl_2 and DMAc are likely due to (1) the increase in the rate of intersystem crossing and therefore an increase in the total nonradiative decay rate constant ($k_{NR} = k_{IC} + k_{ISC}$) and (2) energy transfer from the electron donor to the electron acceptor (AQ) (see Jablonski state energy-level diagram).

Both the Stern-Volmer constant (K_Q) and bimolecular quenching rate constant (k_q) in polyimides (series I and II) in both solvents decreased from 5% to 30% PI. As observed, the K_Q decreased dramatically from 252.2 to 87.7 M^{-1} and k_q slightly decreased from 2.86×10^{10} to 1.08×10^{10} $\text{M}^{-1} \text{s}^{-1}$ in PI-C1 to PI-C4. Similarly, the K_Q values in both PI-T1 and PI-T4 were found to be 273.7 and 102.9 M^{-1} and the bimolecular rate constants (k_q) were found to be 3.16×10^{10} and 1.26×10^{10} $\text{M}^{-1} \text{s}^{-1}$ in CH_2Cl_2 . In DMAc, the K_Q values decreased less significantly than in CH_2Cl_2 , from 76.0 to 48.6 M^{-1} and k_q decreased from 6.51×10^9 to 4.32×10^9 $\text{M}^{-1} \text{s}^{-1}$ in PI-C1 to PI-C4. Likewise, the K_Q values in PI-T1 and PI-T4 were found to be 90.1 to 51.3 M^{-1} and k_q values were found to be equal to 7.79×10^9 to 4.59×10^9 $\text{M}^{-1} \text{s}^{-1}$. As expected, polyimide-containing *trans*-DATPP is more efficient in being quenched by AQ than *cis*-DATPP in both CH_2Cl_2 and DMAc. The k_q polyimides in series I and II in CH_2Cl_2 are higher than in DMAc due to more rapid quenching of the coiling polymer by AQ in less polar media.

Table 4.14 Summary of photophysical data of polyimides (series I and II) in CH₂Cl₂ and DMAc

Compound	Solvent	τ_0 (ns)	τ_F (ns)	K_Q (M ⁻¹)	k_q (M ⁻¹ s ⁻¹)
TPP	CH ₂ Cl ₂	9.21	8.66	145.98	1.59x10 ¹⁰
<i>cis</i> -DATPP	CH ₂ Cl ₂	8.02	7.50	156.27	1.99x10 ¹⁰
<i>trans</i> -DATPP	CH ₂ Cl ₂	8.06	7.53	169.68	2.11x10 ¹⁰
Series I					
<i>cis</i> -DATPP					
PI-C1	CH ₂ Cl ₂	8.83	7.68	252.24	2.86x10 ¹⁰
PI-C2	CH ₂ Cl ₂	8.47	7.90	134.77	1.59x10 ¹⁰
PI-C3	CH ₂ Cl ₂	8.38	8.10	116.96	1.40x10 ¹⁰
PI-C4	CH ₂ Cl ₂	8.09	7.94	87.71	1.08x10 ¹⁰
Series II					
<i>trans</i> -DATPP					
PI-T1	CH ₂ Cl ₂	8.65	7.54	273.67	3.16x10 ¹⁰
PI-T2	CH ₂ Cl ₂	8.51	8.01	176.52	2.08x10 ¹⁰
PI-T3	CH ₂ Cl ₂	8.27	7.90	159.00	1.91x10 ¹⁰
PI-T4	CH ₂ Cl ₂	8.11	7.95	102.92	1.26x10 ¹⁰
Series I					
TPP	DMAc	11.94	11.37	95.56	8.00x10 ⁹
<i>cis</i> -DATPP	DMAc	4.93	4.74	126.19	2.56x10 ¹⁰
<i>trans</i> -DATPP	DMAc	4.93	4.73	116.37	2.36x10 ¹⁰
<i>cis</i> -DATPP					
PI-C1	DMAc	11.67	10.95	76.00	6.51x10 ⁹
PI-C2	DMAc	11.50	11.07	60.09	5.22x10 ⁹
PI-C3	DMAc	11.32	11.03	52.86	4.67x10 ⁹
PI-C4	DMAc	11.30	11.17	48.56	4.32x10 ⁹
Series II					
<i>trans</i> -DATPP					
PI-T1	DMAc	11.56	10.67	90.06	7.79x10 ⁹
PI-T2	DMAc	11.40	10.88	66.70	5.85x10 ⁹
PI-T3	DMAc	11.30	11.04	63.85	5.65x10 ⁹
PI-T4	DMAc	11.17	11.03	51.30	4.59x10 ⁹

Table 4.15 Summary of photophysical data of polyimides (Series III and IV) in CH₂Cl₂ and DMAc

Compound	Solvent	τ_0 (ns)	τ_f (ns)	K_Q (M ⁻¹)	k_q (M ⁻¹ s ⁻¹)
ZnTPP	CH ₂ Cl ₂	1.97	1.82	93.03	4.72x10 ¹⁰
<i>cis</i> -ZnDATPP	CH ₂ Cl ₂	1.55	1.40	117.92	7.62x10 ¹⁰
<i>trans</i> -ZnDATPP	CH ₂ Cl ₂	1.50	1.38	124.01	8.25x10 ¹⁰
Series III					
<i>cis</i> -ZnDATPP					
PI-ZnC1	CH ₂ Cl ₂	1.73	1.61	83.32	4.83x10 ¹⁰
PI-ZnC2	CH ₂ Cl ₂	1.67	1.56	79.46	4.76x10 ¹⁰
PI-ZnC3	CH ₂ Cl ₂	1.65	1.57	85.52	5.17x10 ¹⁰
PI-ZnC4	CH ₂ Cl ₂	1.67	1.61	79.32	4.76x10 ¹⁰
Series IV					
<i>trans</i> -ZnDATPP					
PI-ZnT1	CH ₂ Cl ₂	1.75	1.61	75.63	4.33x10 ¹⁰
PI-ZnT2	CH ₂ Cl ₂	1.66	1.57	70.26	4.23x10 ¹⁰
PI-ZnT3	CH ₂ Cl ₂	1.67	1.56	73.03	4.37x10 ¹⁰
PI-ZnT4	CH ₂ Cl ₂	1.68	1.60	73.13	4.36x10 ¹⁰
<hr/>					
ZnTPP	DMAc	1.94	1.92	61.97	3.19x10 ¹⁰
<i>cis</i> -ZnDATPP	DMAc	1.90	1.77	93.66	4.94x10 ¹⁰
<i>trans</i> -ZnDATPP	DMAc	1.86	1.72	100.34	5.39x10 ¹⁰
Series III					
<i>cis</i> -ZnDATPP					
PI-ZnC1	DMAc	1.80	1.69	67.89	3.78x10 ¹⁰
PI-ZnC2	DMAc	1.78	1.68	61.02	3.42x10 ¹⁰
PI-ZnC3	DMAc	1.78	1.68	62.29	3.51x10 ¹⁰
PI-ZnC4	DMAc	1.78	1.68	57.66	3.23x10 ¹⁰
Series IV					
<i>trans</i> -ZnDATPP					
PI-ZnT1	DMAc	1.78	1.65	82.20	4.62x10 ¹⁰
PI-ZnT2	DMAc	1.78	1.65	65.38	3.69x10 ¹⁰
PI-ZnT3	DMAc	1.78	1.70	64.71	3.63x10 ¹⁰
PI-ZnT4	DMAc	1.77	1.69	60.47	3.42x10 ¹⁰

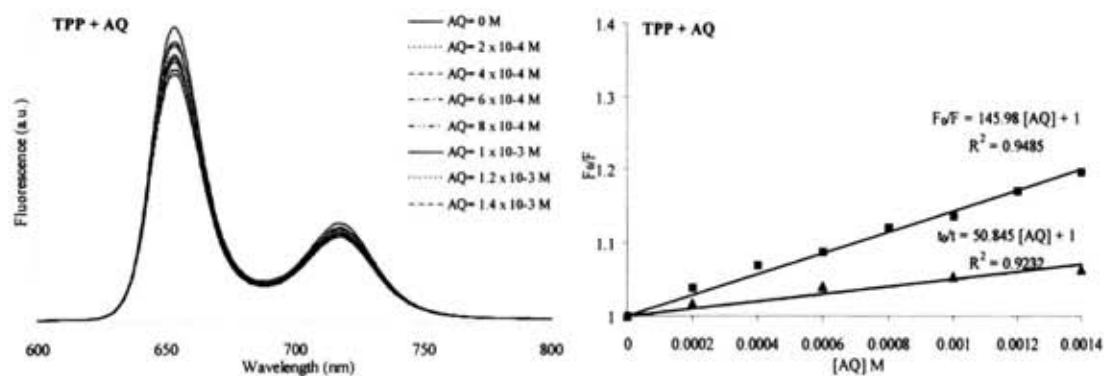


Fig.4.22 Fluorescence quenching of 5×10^{-6} mol.dm⁻³ of TPP and Stern-Volmer plot of fluorescence quenching by anthraquinone [2×10^{-4} - 1.4×10^{-3} M] in CH₂Cl₂

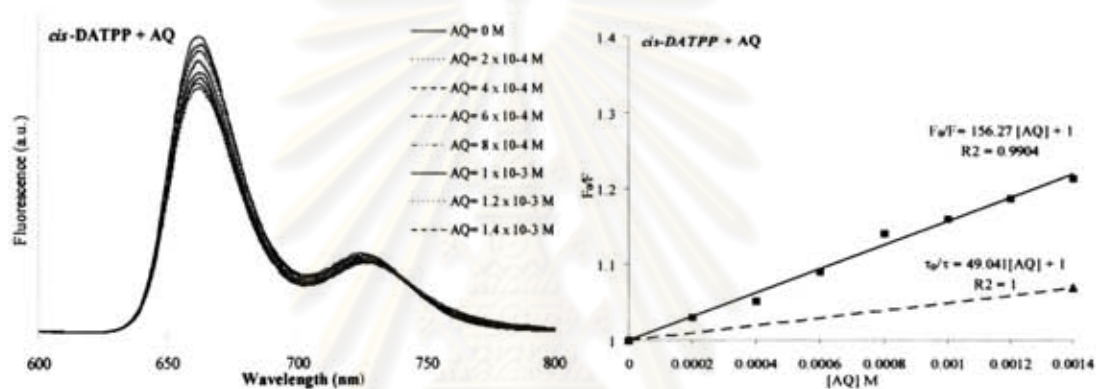


Fig.4.23 Fluorescence quenching of 5×10^{-6} mol.dm⁻³ of *cis*-DATPP and Stern-Volmer plot of fluorescence quenching by anthraquinone [2×10^{-4} - 1.4×10^{-3} M] in CH₂Cl₂

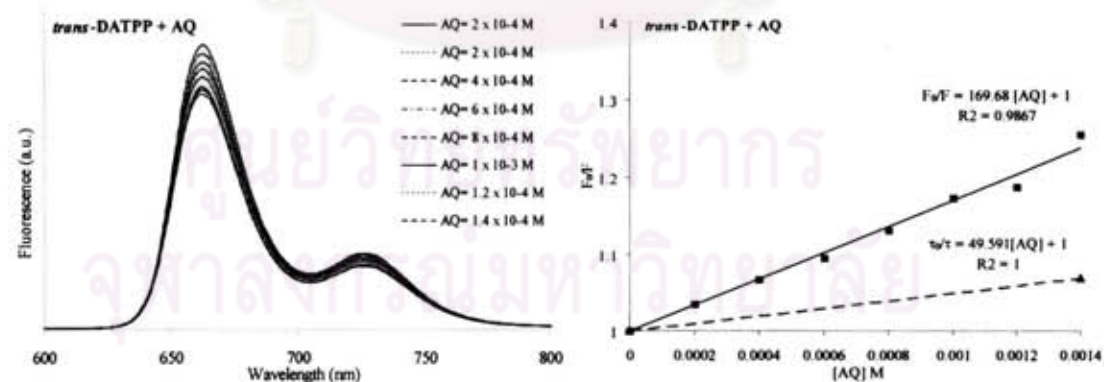


Fig.4.24 Fluorescence quenching of 5×10^{-6} mol.dm⁻³ of *trans*-DATPP and Stern-Volmer plot of fluorescence quenching by anthraquinone [2×10^{-4} - 1.4×10^{-3} M] in CH₂Cl₂

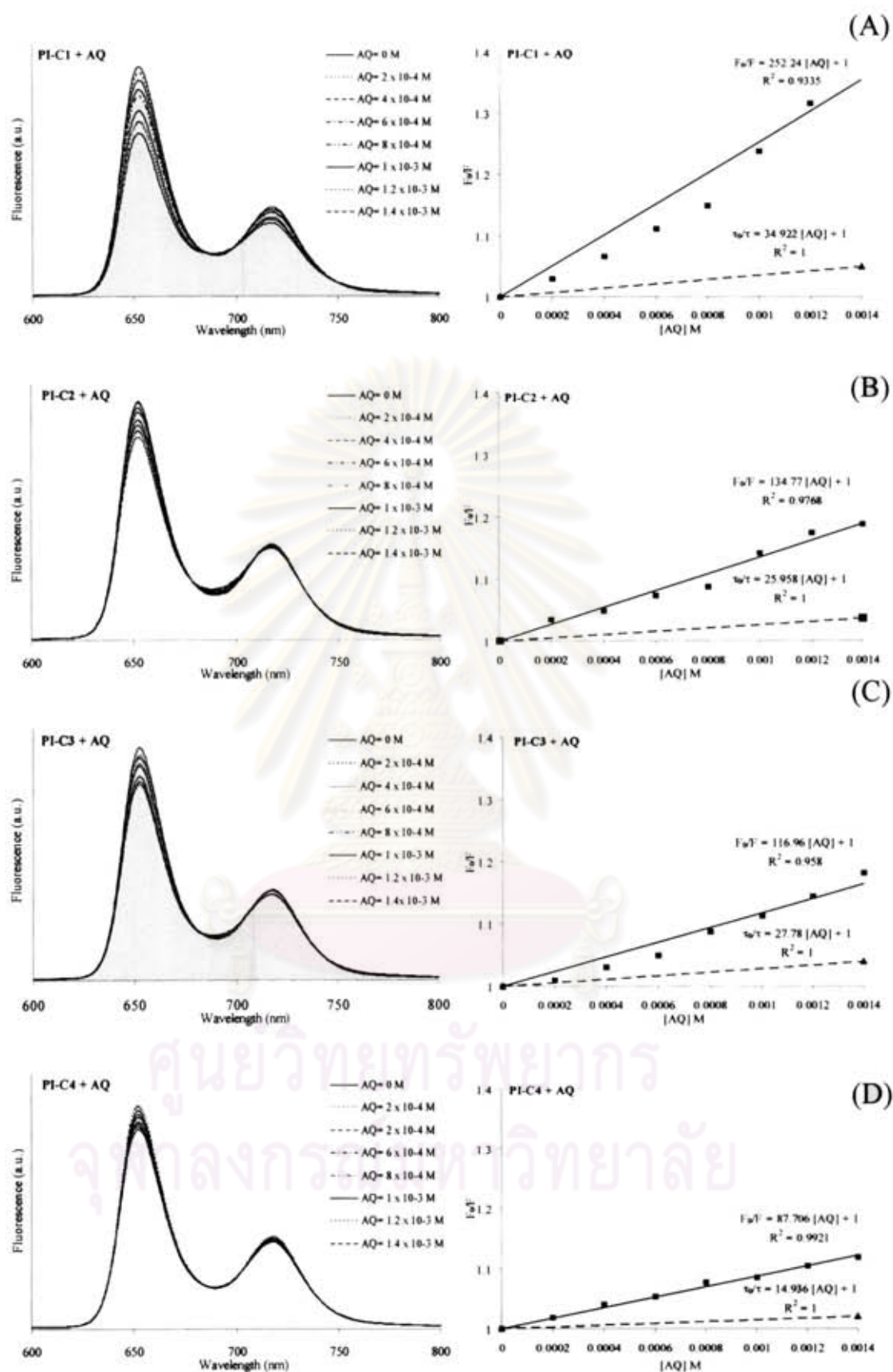


Fig.4.25A-D Fluorescence quenching of polyimide containing 5-30% *cis*-DATPP moieties and Stern-Volmer plots of fluorescence quenching by anthraquinone [2×10^{-4} - 1.4×10^{-3} M] in CH_2Cl_2

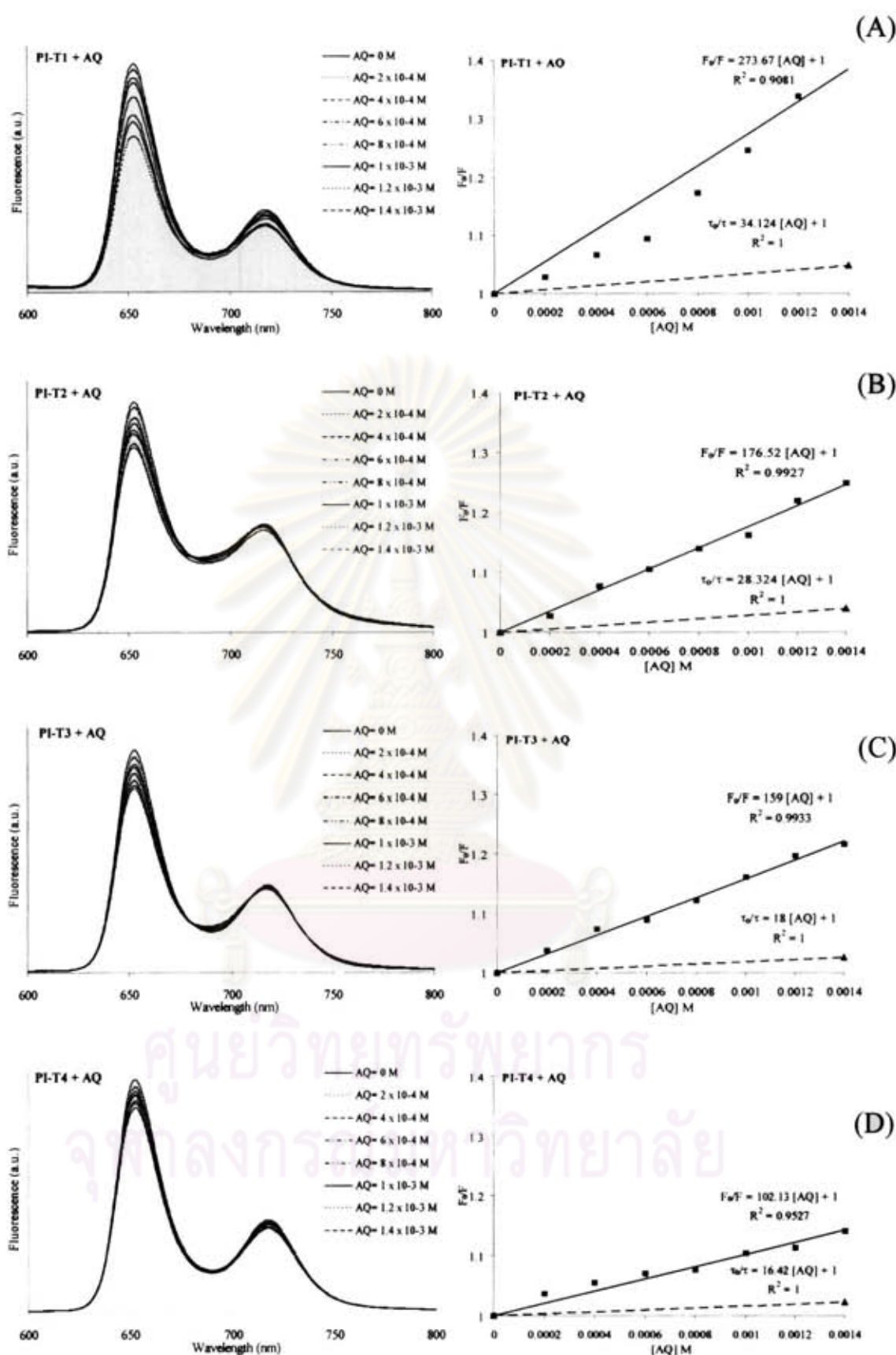


Fig.4.26A-D Fluorescence quenching of polyimide containing 5-30% *trans*-DATPP moieties and Stern-Volmer plots of fluorescence quenching by anthraquinone [2×10^{-4} - 1.4×10^{-3} M] in CH_2Cl_2

In the fluorescence quenching of polyimide-containing porphyrins by external quencher (AQ), the fluorescence intensity is expected to be minimized due to greater number of collisions between the excited singlet state of the polyimide species and the quencher. As expected, the small amount of porphyrin in the polymer chain (e.g. 5%) dissolves in the solvent more freely due to less aggregation of the molecules (less chain packing leads to an increase in free volume and more flexible linkages [35]). Hence, the presence of less aggregation causes AQ to easily collide and attach with the PI species. In contrast, the presence of a greater number of porphyrin molecules in the polymer (30%) increases the effect of aggregation of the polyimide species (higher chain packing leads to a decrease in free volume and less flexible linkages). The cause of aggregation might serve to change the local environment that exists around the porphyrin macrocycle in the polyimides making it more difficult for the quencher to diffuse and interact with porphyrins within the interior of the polymer chain.

In case of polyimides containing metalloporphyrins (series III and IV) in CH_2Cl_2 and DMAc, the fluorescence lifetimes were smaller than those of standard Zn-porphyrin (ZnTPP) as described previously. The lifetime in the absence of AQ quencher (τ_0) in polyimides containing *cis*- and *trans*-ZnDATPP (series III and IV) slightly decrease from 5-30% (1.73 to 1.67 ns for PI-ZnC1 to PI-ZnC4 and 1.75 to 1.68 ns for PI-ZnT1 to PI-ZnT4 in CH_2Cl_2). In DMAc, the τ_0 for polyimide series III and IV were similar to those in CH_2Cl_2 (1.80 to 1.78 ns for PI-ZnC1 to PI-ZnC4 and 1.78 to 1.77 ns for PI-ZnT1 to PI-ZnT4). The fluorescence lifetimes in the presence of AQ quencher (τ_F) in polyimides containing both *cis*- and *trans*-ZnDATPP are smaller than τ_0 . For instance, in series III, the τ_F values for polyimides, PI-ZnC1 to PI-ZnC4, are slightly less than those in the absence of quencher (e.g. for PI-ZnC1 in CH_2Cl_2 , $\tau_F = 1.61$ ns and $\tau_0 = 1.73$ ns; for PI-ZnC4, $\tau_F = 1.61$ ns and $\tau_0 = 1.67$ ns; for PI-ZnC1 in DMAc, $\tau_F = 1.69$ ns and $\tau_0 = 1.80$ ns; for PI-ZnC4, $\tau_F = 1.68$ ns and $\tau_0 = 1.78$ ns). Similar to the free-base porphyrin containing polyimides, an analogous trend is observed in the case of the zinc porphyrins. A small decrease in the lifetimes is observed for the zinc-containing porphyrins perhaps due to a small increase in the rate of ISC.

Both the Stern-Volmer constant (K_Q) and bimolecular quenching rate constant (k_q) in polyimides (series III and IV) in both solvents slightly decreased from 5% to

30% PI. As observed, the K_Q decreased from 83.3 to 79.3 M^{-1} and calculations show that the k_q values are essentially the same ($k_q = 4.83 \times 10^{10}$ to $4.76 \times 10^{10} M^{-1} s^{-1}$ in PI-ZnCl to PI-ZnCl4). Likewise, the K_Q values in both PI-ZnT1 and PI-ZnT4 were found to be 75.6 and 73.1 M^{-1} and the k_q values were essentially the same ($k_q = 4.33 \times 10^{10}$ to $4.36 \times 10^{10} M^{-1} s^{-1}$ in CH_2Cl_2). In DMAc, the K_Q values decreased similar to those in CH_2Cl_2 , from 67.9 to 57.6 M^{-1} with k_q values close to each other from 3.78×10^{10} to $3.23 \times 10^{10} M^{-1} s^{-1}$ in PI-ZnCl to PI-ZnCl4. Likewise, the K_Q values in PI-ZnT1 and PI-ZnT4 were found to be 82.2 to 60.5 M^{-1} and k_q values were found to be equal to 4.62×10^{10} to $3.42 \times 10^{10} M^{-1} s^{-1}$. As observed, the k_q polyimides in series III and IV in CH_2Cl_2 are similar in DMAc, perhaps indicating that solvent polarity is not a significant effect on the fluorescence quenching of the excited-state polyimides and the amount of zinc-porphyrin in the polymer chain. This is due to the incorporation of *cis*- and *trans*-ZnDATPP in the polymer structure, resulting in an increase in chain rigidity and less free volume for diffusion maybe difficult to collided or attached between AQ and fluorophore.



ศูนย์วิทยทรัพยากร
จุฬาลงกรณ์มหาวิทยาลัย

4.5 Fluorescence quenching at high anthraquinone concentration of TPP and ZnTPP in CH₂Cl₂ and DMAc

Departure from linearity observed in the Stern-Volmer plots (Figure 4.19-4.26) can be explained by involving both static and dynamic quenching mechanisms.

The fluorophore can be quenched both by collisions and by complex formation with the same external quencher. The characteristic feature of the SV plots in these circumstances is an upward curvature, concave toward the y-axis. The upward-curving SV plots could be analyzed in terms of both the static and dynamic quenching constants (K_D and K_S). The fractional fluorescence intensity, F_0/F , is given by the product of static and dynamic quenching. Hence,

$$\frac{F_0}{F} = (1 + K_D[AQ])(1 + K_S[AQ]) \quad \text{Eq. 2.6}$$

where K_D and K_S are the dynamic and static quenching constants, respectively [49].

In case of fluorescence quenching of 5×10^{-6} mol.dm⁻³, free-base porphyrin; TPP and metallic; ZnTPP by increasing concentration of external quencher (AQ) from 0.002-0.016 M in CH₂Cl₂ did not obey the simple Stern-Volmer linear relationship; that is, the plot deviated upward from the straight line (Figures 4.28 and 4.30). The plot of the ratio of fluorescence lifetimes both in the absence and presence of quencher against [AQ] in the Stern-Volmer plots is linear and shows less quenching than the fluorescence intensity data. According to the SV plots, the positive deviation indicates the simultaneous presence of dynamic and static quenching. That is fluorophore is quenched by excited state collisions and by ground state complex formation with the quencher as shown in Figure 4.27 [54].

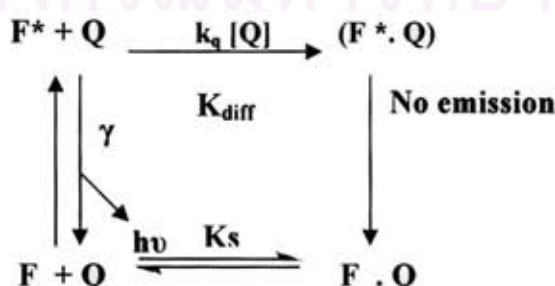


Figure 4.27 Pathway of dynamic (collisional) quenching and static quenching

From the fluorescence quenching data of TPP and ZnTPP by AQ in CH₂Cl₂, the static and dynamic quenching constants can be determined from a plot of the apparent quenching constant (K_{app}) versus [AQ] (Figures 4.29 and 4.31), which is found to be sufficiently linear.

$$K_{app} = (F_0 / F) - 1[AQ] \quad \text{Eq.4.1}$$

This indicates the presence of parallel quenching process, such as static or transient quenching along with dynamic quenching. The plot of (τ_0/τ) versus [Q] of TPP and ZnTPP (Figure 4.28B and 4.30B) for these systems gives a straight line with a slope equal to K_D (36.1 and 13.5 M⁻¹). The lifetimes of fluorophore with different concentration of quencher in CH₂Cl₂ are given in Table 4.16. Most of the fluorescence lifetimes were found to be best to a two-component exponential decay composed of one major component and one minor component. The value of τ_1 presence of quencher high concentration [AQ] were uniformly smaller than those of τ_1 absence of quencher as 6.07, 9.04 ns for TPP and 1.44, 1.74 ns for ZnTPP. Similarly, DMAc in Table 4.17, the value of τ_1 presence of quencher high concentration [AQ] and τ_1 absence of quencher calculated as 8.72, 10.84 ns for TPP and 1.56, 1.81 ns in ZnTPP respectively.

According to the calculated K_D values of TPP and ZnTPP (36.1 and 13.5 M⁻¹), the other static component is determined from the slope of the second order SV plot (Figures 4.29 and 4.31) and it is found to be 101.3 and 169.9 M⁻¹ (K_S) for TPP and ZnTPP. The static quenching component (K_S) is larger when compared to the dynamic component (K_D), indicating a high rate of complex formation.

The results suggest that the positive deviation in the SV plot of TPP and ZnTPP in the presence of external quencher (AQ) in CH₂Cl₂ is due to the presence of a high static quenching component in the overall dynamic quenching.

Table 4.16 Lifetimes of TPP and ZnTPP (ns) with different concentration of AQ in CH₂Cl₂

Compound	[AQ] 10 ⁻³ M	Lifetime		K _D M ⁻¹	K _S M ⁻¹
		τ ₁ (ns)	τ ₂ (ns)		
TPP	0.0	9.038(68.31±1.05%)	0.178(31.69±41.30%)	36.10	101.31
	1.6	6.067(61.16±2.12%)	0.092(38.84±24.10%)		
ZnTPP	0.0	1.743(78.11±10.12%)	0.260(21.89±20.80%)	13.50	169.91
	1.6	1.441(79.03±8.48%)	0.345(20.97±26.07%)		

Table 4.17 Lifetimes of TPP and ZnTPP (ns) with different concentration of AQ in DMAc

Compound	[AQ] 10 ⁻³ M	Lifetime		K _D M ⁻¹	K _S M ⁻¹
		τ ₁ (ns)	τ ₂ (ns)		
TPP	0.0	10.840(70.79±0.01%)	0.036(29.21±0.01%)	12.42	176.55
	1.6	8.723(67.57±0.62%)	0.063(32.43±15.50%)		
ZnTPP	0.0	1.813(70.66±5.32%)	0.170(29.34±1.63%)	21.91	91.51
	1.6	1.563(72.03±5.40%)	0.250(27.97±10.0%)		

ศูนย์วิทยทรัพยากร
จุฬาลงกรณ์มหาวิทยาลัย

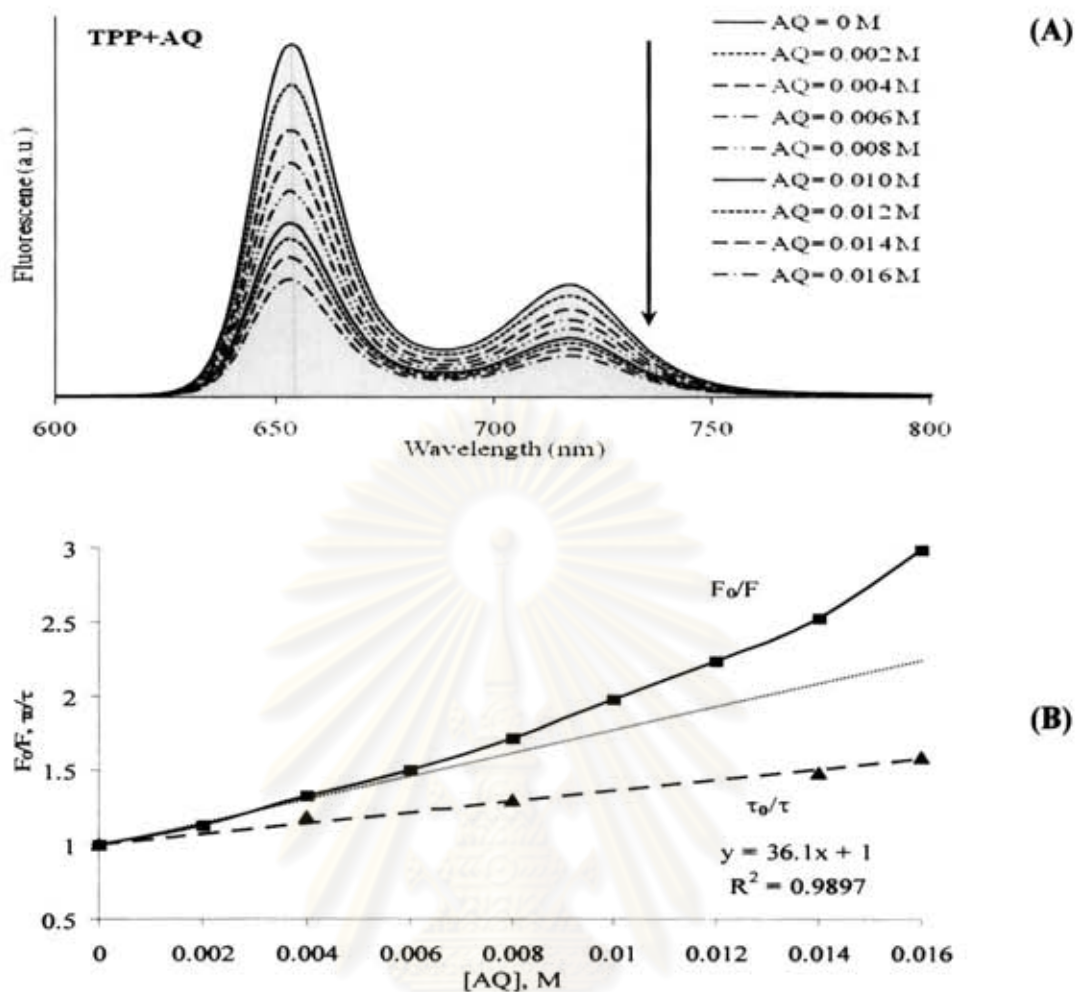


Figure 4.28 Fluorescence quenching (A) and Stern-Volmer plots (B) of fluorescence quenching of $5 \times 10^{-6} \text{ mol} \cdot \text{dm}^{-3}$ TPP by AQ concentration 0.002-0.016 M in CH_2Cl_2

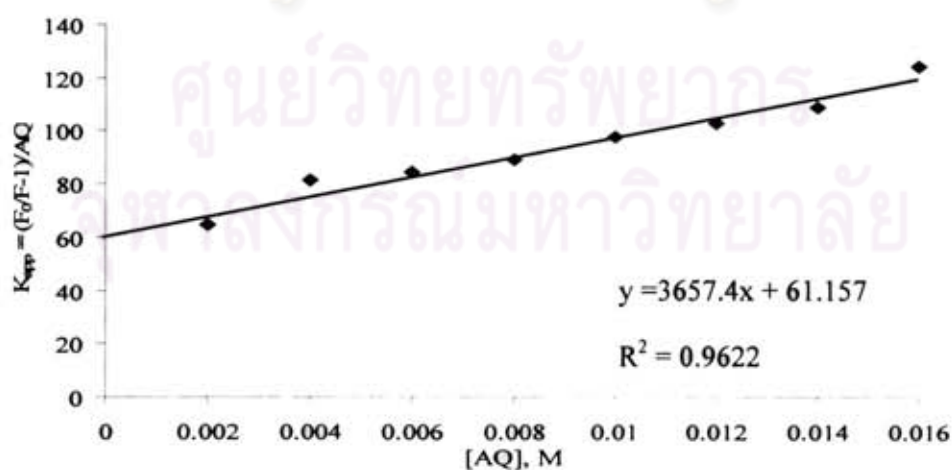


Figure 4.29 Plot of $[(F_0/F) - 1]/[AQ]$ vs. AQ for TPP fluorescence quenching by AQ in CH_2Cl_2

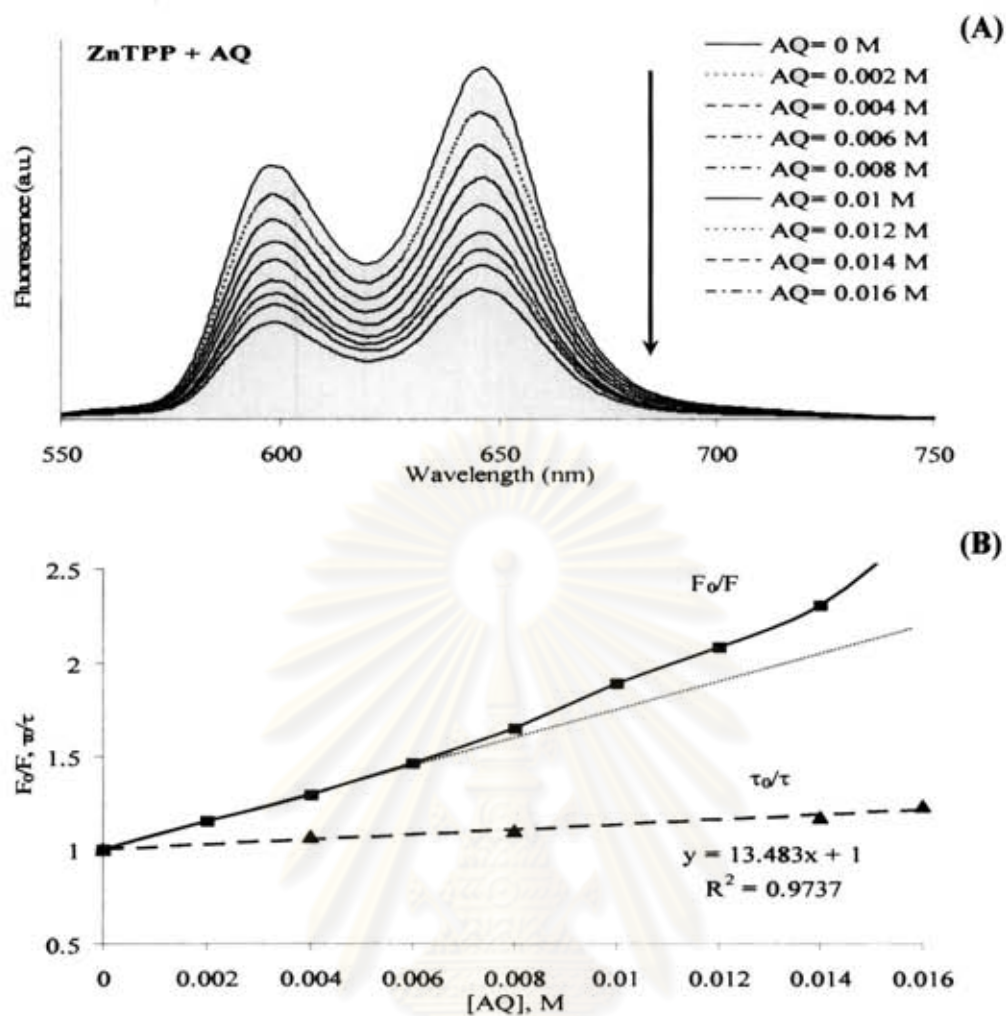


Figure 4.30 Fluorescence quenching (A) and Stern-Volmer plots (B) of fluorescence quenching of $5 \times 10^{-6} \text{ mol} \cdot \text{dm}^{-3}$ ZnTPP by AQ concentration 0.002-0.016 M in CH_2Cl_2

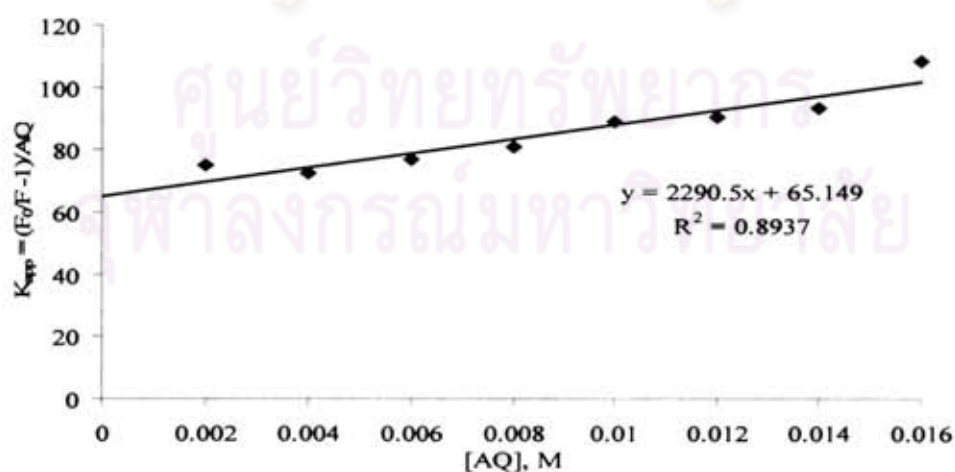


Figure 4.31 Plot of $[(F_0/F) - 1]/[\text{AQ}]$ vs. AQ for ZnTPP fluorescence quenching by AQ in CH_2Cl_2

As similarly with CH_2Cl_2 , the fluorescence quenching of $5 \times 10^{-6} \text{ mol.dm}^{-3}$ in DMAc, free-base porphyrin TPP and metallic ZnTPP were examined by increasing the concentration of external quencher (AQ) from 0.002-0.016 M. Likewise, the monomers did not obey the simple Stern-Volmer linear relationship; that is, the plot deviated upward from the straight line (Figures 4.32B and 4.34B). The static and dynamic quenching constants can be determined from a plot of the apparent quenching constant (K_{app}) versus [AQ] (Figures 4.33 and 4.35), found to be sufficiently linear. The plot of (τ_0/τ) versus [Q] of TPP and ZnTPP (Figure 4.32B and 4.34B) for these systems gives a straight line with a slope equal to K_D (12.4 and 21.9 M^{-1}). The lifetimes of fluorophore with different concentration of quencher in DMAc are given in Table 4.17. The other static component is determined from the slope of the second order SV plot (Figures 4.33 and 4.35) and it is found to be 176.5 and 91.5 M^{-1} (K_S) for TPP and ZnTPP, respectively. The static quenching component (K_S) is larger when compared to the dynamic component in DMAc and possible explanation could be due to the presence of a high static quenching component in the overall dynamic quenching. These observations suggest a significant contribution of static quenching in CH_2Cl_2 and DMAc. A possibility for the static contribution to the quenching may be a ground-state donor-acceptor (D-A) interaction between TPP, ZnTPP and AQ quencher.

ศูนย์วิทยทรัพยากร
จุฬาลงกรณ์มหาวิทยาลัย

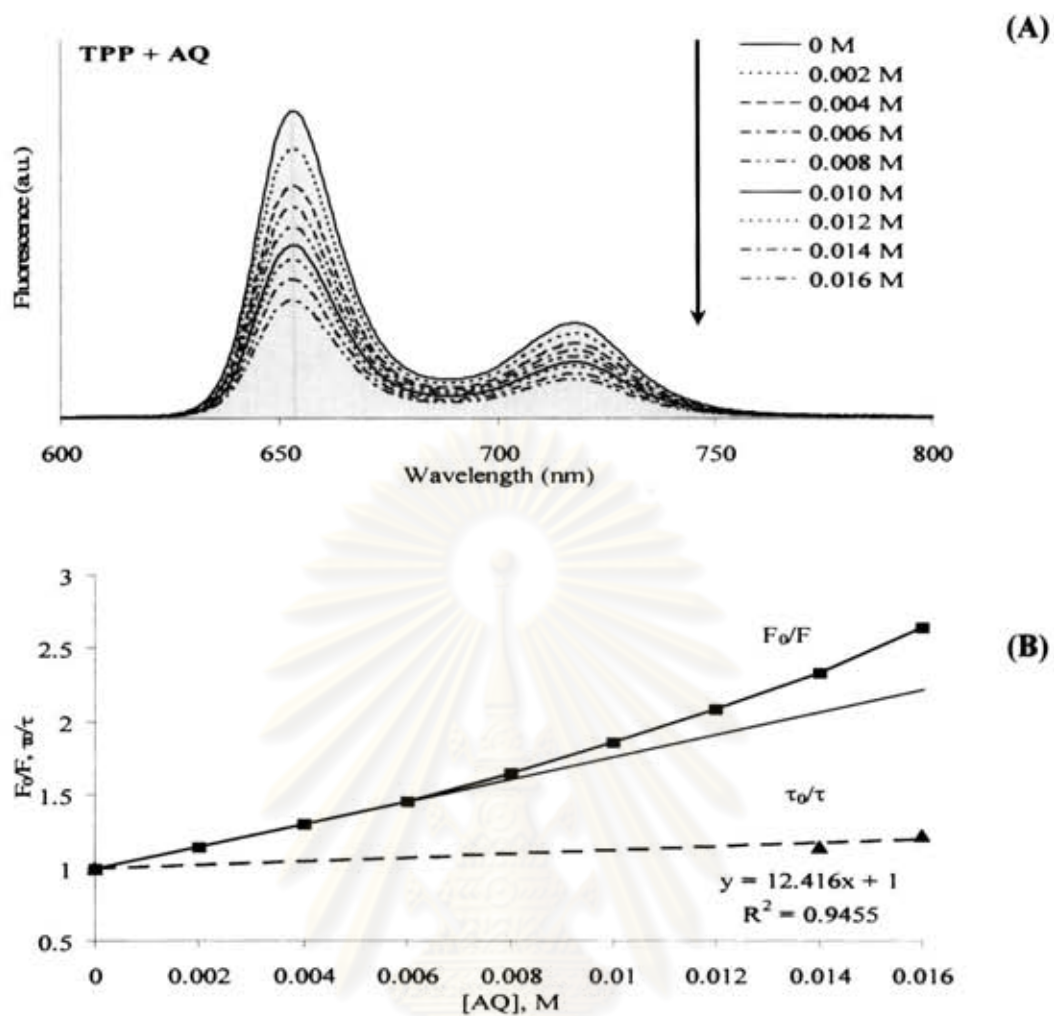


Figure 4.32 Fluorescence quenching (A) and Stern-Volmer plots (B) of fluorescence quenching of $5 \times 10^{-6} \text{ mol.dm}^{-3}$ TPP by AQ concentration 0.002-0.016 M in DMAc

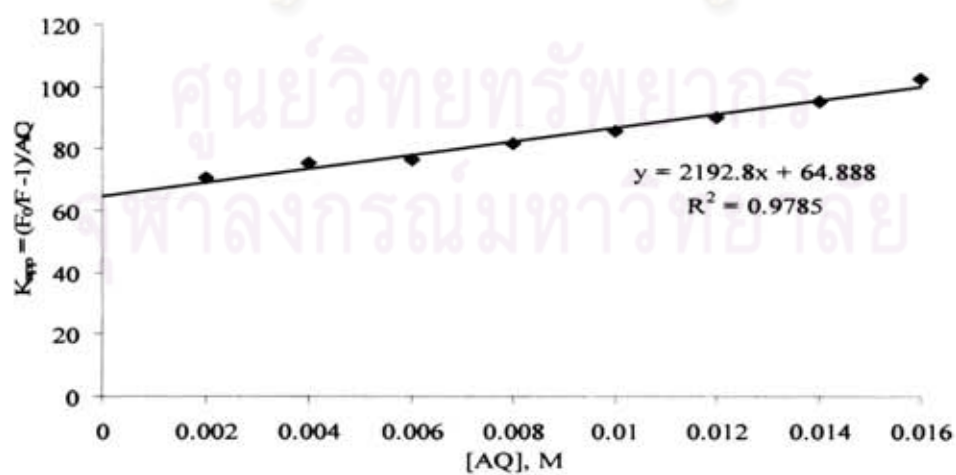


Figure 4.33 Plot of $[(F_0/F) - 1]/[AQ]$ vs. AQ for TPP fluorescence quenching by AQ in DMAc

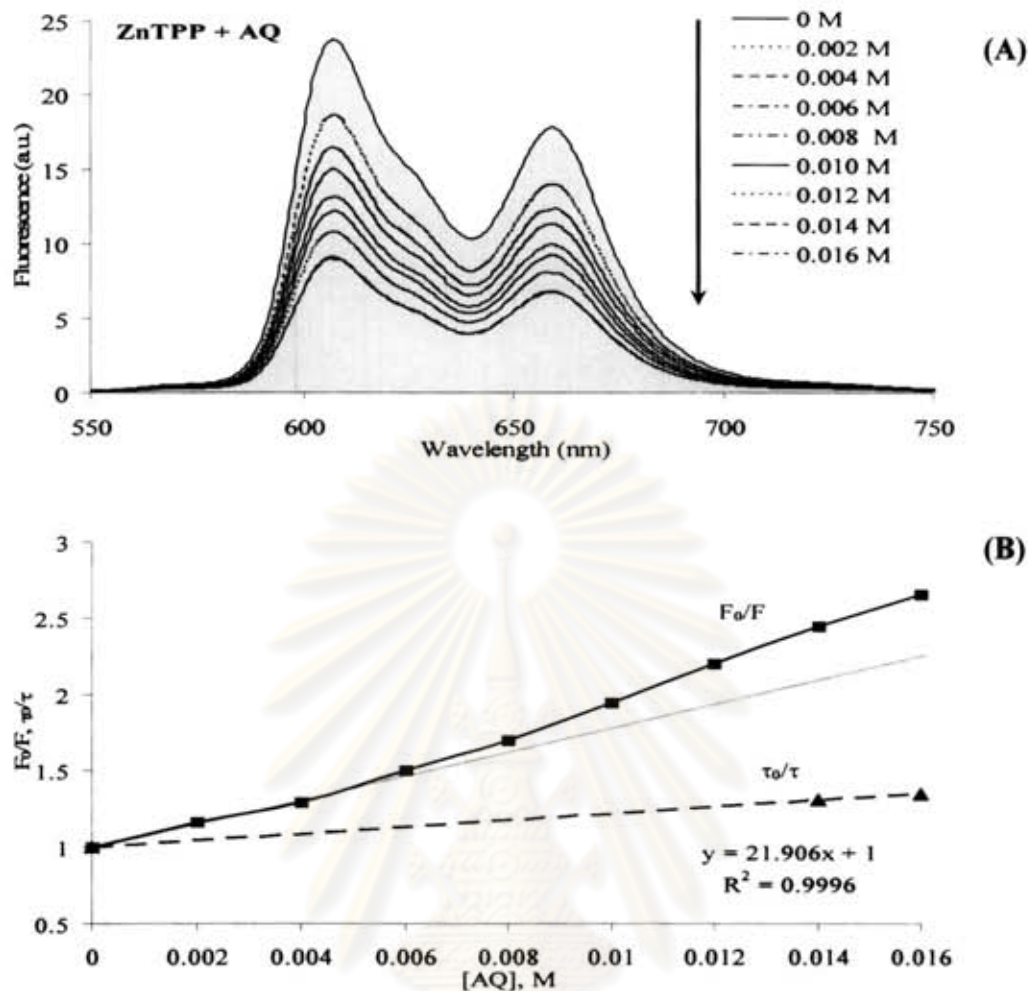


Figure 4.34 Fluorescence quenching (A) and Stern-Volmer plots (B) of fluorescence quenching of $5 \times 10^{-6} \text{ mol.dm}^{-3}$ ZnTPP by AQ concentration 0.002-0.016 M in DMAc

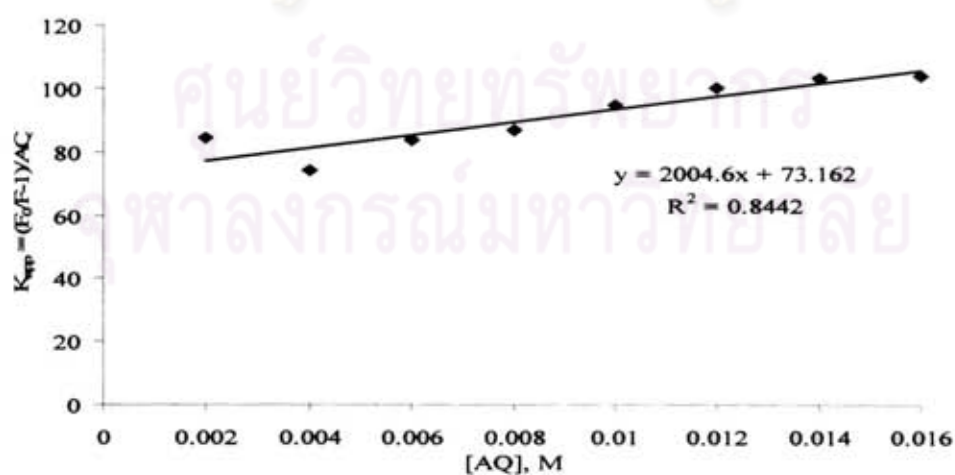


Figure 4.35 Plot of $[(F_0/F) - 1]/[AQ]$ vs. AQ for ZnTPP fluorescence quenching by AQ in DMAc

CHAPTER V

CONCLUSION

Four series of porphyrin-containing polyimides were synthesized. All of them showed good thermal and thermooxidative properties measured by TGA analysis. They all had high decomposition temperature at above 500 °C. It was found that the existence of either one of *cis*-DATPP or *trans*-DATPP or *cis*-ZnDATPP or *trans*-ZnDATPP in the polymer did not significantly affect the thermal stabilities of these polyimides as compared to the polyimide without porphyrin. They exhibited significantly higher viscosities than polyimides without porphyrin. It was postulated that the aggregation of polyimide chain might occur *via* pi-pi interaction of porphyrin units, and in case of zinc porphyrin-containing polyimides, the axial ligation to the zinc porphyrin additionally influenced on the decrease in viscosity.

These porphyrin-containing polyimides were soluble in common organic solvents. Their spectroscopic properties were determined in two solutions as CH₂Cl₂ and DMAc. The absorption and fluorescence spectra of polyimides containing *cis*- and *trans*-DATPP were essentially the same in their absorption, fluorescence maxima and band profiles as TPP while the polyimides containing *cis*- and *trans*-ZnDATPP were the same as ZnTPP. Accordingly incorporation of either *cis*- or *trans*-DATPP or *cis*- or *trans*-DATPP gave the polyimides with the same thermal and spectroscopy properties. In other words the pattern of the incorporation did not have a significant effect on the molecular arrangement of the polymers.

The fluorescence quantum yields of these polyimides in the absence of quencher was found that the rate of electron transfer (k_{ET}) from excited-state porphyrin unit within the polymer to diimide acceptor groups in both CH₂Cl₂ and DMAc are very fast when increasing the porphyrin moiety due to self quenching. In the case of metalloporphyrins, k_{ET} was significantly larger than the corresponding porphyrins. The lower values of Φ_f and more rapid k_{ET} in both CH₂Cl₂ and DMAc for the zinc porphyrin-containing polymers appeared to support the chain coiling effect. Accordingly, these polyimides have great potential in photonic applications.

Fluorescence quenching of porphyrin monomers and polyimides-containing porphyrin by an external electron acceptor (AQ) were found that the fluorescence

intensity decreases upon successive addition of AQ. The Stern-Volmer plots are linear in the relatively low concentration range investigated for free-base porphyrin and metalloporphyrin by AQ. The observed decrease in the fluorescence intensity is due to quenching of the excited singlet state of the porphyrin in the presence of AQ. TPP ($\tau_0=9.21$ ns in CH_2Cl_2 and 11.94 ns in DMAc) was characterized by longest lifetimes compared to ZnTPP ($\tau_0=1.97$ ns in CH_2Cl_2 and 1.94 ns in DMAc). This result implied that TPP could interact with the anthraquinone quencher for a longer period of time in the nanosecond time range. The bimolecular quenching rate constant k_q of TPP and ZnTPP were found to be 1.59×10^{10} and $4.72 \times 10^{10} \text{ M}^{-1} \text{ s}^{-1}$ in CH_2Cl_2 and 8.00×10^9 and $3.19 \times 10^{10} \text{ M}^{-1} \text{ s}^{-1}$ in DMAc. A possible explanation for the high k_q values of ZnTPP could be due to rapid fluorescence quenching by AQ.

Fluorescence quenching of the excited singlet states of porphyrin-containing polyimides in the presence of AQ were also observed. These observations suggest that the small amount of porphyrin in the polymer chain (e.g. 5%) dissolves in the solvent more freely and less aggregation causes AQ to easily collide and attach with the PI species. In contrast, the greater amount 30% of ZnTPP moiety in the polymer, which is crowded with bulky polyimide pendants, is sterically protected from a direct contact with AQ, a quencher with a large molecular size. The polyimides-containing metalloporphyrins (series III and IV). The k_q of polyimides in CH_2Cl_2 and DMAc were similar, indicating that solvent polarity was not significantly affected the fluorescence quenching of the excited-state polyimides and the amount of zinc-porphyrin in the polymer chain.

At high anthraquinone concentration of TPP and ZnTPP in both of CH_2Cl_2 and DMAc can be explained involving both static and dynamic quenching mechanisms. It was found that increasing concentration of AQ the plot of (τ_0/τ) versus $[Q]$ upward formed the straight line. This indicates the presence of parallel quenching process, such as static and dynamic quenching. This result was concluded that the static quenching component (K_s) is larger when compared to the dynamic component (K_D) both of CH_2Cl_2 and DMAc.

This result was concluded that the pattern of incorporation of porphyrin by using *cis*- or *trans*-porphyrin in polyimides did not have a significant effect on the molecular arrangement, optical properties and the effect rate of electron transfer.

Suggestions for further work

1. Study glass transition temperature (T_g) of all polyimides using thermomechanical analysis (TMA) of thin films.
2. Optimize the electron transfer properties of these polymers by modifying the acceptor group as well as the ratio of porphyrin/acceptor within the copolymer to determined Organic light-emitting devices.



ศูนย์วิทยทรัพยากร
จุฬาลงกรณ์มหาวิทยาลัย

REFERENCES

- [1] Leupold, D., Freyer, W. *Photochem Photobiol B: Biol.* 21 (1992): 311.
- [2] Freyer, W., Stiel, H., Truchner, K., Leupold, D. *Photochem Photobiol A.*, 80 (1994): 161.
- [3] Vicente, M. G. H.; Shetty, S., Wickramasinghe, A., Smith, K. M. Syntheses of carbon-carbon linked carboranylated porphyrins for application in boron neutron capture therapy of cancer. *Tetrahedron Lett.* 41 (2000): 7623.
- [4] Gust, D., Very Small Arrays, *Nature.* 386 (1997): 21.
- [5] Kalyanasundaram, K. Photochemistry of polypyridine and porphyrin complexes. London and New York: Academic Press, 1992.
- [6] Berezin, BD. *Russ J Inorg Chem.* 37 (1992): 634.
- [7] Bensasson, RV., Land, EJ., Trucott, TG. Primary photoprocesses in biology and medicine. New York: Plenum Press, 1985.
- [8] Jori, G., Perria, C. Photodynamic therapy of tumors and other diseases. *Libreria Progetto Padova*, 1985.
- [9] Arnold, Jr F. E., Cheng, S. Z. D., Hsu, S. L. C., Lee, C. J. and Harris, F. W. Organo-soluble, segmented rigid-rod polyimide films: 2 properties for microelectronic application. *Polymer.* 33 (1992): 5179.
- [10] Harris, F W., Lin, S. H., Li, F. and Cheng, S. Z. D. Organo-soluble polyimides: synthesis and polymerization of 2,2'-disubstituted-4,4',5,5'-biphenyl tetracarboxylic dianhydrides. *Polymer.* 37 (1996): 5049.
- [11] Lin, S. H., Li, F., Cheng, S. Z. D. and Harris, F. W. Organo-soluble polyimides: synthesis and polymerization of 2,2'-bis(trifluoromethyl)-4,4',5,5'-biphenyltetracarboxylic dianhydride. *Macromolecules.* 31 (1998): 2080.
- [12] Nisikata, Y., Morikawa, A., Kakimoto, M. A., Imai, Y., Nishiyama, K. and Fujihira, M. Preparation and photocurrent properties of tin dioxide electrode modified by polyimide langmuir blodgett films possessing tetraphenylporphyrin unit. *Polymer J.* 22 (1990): 593.

- [13] Xu, Z. K., Zhu, B. K. and Xu, Y. Y. Photoinductivity of copolyimide films containing tetraphenylporphyrin and carbazole moieties. *Chem. Mater.* 10 (1998): 1350.
- [14] Zhu, B. K., Xu, Z. K. and Xu, Y. Y. Synthesis and electrophotographic properties of copolyimides containing tetraphenylporphyrin. *Eur Polym J.* 35 (1999): 77.
- [15] Zhu, B. K., Xu, Y. Y., Wei, X. Z. and Xu, Z. K. Synthesis and photoconductive characteristics of biphenylporphyrin-containing poly(amic acid) and Polyimides. *Polym. Int.* 53 (2004): 708.
- [16] Abraham, R. J., Smith, K. M., Goff, D. A., Simpson, D.J. NMR spectra of porphyrins ring currents in hydroporphyrins. *J. Am. Chem. Soc.* 109 (1987): 4786.
- [17] Kadish, K. M., Smith, K. M., Guillard, R. *The porphyrin handbook.* Burlington: Academic Press. 1999.
- [18] Hewson, W, D. and L, P. Hager. Peroxidases, vatalases and chloroperoxidase. Academic Press. 7 (1979): 295.
- [19] Ferguson-Miller, S., D. L. Brautigan and E. Margoliash. The electron transfer function of cytochrome C. Academic Press. (1979): 149.
- [20] Gibson, Q. H. The oxygenation of hemoglobin. Academic Press. (1979): 153.
- [21] Smith, K. M. Porphyrin and metalloporphyrins. *Elsevier Science Publishers.* 1975.
- [22] Mittal, K. L. Polyimides: Synthesis, characterization and applications. *Plenum,* New York. 1984.
- [23] Bessonov, M.T., Koton, M.M., Kudryavtsev, V.V. and Laius, L.A. Polyimides: thermally stable polymers consultants bureau. New York. 1987.
- [24] Wilson, D., Stenzenberge, H. D. and Hergenrother, P.M. Polyamides blackie glasgow. *Eur. Polym. J.* 1990.
- [25] Ghosh, M.K. and Mittal, K. L. Polyimides: Fundamentals and Applications. New York. 1996.
- [26] Seino, H., Mochizuki, A. and Ueda, M. *J. Polym. Sci.* 37 (1999): 3584.

- [27] Tamai, S., Yamashita, A. and Yamaguchi, A. *J. Polym. Sci.* 36 (1998): 1717.
- [28] Harris, F. W. in *Polyimides* (Eds D. Wilson, H. D. Stenzenberger and P. M. Hergenrother). New York: Blackie and Son. 1990, 1-37.
- [29] Takahashi, K., Takano, Y., Yamaguchi, T., Nakamura, J. I, Yokoe, C. and Murata, K. Porphyrin dye-sensitization of polythiophene in a conjugated polymer/TiO₂ p-n hetero-junction solar cell. *Synthetic Metals*. 155 (2005): 51.
- [30] Takechi, K., Shiga, T., Motohiro, T., Akiyamab, T., Yamada, S., Nakayama, H. and Kohama, K. Solar cells using iodine-doped polythiophene-porphyrin polymer films. *Solar Energy Materials & Solar Cells*. 90 (2006): 1322.
- [31] Johanson, U., Marandi, M., Sammelseg, V. and Tamm, J. Electrochemical properties of porphyrin-doped polypyrrole Films. *Journal of Electroanalytical Chemistry*. 575 (2005): 267.
- [32] Bao, Z. N., Chen, Y. M. and Yu, L. P. New Metalloporphyrin Containing Polymers from the Heck Coupling Reaction. *Macromolecules*. 27 (1994): 4629.
- [33] Wagner, R. W. and Lindsey, J. S. A Molecular Photonic Wire. *J. Am. Chem. Soc.* 116 (1994): 9759
- [34] Harris, F. W. in *Polyimides* (Eds D. Wilson, H. D. Stenzenberger and P. M. Hergenrother). New York: Blackie and Son. 1990.
- [35] Anannarukan, W., Tantayanon, S., Zhang, D., Aleman, E. A., Modarelli, D. A. and Harris, F. W. Soluble polyimides containing *trans*-diaminotetraphenyl porphyrin: Synthesis and photoinduced electron transfer. *Polymer*. 47 (2006): 4936.
- [36] Adler, A.D., Longo, F. R., Finarelli, J. D., Goldmacher, J., Assour, J., Korsakoff, L. A simplified synthesis for meso-tetraphenylporphine. *J. Org. Chem.* 32 (1967): 476.

- [37] Arunwattanachok, T., Bhanthumnavin, W. and Sritana-anant, Yongsak. Synthesis of pyridylporphyrin metal complexes. Thesis; The Degree of Master of Science Program in Petrochemistry and Polymer Science, Chulalongkorn University of Thailand 2006.
- [38] Raymond, L., Laurent, J., Frank, R., Fronczek, M., Graca, H. V. and Kevin, M.S. Synthesis and reactions of *meso*-(*p*-nitrophenyl)porphyrins. *Tetrahedron*. 60 (2004): 2757.
- [39] Shiang, W. R. and Woo, E. P. Soluble Copolyimides with High Modulus and Low Moisture Absorption. *J. Polym. Sci.* 31 (1993): 2081.
- [40] Li, F., Fang, S., Ge, J. J., Honigfort, P. S., Chen, J. C., Harris, F. W. and Cheng, S. Z. D. Diamine architecture effects on glass transitions, relaxation processes and other material properties in organo-soluble aromatic polyimide films. *Polymer*. 40 (1999): 4571.
- [41] Yin, J., Ye, Y. F. and Wang, Z. G. Study on Preparation and Properties of Polyimides Containing Long Flexible Chain in the Backbone. *Eur. Polym. J.* 34 (1998): 1839.
- [42] Karangu, N. T., Rezac, M. E. and Beckham, H. W. Synthesis and properties of processable polyimides containing diacetylene group. *Chem. Mater.* 10 (1998): 567.
- [43] Chung, I. S and Kim, S. Y. Soluble polyimides from unsymmetrical diamine with trifluoromethyl pendent group. *Macromolecules*. 33 (2000): 3190.
- [44] Harris, F. W., Sakaguchi, Y., Shibata, M and Cheng, S. Z. D. Organo-soluble polyimides: Synthesis and Characterization of Polyimides Containing phenylated *p*-biphenyl and *p*-terphenyl units. *High Perform. Polym.* 9 (1997): 251.
- [45] Agnieszka, D., Krystyna, U., Zenon, M., Marta, P., Luis, G. A., Jan, H., Alicja, R. and Grazyna, S. Tritolporphyrin dimer as a new potent

- hydrophobic sensitizer for photodynamic therapy of melanoma. *Acta Biochimica Polonica* 48 (2001).
- [46] Strachan, J. P., Gentemann, S., Seth, J., Kalsbeck, W. A., Lindsey, J. S., Holten, D. and Bocian, D. F. Effects of orbital ordering on electronic communication in multiporphyrin arrays. *J. Am. Chem. Soc.* 119 (1997).
- [47] David, R. L. Fluid properties. *CRC Handbook of chemistry and physics*, 77 (1996): 208.
- [48] Hunter, C. A. and Sanders, J.K. M. The nature of π - π interactions. *J. Am. Chem. Soc.* 112 (1990): 5525.
- [49] Lakowicz, J. R. Quenching of fluorescence. *Principles of Fluorescence Spectroscopy*. 3 (2006): 237.
- [50] Yasa, S., Kamachi, M. and Morishima, Y. Photophysical behavior of zinc(II) tetraphenylporphyrin covalently incorporated in a cholesterol-bearing polymethacrylate. *Photochemistry and Photobiology*. 67 (1998): 519.
- [51] Yingyan, S., Wenqi, Z., Ziheng, L., Xingqiao, W., Dejun, W., Shilun, Q. and Xiangqing, Li. Electro-optical properties investigation of a series of hydroxylphenylporphyrins. *Optical Materials*. 28 (2006): 1178.
- [52] Danuta, W., Jędrzej, L. and Henryk, M. Fluorescence quenching and ESR spectroscopy of metallic porphyrins in the presence of an electron acceptor. *Dyes and Pigments*. 58 (2003): 7.
- [53] Kavarnos, GJ. and Turro, NJ. *Chem Rev.* 86 (1986): 401.
- [54] Swaminathan, M. and Radha, N. Static and dynamic model for 4-aminodiphenyl fluorescence quenching by carbontetrachloride in hexane. *Spectrochimica Acta Part A*. 60 (2004): 1839.
- [55] Sunao, Y., Toshinori, S., Koji, K. and Teiichiro, O. Fluorescence quenching of 5,10,15,20-tetra(*p*-TOLYL) porphine and its zinc complex by quinones. Charge-transfer interaction and transient effect. *Photochemistry and photobiology*. 37 (1982): 257.
- [56] Blatt, E. and W.H. Sawyer. *Biohem. Biophys. Acta*. 822 (1985): 43.

- [57] Azenha, EG., Serra, AC., Pineiro, M., Pereira, MM., Melo, JS. and Arnaut, LG. Heavy-atom effects on metalloporphyrins and polyhalogenated porphyrins. *Chemical Physics*. 280 (2002): 90.



ศูนย์วิทยทรัพยากร
จุฬาลงกรณ์มหาวิทยาลัย



APPENDICES

ศูนย์วิทยทรัพยากร
จุฬาลงกรณ์มหาวิทยาลัย

APPENDIX A

Absorption spectra of porphyrins and polyimides

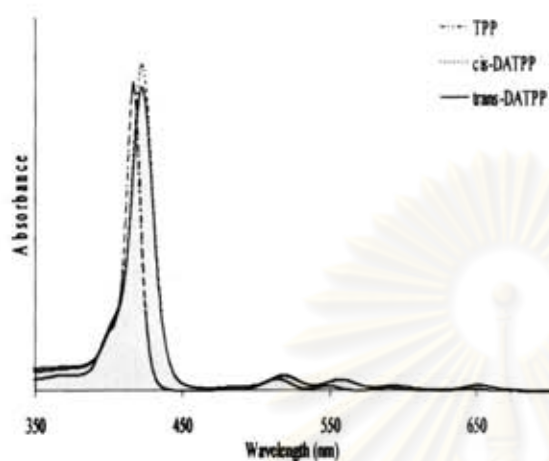
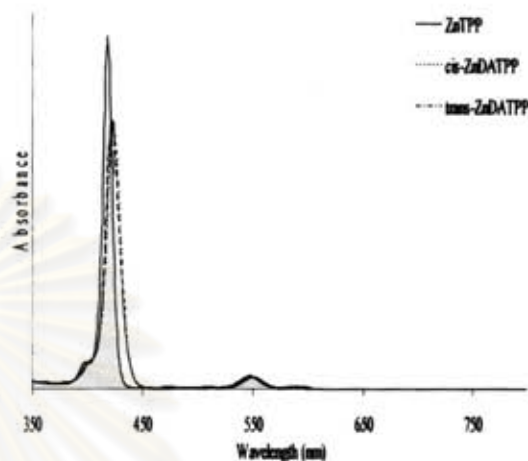
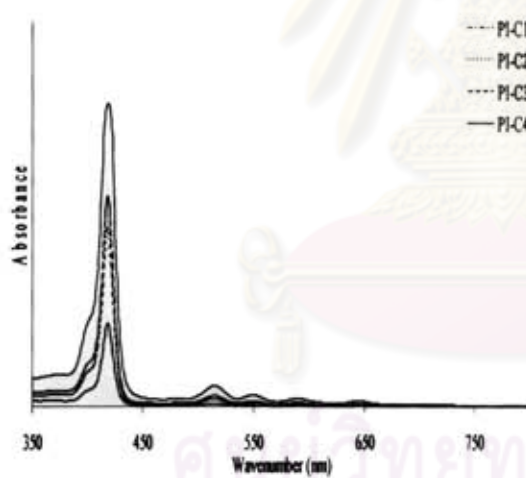
A.1 Absorption spectra of porphyrin and polyimide in CH_2Cl_2 Figure A.1.1 Absorption spectra of TPP, *cis*- and *trans*-DATPP.Figure A.1.2 Absorption spectra of ZnTPP, *cis*- and *trans*-ZnDATPP.

Figure A.1.3 Absorption spectra of polyimides in Series I.

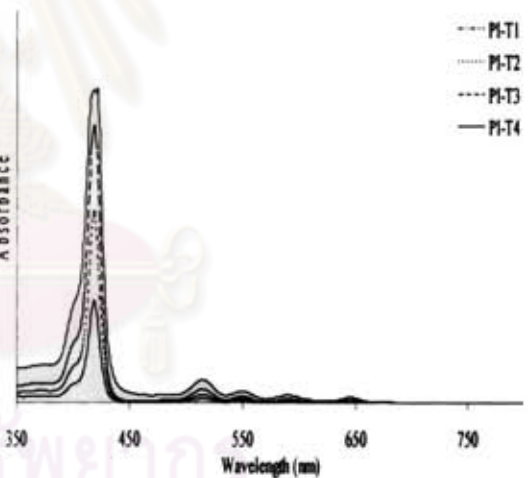


Figure A.1.4 Absorption spectra of polyimides in Series II.

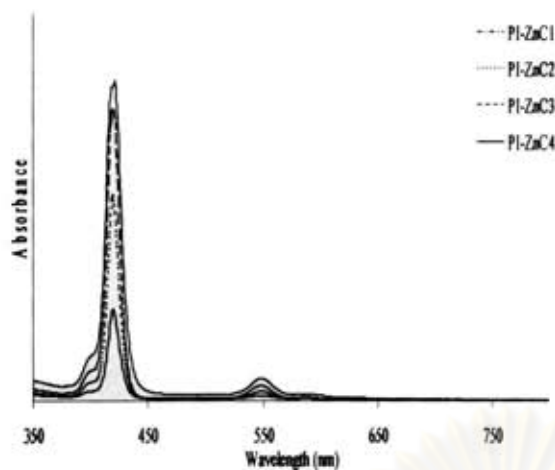


Figure A.1.5 Absorption spectra of polyimides in Series III.

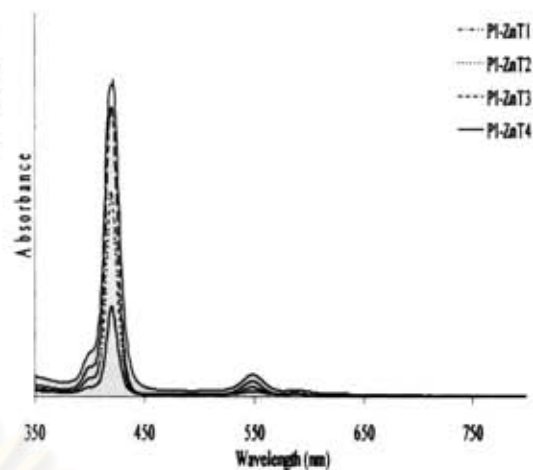
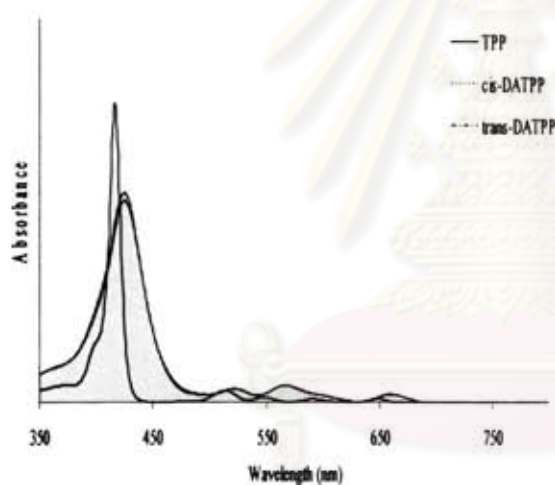
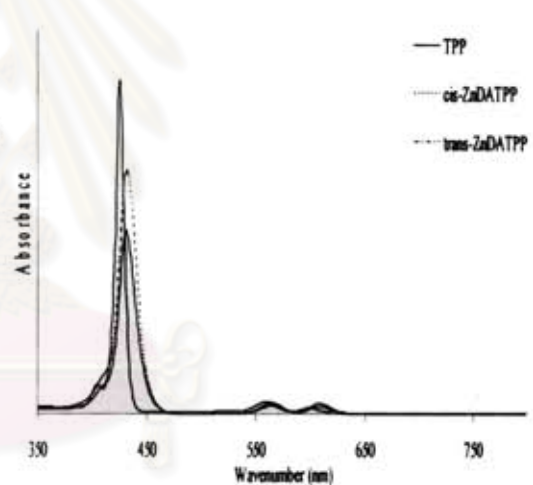


Figure A.1.6 Absorption spectra of polyimides in Series IV.

A.2 Absorption spectra of porphyrin and polyimide in DMAc

Figure A.2.1 Absorption spectra of TPP, *cis*- and *trans*-DATPP.Figure A.2.2 Absorption spectra of ZnTPP, *cis*- and *trans*-ZnDATPP.

ศูนย์วิจัยทรัพยากร
จุฬาลงกรณ์มหาวิทยาลัย

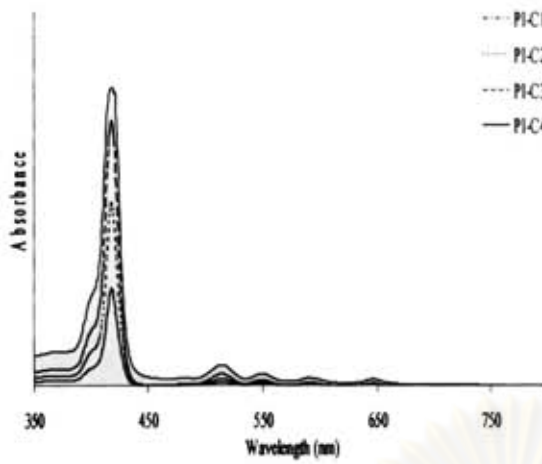


Figure A.2.3 Absorption spectra of polyimides in Series I.

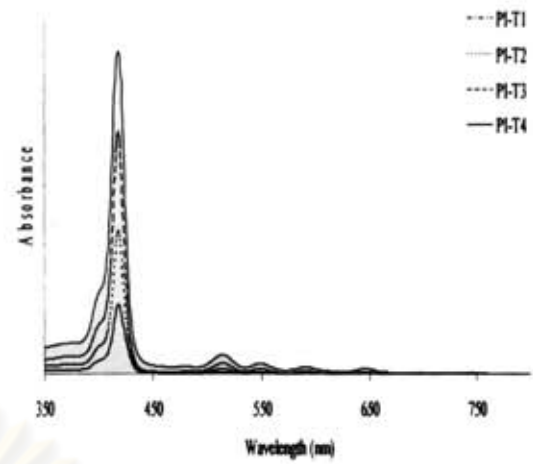


Figure A.2.4 Absorption spectra of polyimides in Series II.

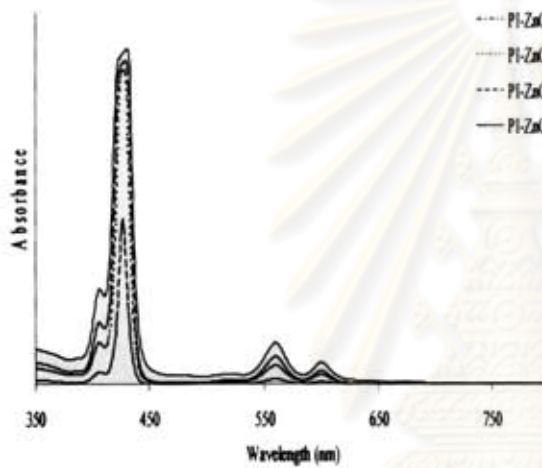


Figure A.2.5 Absorption spectra of polyimides in Series III.

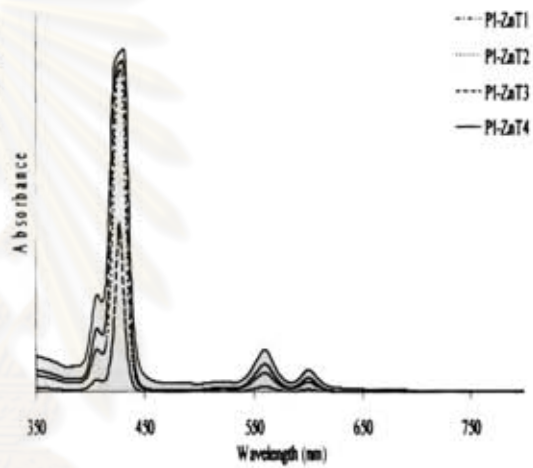


Figure A.2.6 Absorption spectra of polyimides in Series IV.

ศูนย์วิทยทรัพยากร
จุฬาลงกรณ์มหาวิทยาลัย

APPENDIX B

Fluorescence spectra of porphyrin and polyimides

B1. Fluorescence spectra of porphyrins and polyimides in CH_2Cl_2

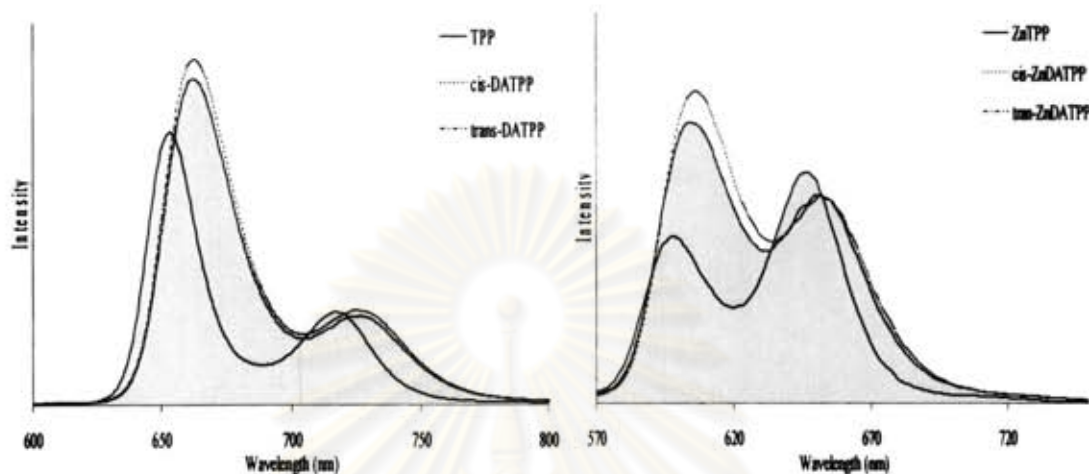


Figure B.1.1 Fluorescence spectra of TPP, *cis*- and *trans*-DATPP.

Figure B.1.2 Fluorescence spectra of ZnTPP, *cis*- and *trans*-ZnDATPP.

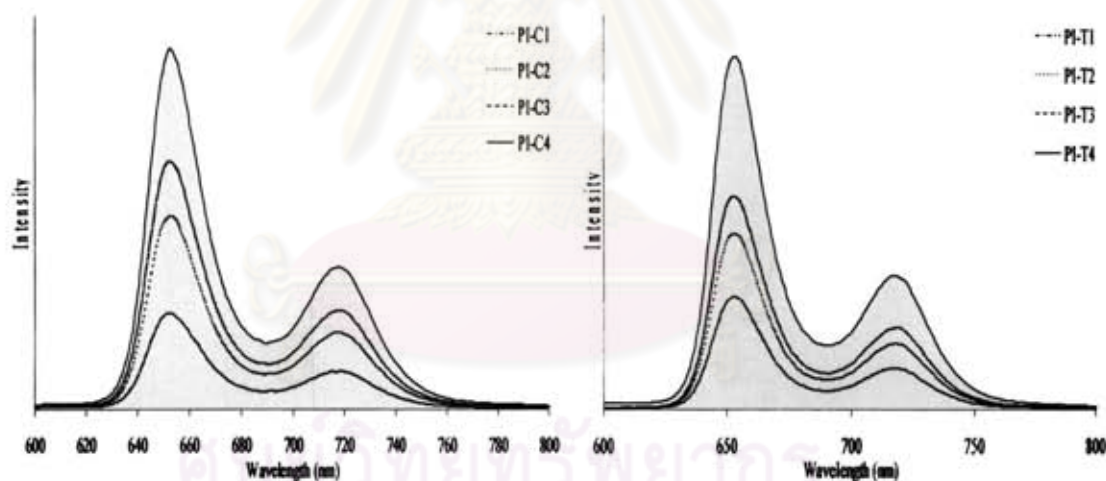


Figure B.1.3 Fluorescence spectra of polyimides in Series I.

Figure B.1.4 Fluorescence spectra of polyimides in Series II.

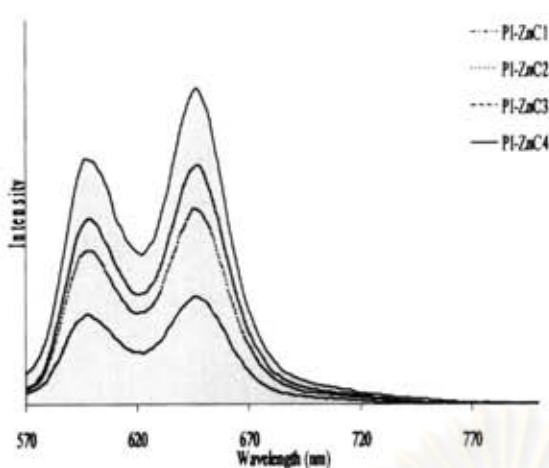


Figure B.1.5 Fluorescence spectra of polyimides in Series III.

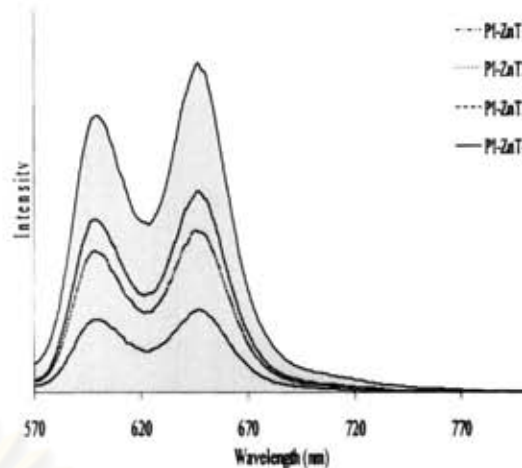


Figure B.1.6 Fluorescence spectra of polyimides in Series IV.

B2. Fluorescence spectra of porphyrins and polyimides in DMAc

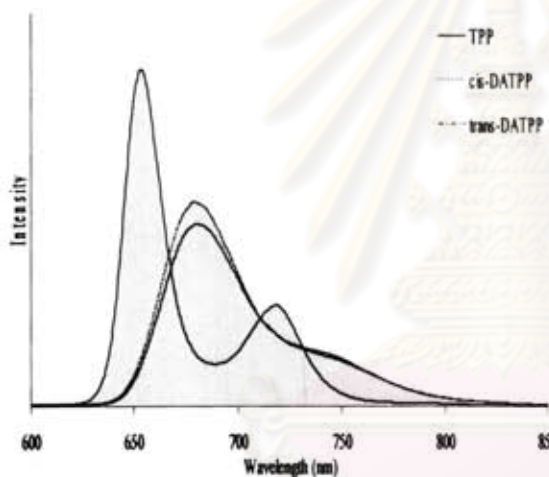
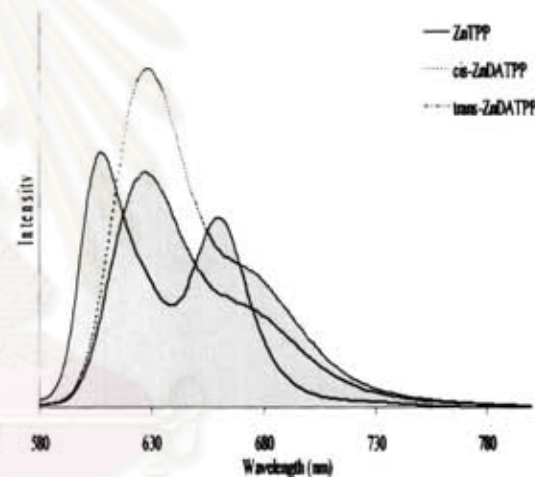
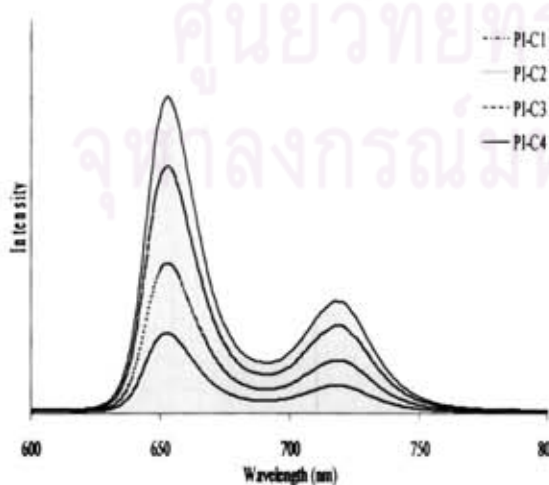
Figure B.2.1 Fluorescence spectra of TPP, *cis*- and *trans*-DATPP.Figure B.2.2 Fluorescence spectra of ZnTPP, *cis*- and *trans*-ZnDATPP.

Figure B.2.3 Fluorescence spectra of polyimides in Series I.

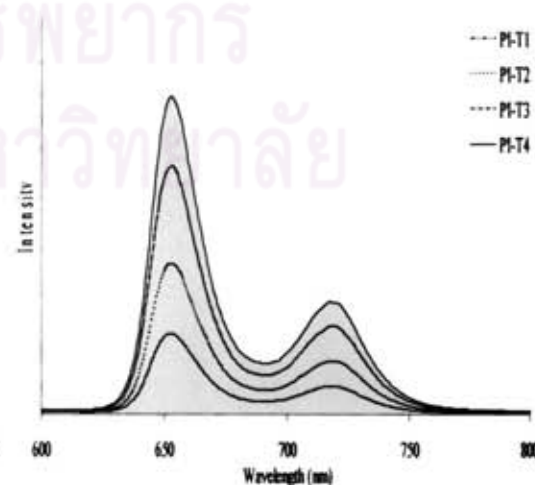


Figure B.2.4 Fluorescence spectra of polyimides in Series II.

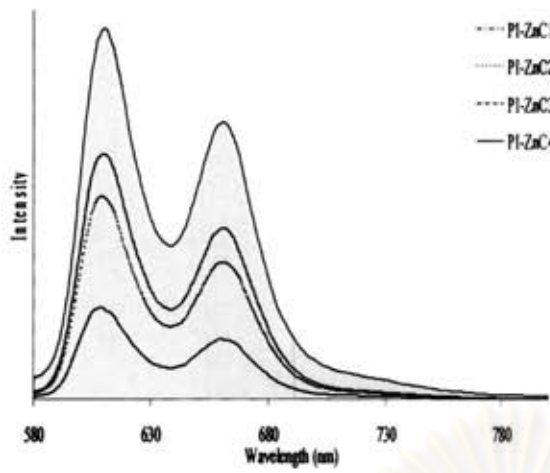


Figure B.2.5 Fluorescence spectra of polyimides in Series III.

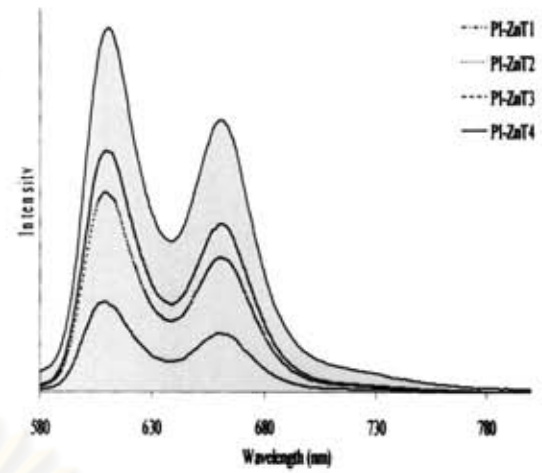


Figure B.2.6 Fluorescence spectra of polyimides in Series IV.

ศูนย์วิทยทรัพยากร
จุฬาลงกรณ์มหาวิทยาลัย

APPENDIX C

Infrared spectra of polyimides

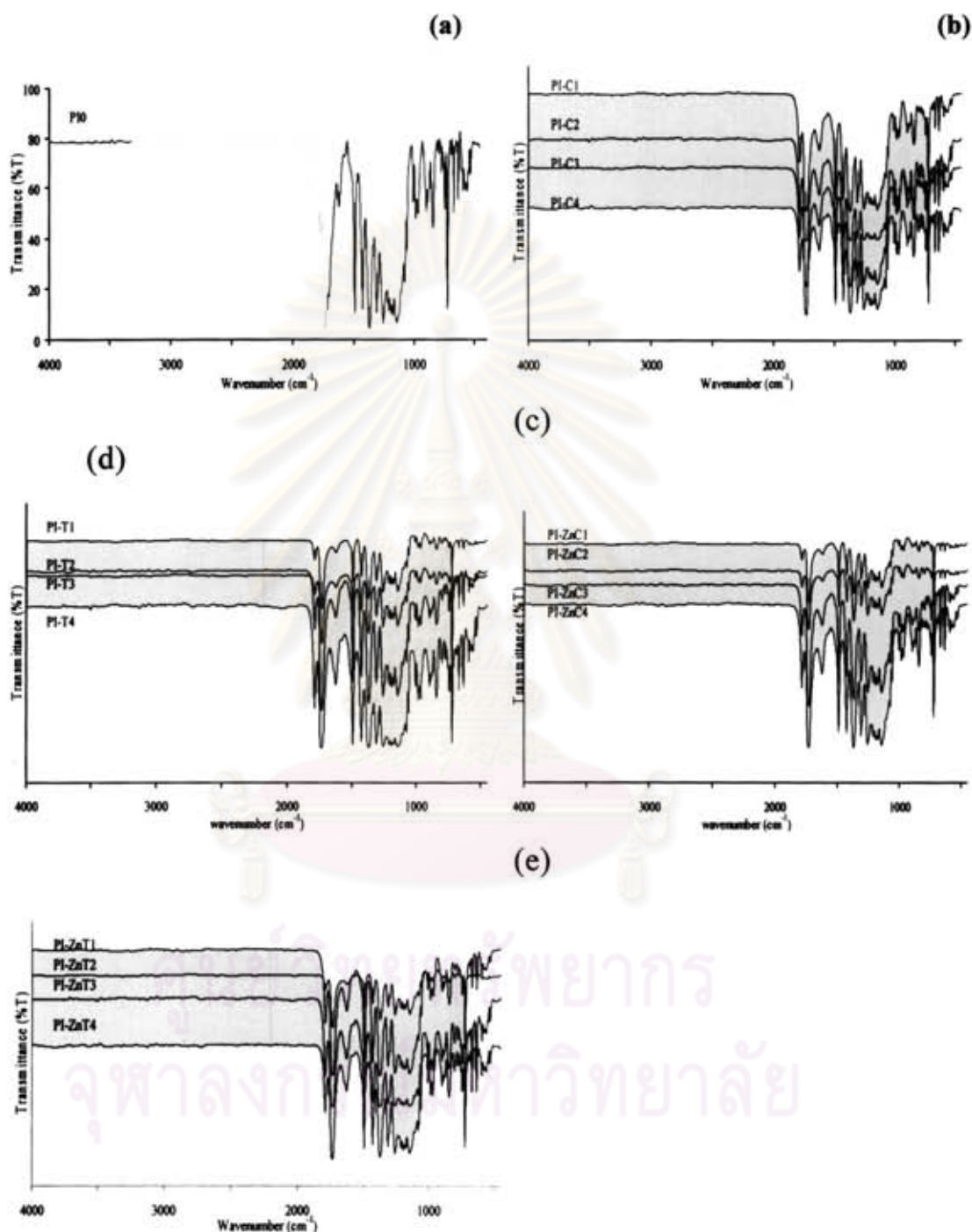


Figure C. IR spectra of polyimides; (a)PI0, (b) series I, (c) series II, (d) series III and (e) series IV.

APPENDIX D

Determination of porphyrin content in polyimides

Determination of porphyrin can be obtained by using equation

$$A = \epsilon bc$$

where A = absorbance (optical density)

ϵ = molar extinction coefficient

b = path length through the sample

c = concentration of solute

Table D. Concentration of porphyrin in polyimides

Polyimide	absorbance	ϵ^a (M ⁻¹ cm ⁻¹)	concentration	mole of porphyrin
Series I				
<i>cis</i> -DATPP				
PI-C1	0.643	461000	1.395x10 ⁻⁶	3.487 x10 ⁻⁹
PI-C2	0.832	461000	1.805x10 ⁻⁶	4.512 x10 ⁻⁹
PI-C3	1.271	461000	2.757x10 ⁻⁶	6.893 x10 ⁻⁹
PI-C4	2.420	461000	5.249x10 ⁻⁶	1.312 x10 ⁻⁸
Series II				
<i>trans</i> -DATPP				
PI-T1	0.678	461000	1.471x10 ⁻⁶	3.677 x10 ⁻⁹
PI-T2	0.880	461000	1.909x10 ⁻⁶	4.772 x10 ⁻⁹
PI-T3	1.307	461000	2.835x10 ⁻⁶	7.088 x10 ⁻⁹
PI-T4	2.318	461000	5.028x10 ⁻⁶	1.257 x10 ⁻⁸
Series III				
<i>cis</i> -ZnDATPP				
PI-ZnC1	0.821	559000	1.469x10 ⁻⁶	3.672 x10 ⁻⁹
PI-ZnC2	1.492	559000	2.669x10 ⁻⁶	6.673 x10 ⁻⁹
PI-ZnC3	2.168	559000	3.878x10 ⁻⁶	9.696 x10 ⁻⁹
PI-ZnC4	2.362	559000	4.225x10 ⁻⁶	1.056 x10 ⁻⁸
Series IV				
<i>trans</i> -ZnDATPP				
PI-ZnT1	0.801	559000	1.433x10 ⁻⁶	3.582 x10 ⁻⁹
PI-ZnT2	1.414	559000	2.529x10 ⁻⁶	6.322 x10 ⁻⁹
PI-ZnT3	2.120	559000	3.792x10 ⁻⁶	9.481 x10 ⁻⁹
PI-ZnT4	2.362	559000	4.225x10 ⁻⁶	1.056 x10 ⁻⁸

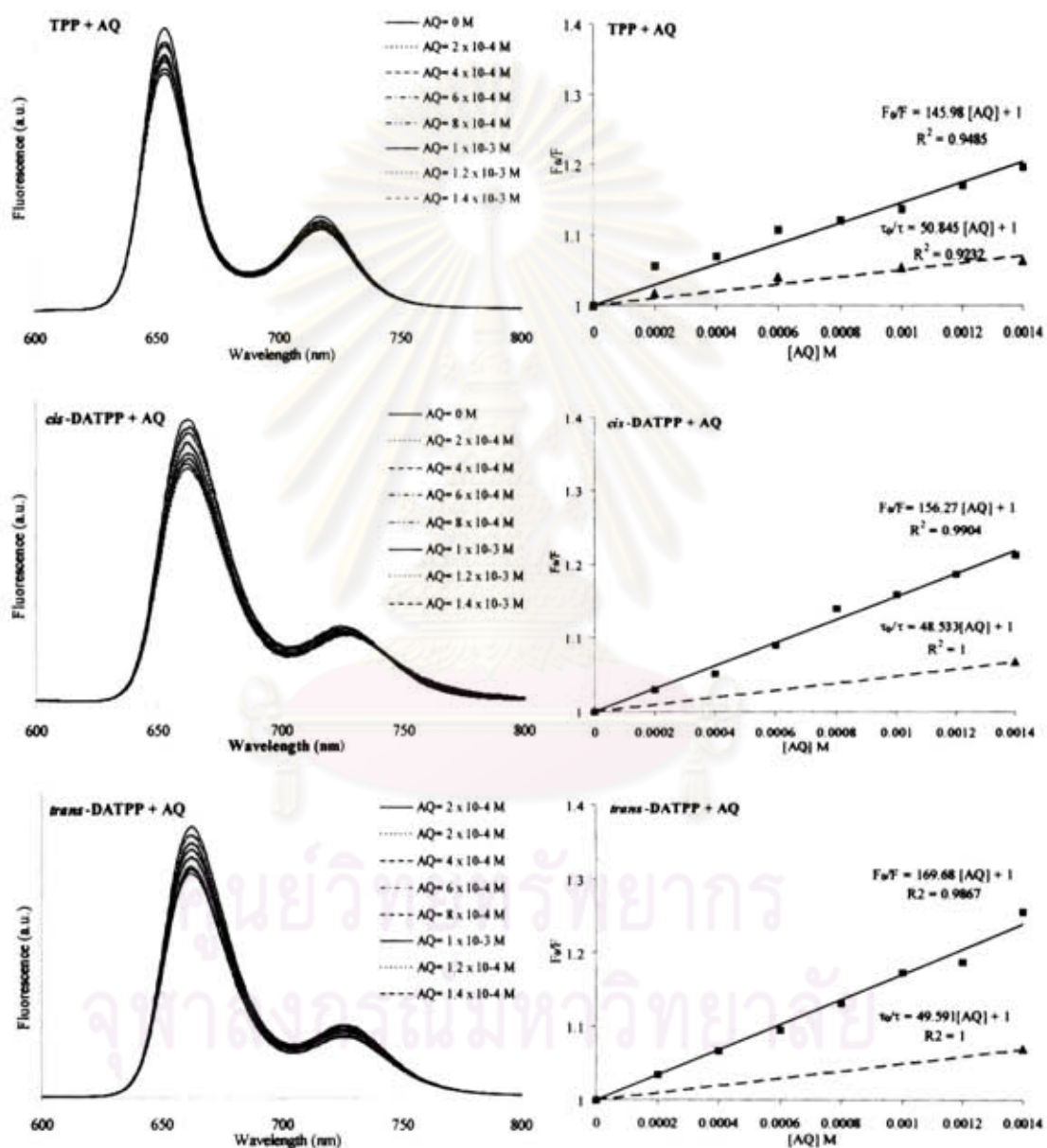
ϵ^a (CH₂Cl₂) = ϵ_{TPP} = 461000 for polyimides containing free base porphyrin.

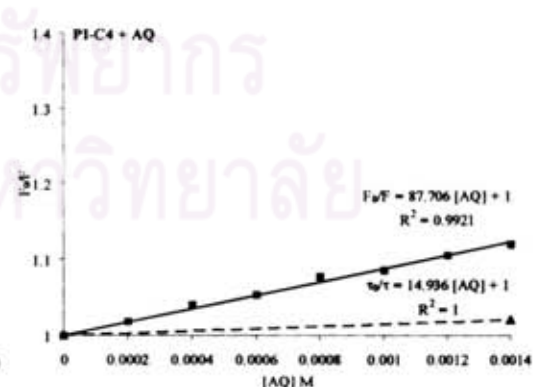
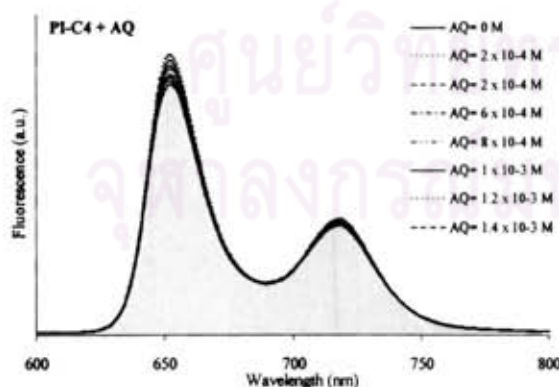
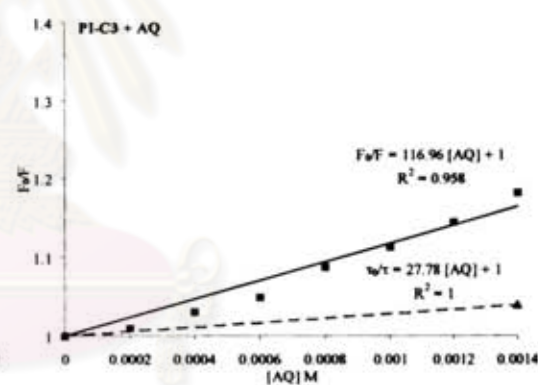
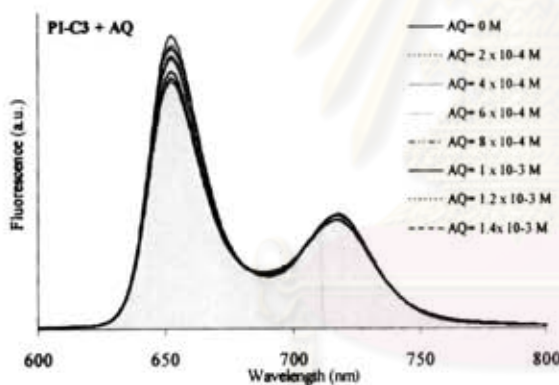
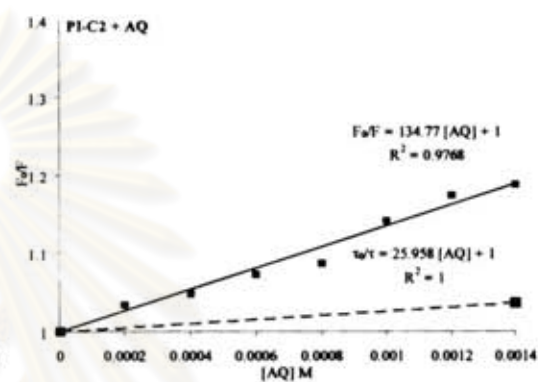
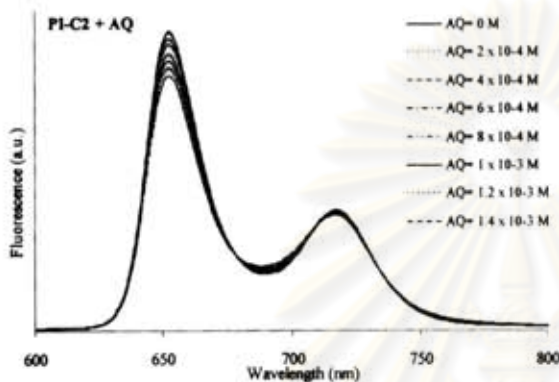
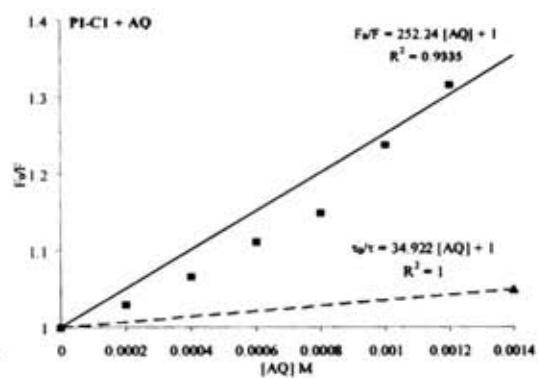
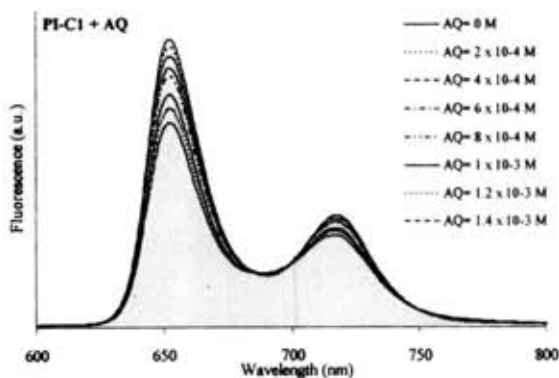
= ϵ_{ZnTPP} = 559000 for polyimides containing zinc porphyrin.

APPENDIX E

Fluorescence spectra and Stern-Volmer plot of porphyrin and polyimides

Fig.E1 Fluorescence spectra and Stern-Volmer plots of TPP, *cis*-, *trans*-DATPP and polyimides containing 5-30% (Series I and II) by Anthraquinone in CH₂Cl₂





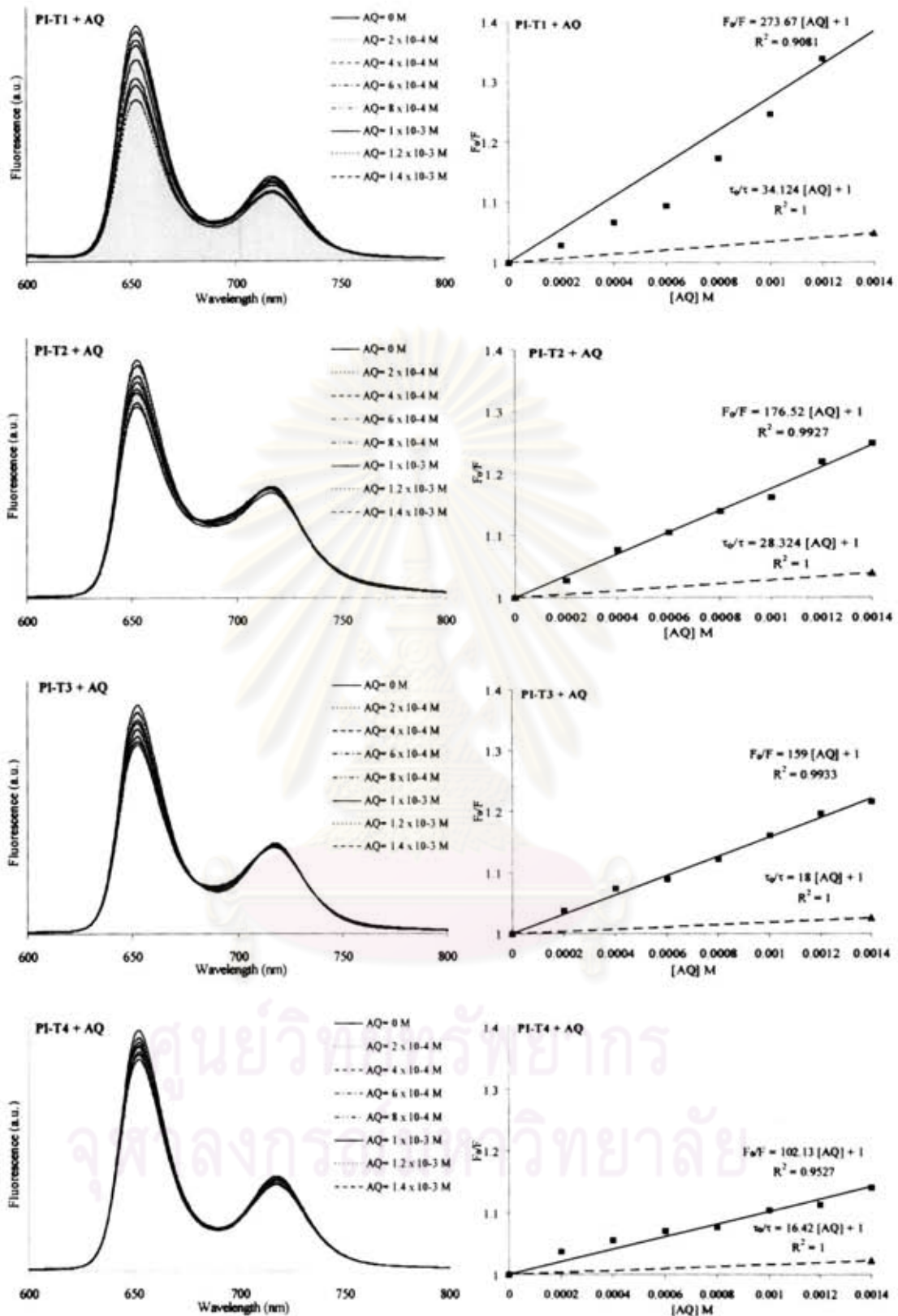
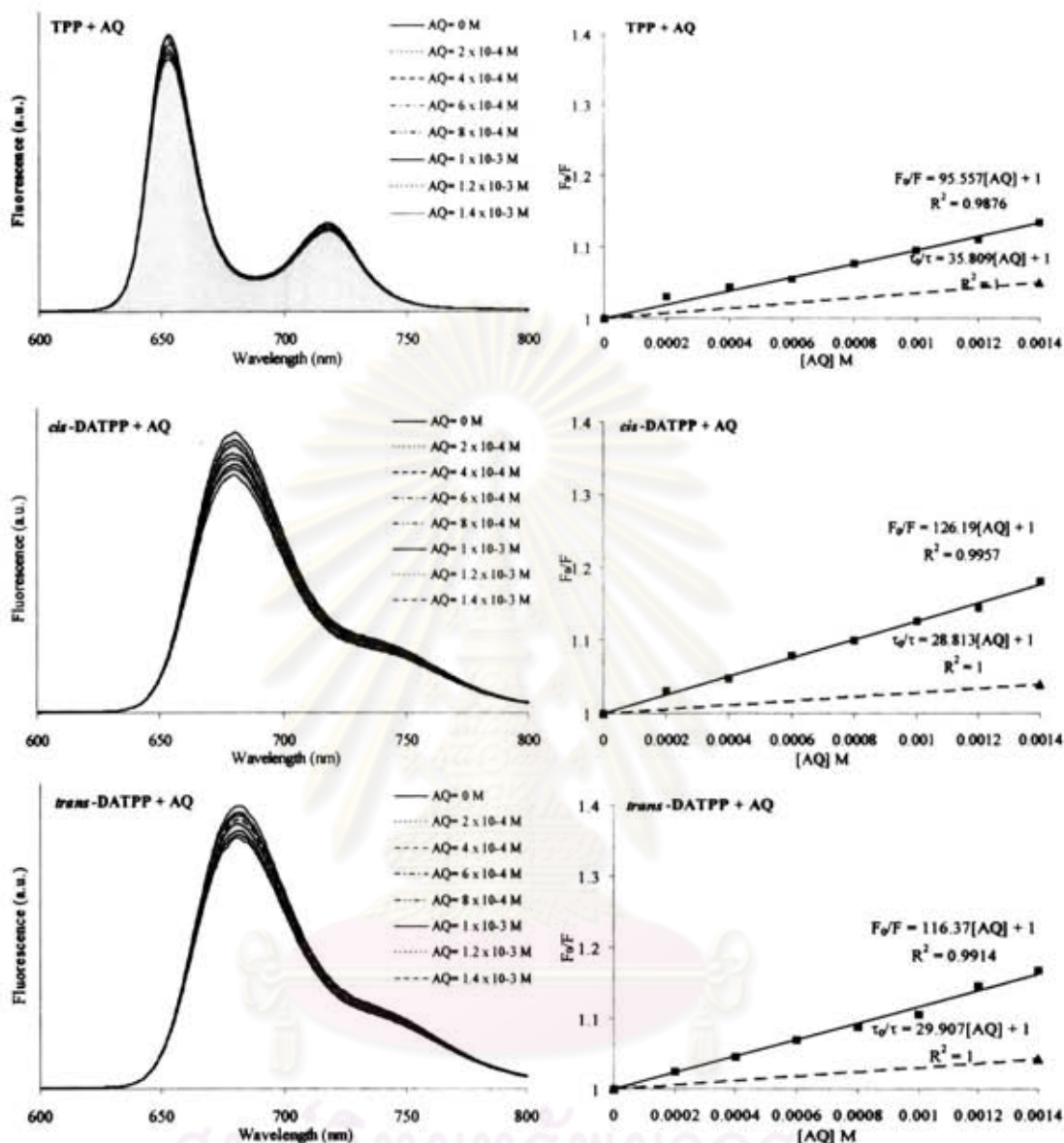
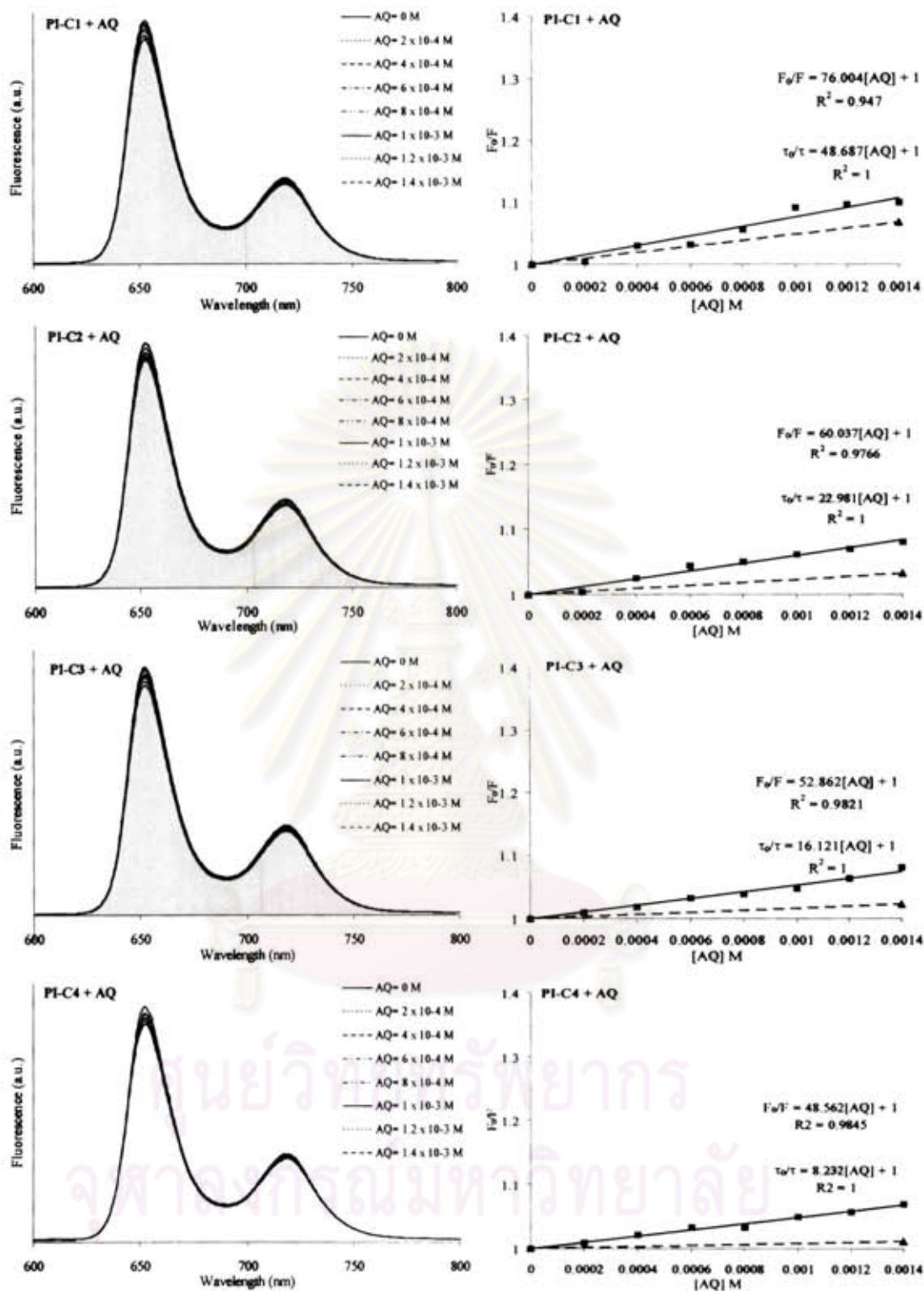


Fig.E2 Fluorescence spectra and Stern-Volmer plots of TPP, *cis*-, *trans*-DATPP and polyimides containing 5-30% (Series I and II) by Anthraquinone in DMAc



ศูนย์วิทยทรัพยากร
จุฬาลงกรณ์มหาวิทยาลัย



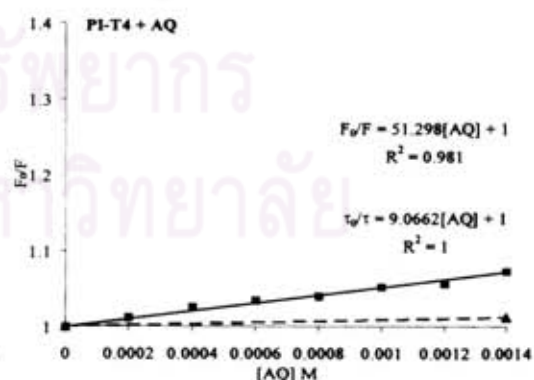
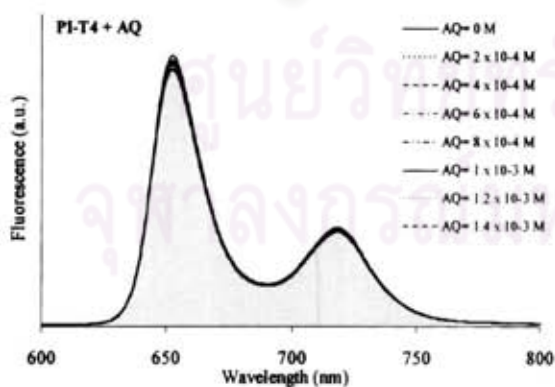
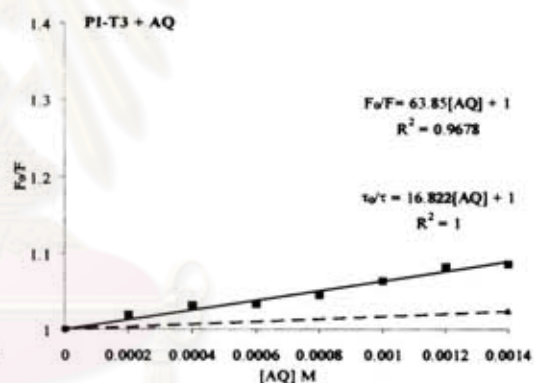
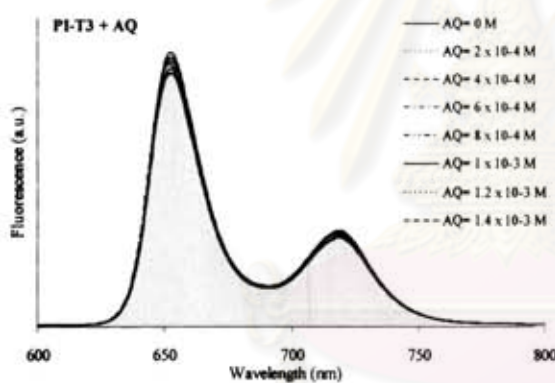
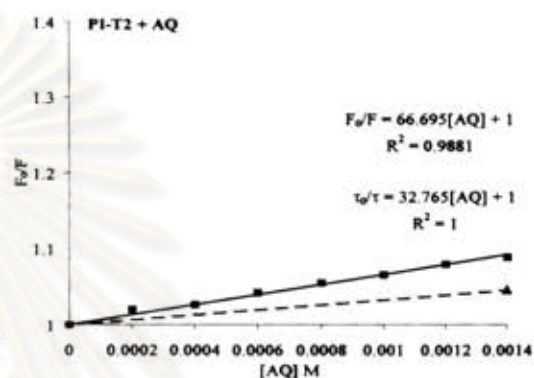
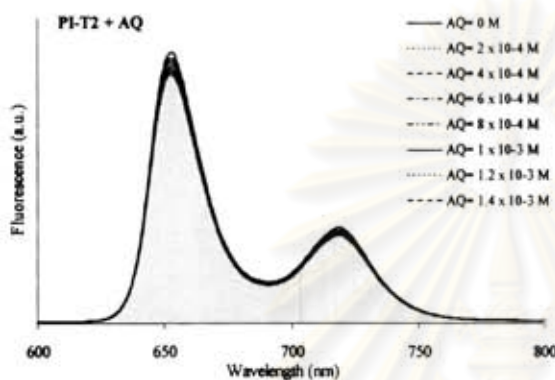
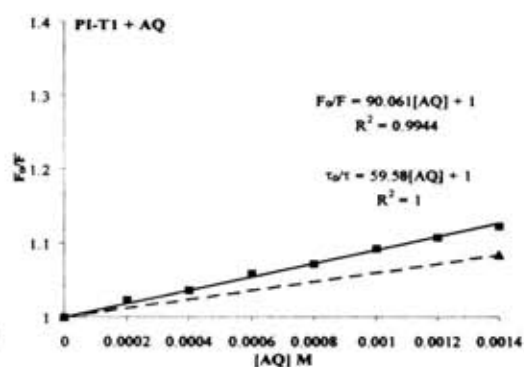
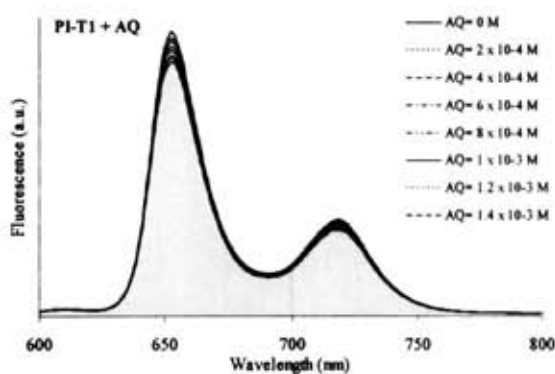
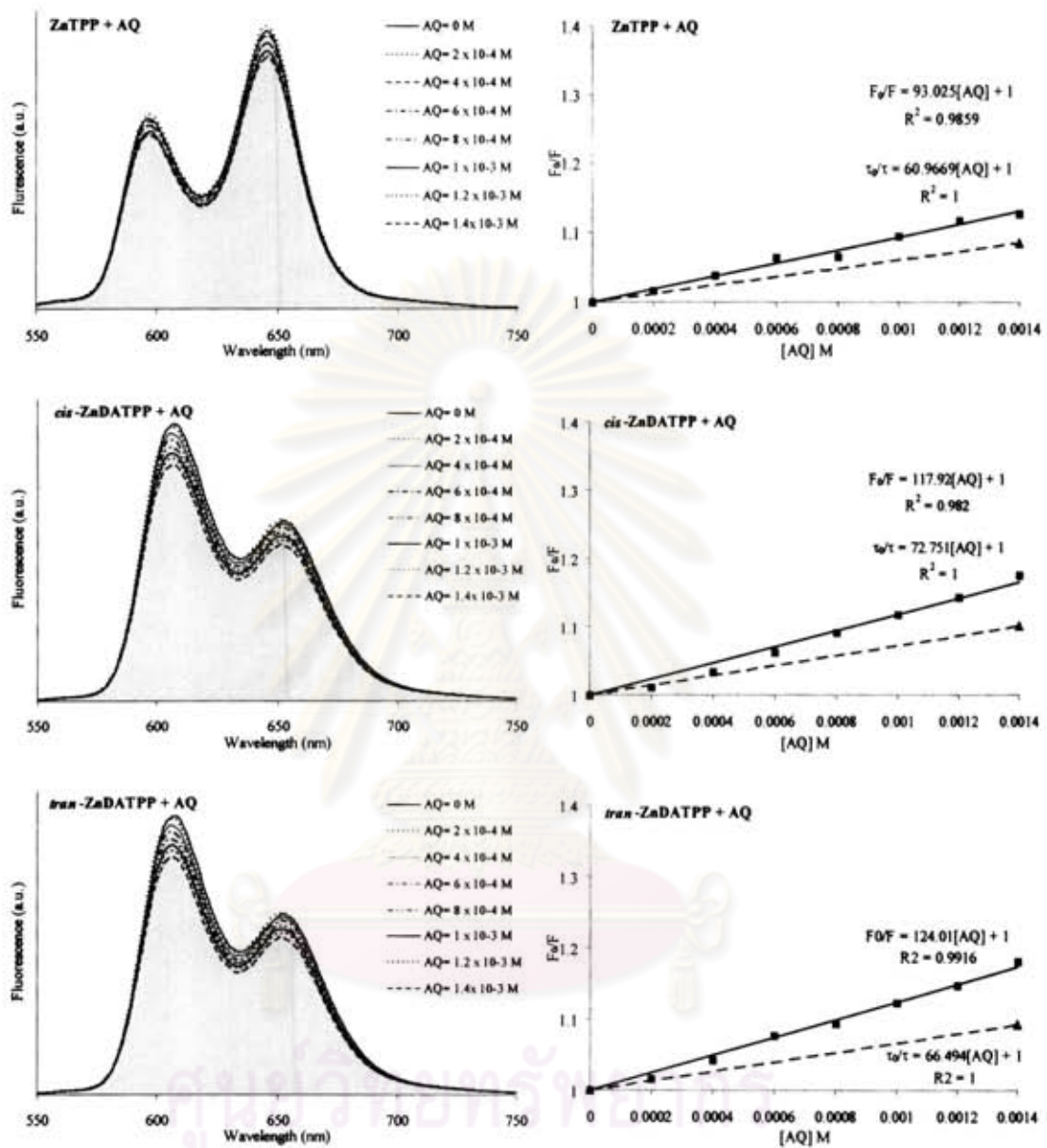
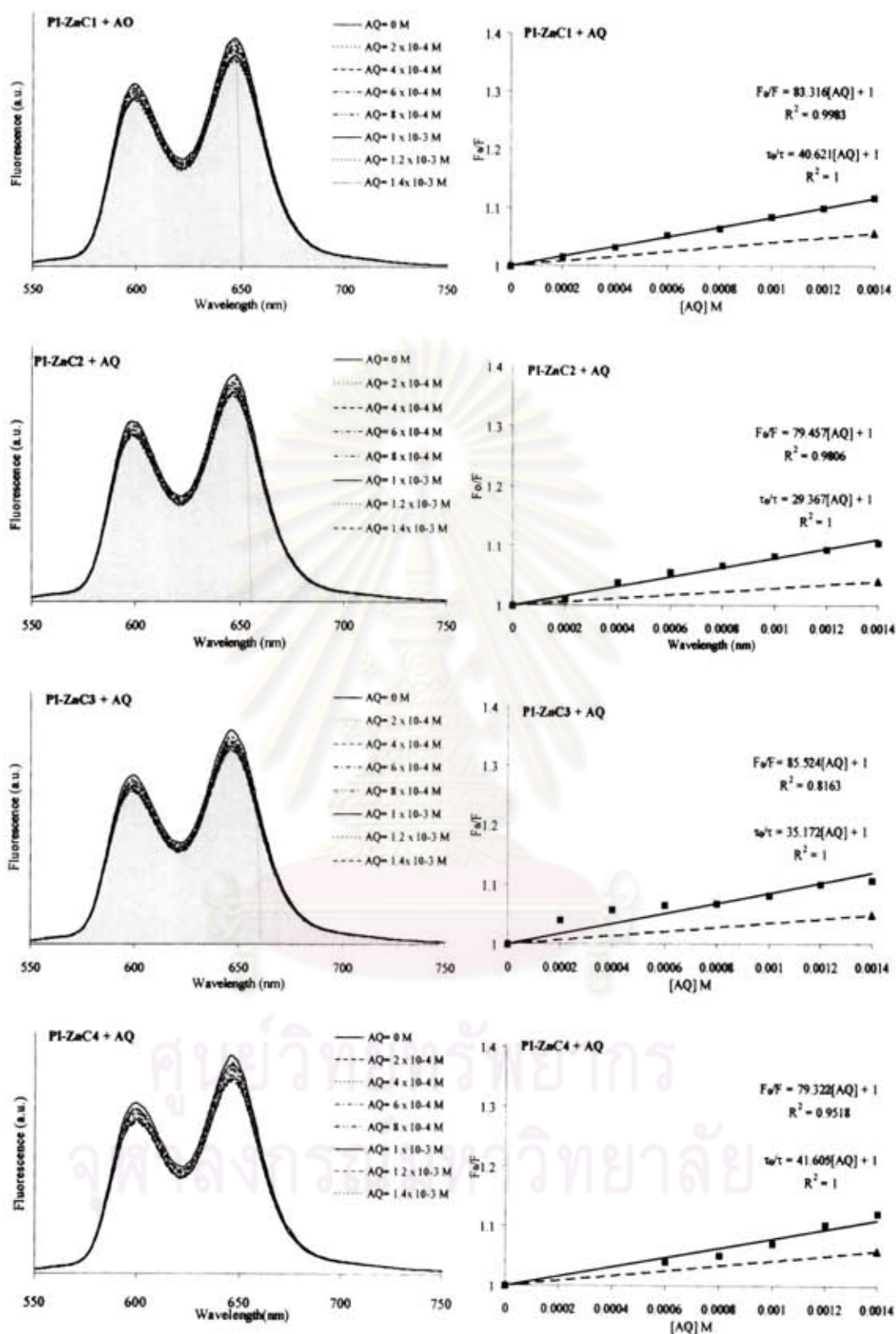


Fig.E3 Fluorescence spectra and Stern-Volmer plots of TPP, cis-, trans-DATPP and polyimides containing 5-30% (Series III and IV) by Anthraquinone in CH_2Cl_2



จุฬาลงกรณ์มหาวิทยาลัย



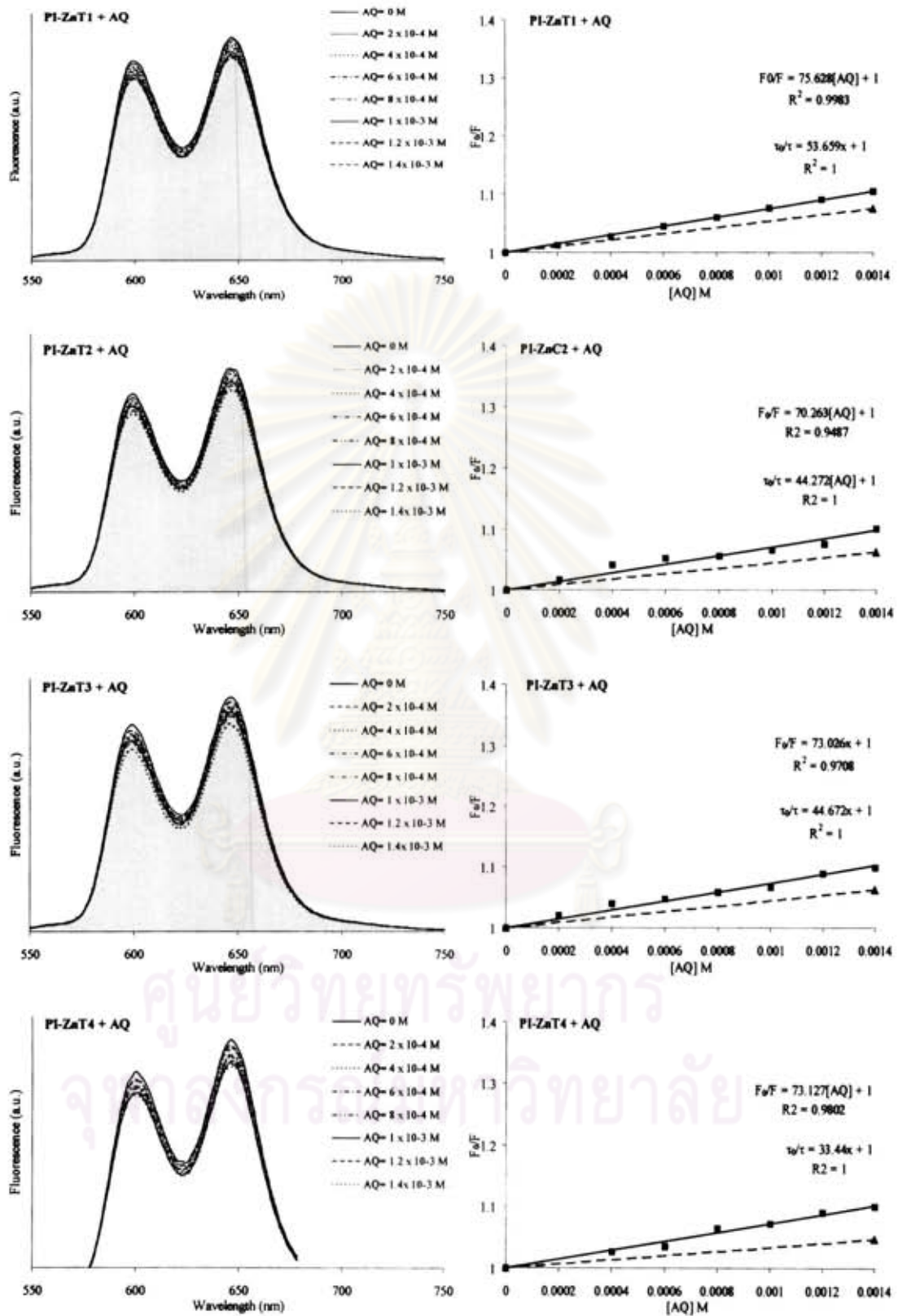
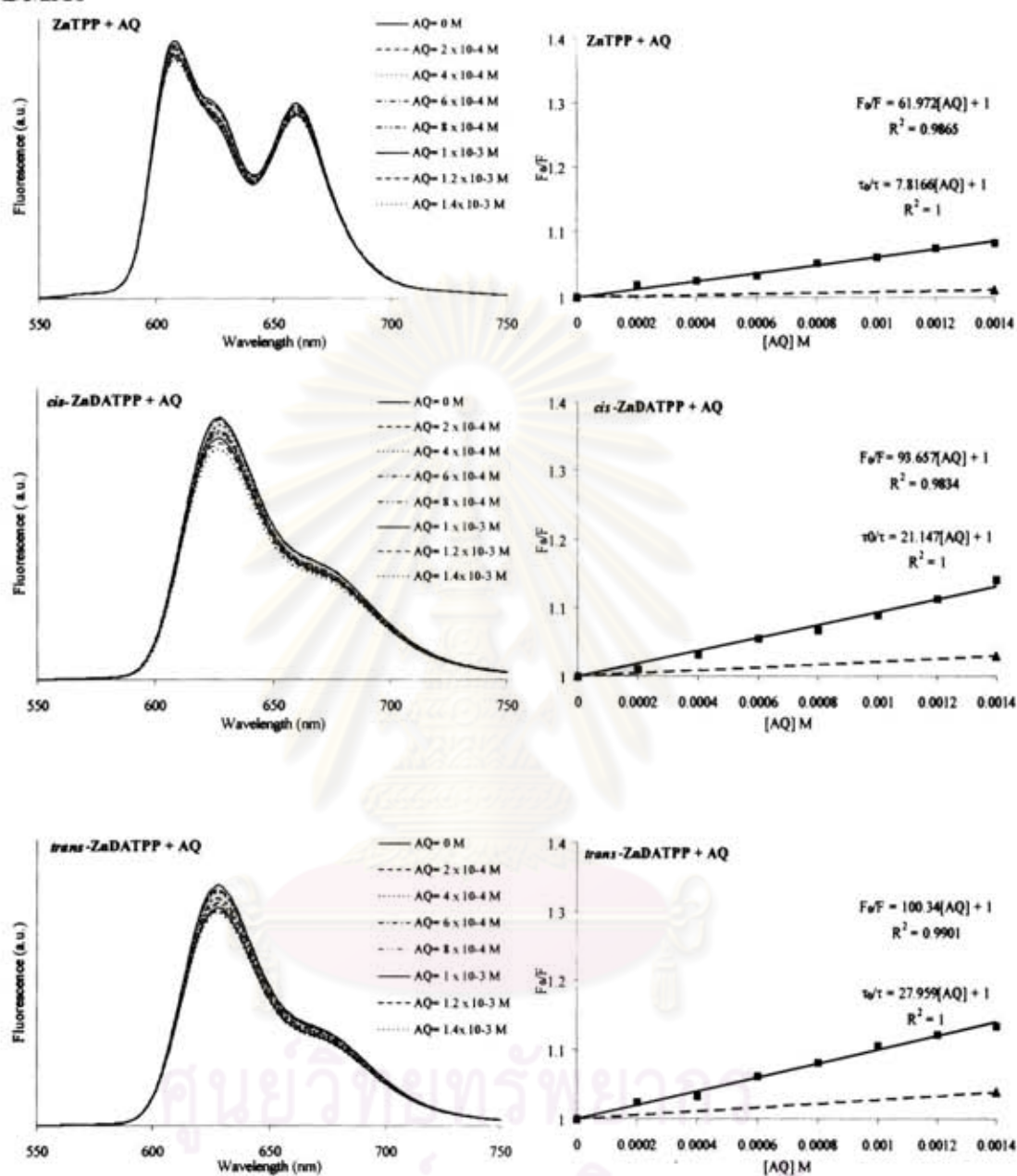
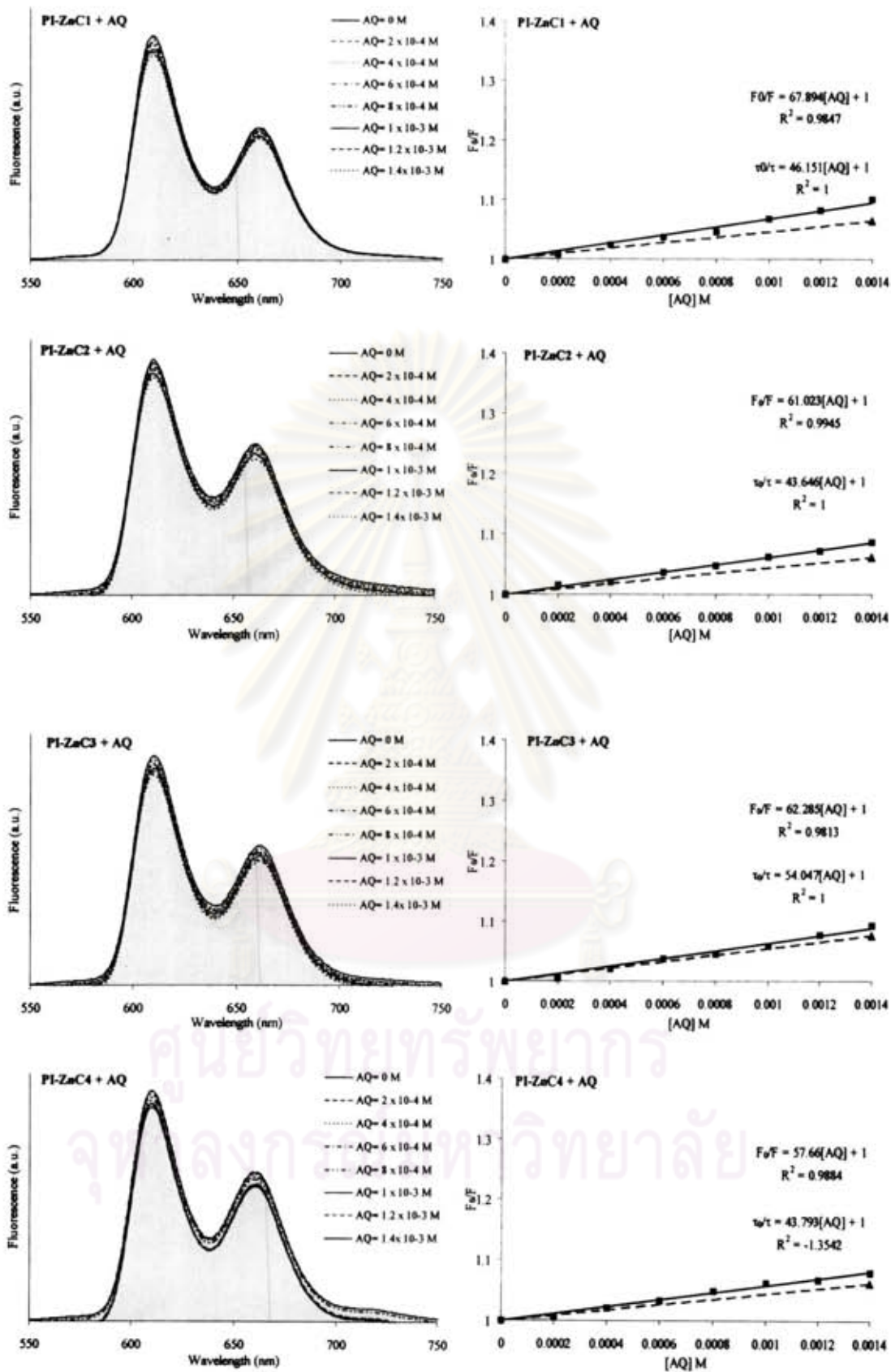
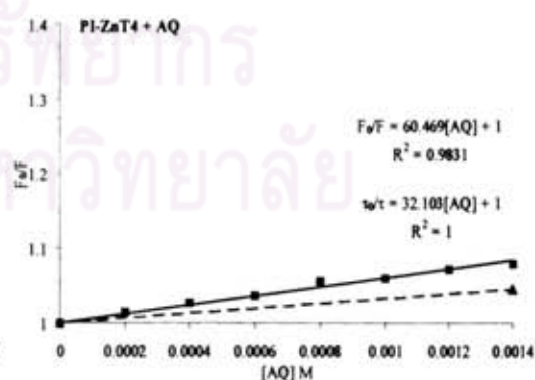
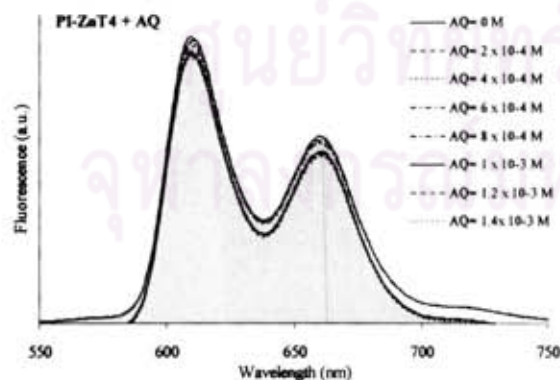
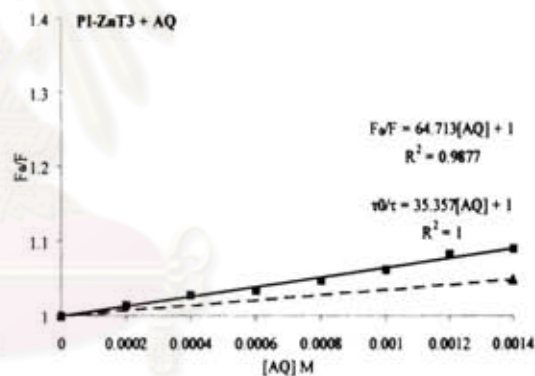
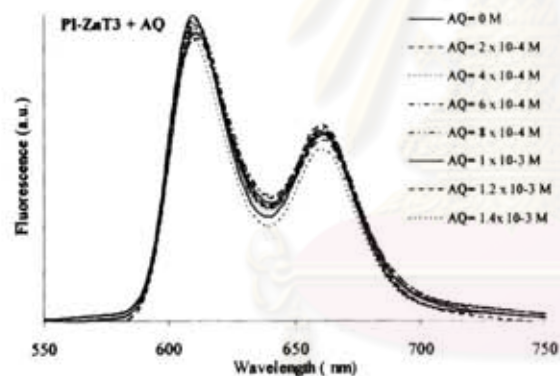
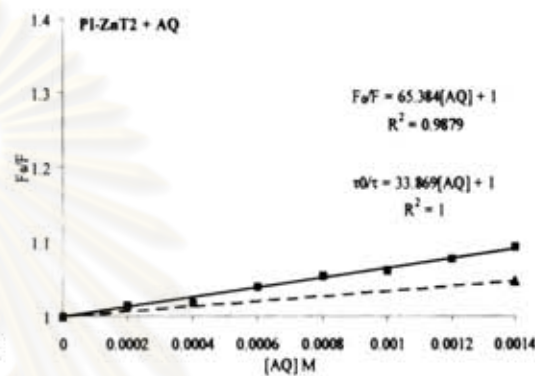
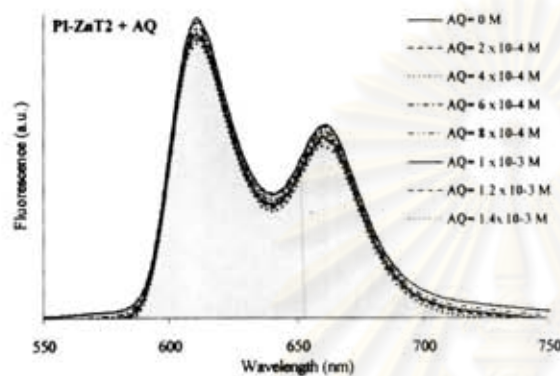
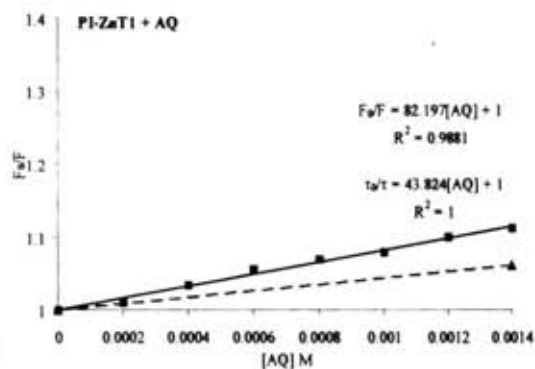
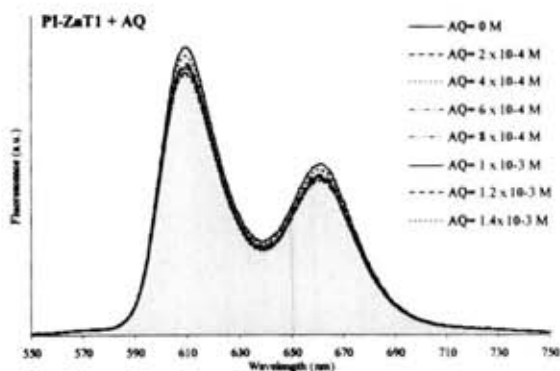


Fig.E4 Fluorescence spectra and Stern-Volmer plots of TPP, cis-, trans-DATPP and polyimides containing 5-30% (Series III and IV) by Anthraquinone in DMAc







APPENDIX F

Fluorescence quantum yield determination

The fluorescence quantum yield (Φ_f) is defined as the ratio of the number of photons emitted and photons absorbed through fluorescence and calculated by using equation F

$$\Phi_f = \Phi_s \frac{A_s D_c n_c^2}{A_c D_s n_s^2} \quad \text{Eq. F}$$

where Φ_s is the fluorescence quantum yield of known standard (from literature)

A_s = Absorbance at $\lambda(\text{ex})$ of standard

A_c = Absorbance at $\lambda(\text{ex})$ of sample

n_s = Index of refraction of standard solvent

n_c = Index of refraction of sample solvent

D_s = Computed area under corrected fluorescence emission spectrum standard

D_c = Computed area under corrected fluorescence emission spectrum sample

Tetraphenylporphyrin (TPP) in toluene ($\Phi_f = 0.1 \pm 0.001$), TPP in CH_2Cl_2 ($\Phi_f = 0.116$) and TPP in DMAc ($\Phi_f = 0.15$). For metallic porphyrin; ZnTPP in toluene ($\Phi_f = 0.033$), $\Phi_f = 0.02$ in CH_2Cl_2 and $\Phi_f = 0.024$ in DMAc as a standard.

ศูนย์วิทยทรัพยากร
จุฬาลงกรณ์มหาวิทยาลัย

Quantum yield determination for TPP in ungasged
Dichloromethane with red sensitive tube.
experiment 1

This QuickSheet demonstrates Mathcad's **cspline** and **interp** functions for connecting X-Y data.



Enter a matrix of X-Y data to be interpolated:

Enter spectral data for compound after converting to wavenumbers, multiplying intensity by lambda squared DO NOT normalize intensity. Insert data from Excel -right key, paste table.

data1 :=

21000	100
20900	1000
20800	2000
20700	...

Click on the **Input Table** above until you see the handles, and enlarge it to see the matrix **data** used in this example.

~~data1~~ := csort(data1, 0)

X := data1⁽⁰⁾

Y := data1⁽¹⁾

Spline coefficients:

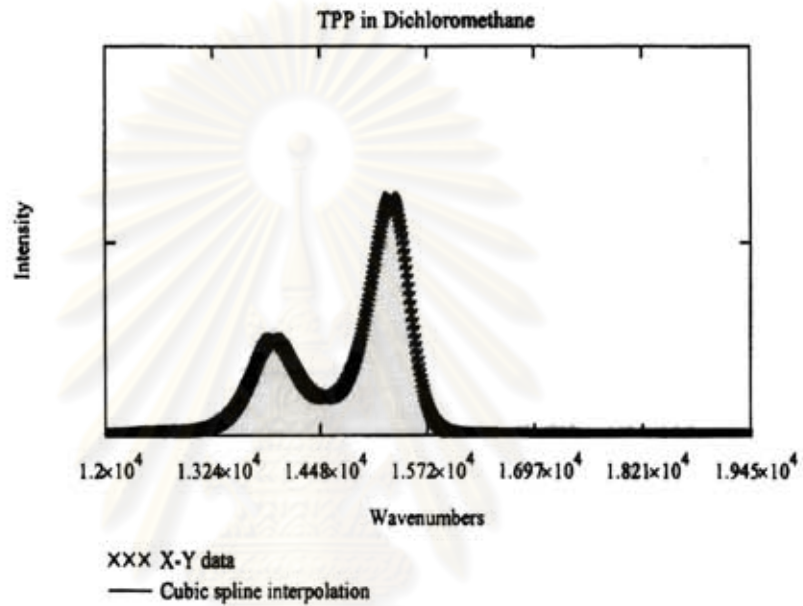
S1 := cspline(X, Y)

Fitting function:

fit(x) := interp(S1, X, Y, x)

ศูนย์วิทยทรัพยากร
จุฬาลงกรณ์มหาวิทยาลัย

Sample interpolated values: $\text{fit}(21000) = 100$
 $\text{fit}(18800) = 2.418 \times 10^4$



Correction factors for LS50B with red sensitive tube
DATA Limits 12,500-22,200 Wavenumbers

corrdata :=

	0	1
0	12500	4.43
1	12550	...

xdata := csort(corrdata, 0)

A := corrdata⁽⁰⁾ B := corrdata⁽¹⁾

Spline coefficients:

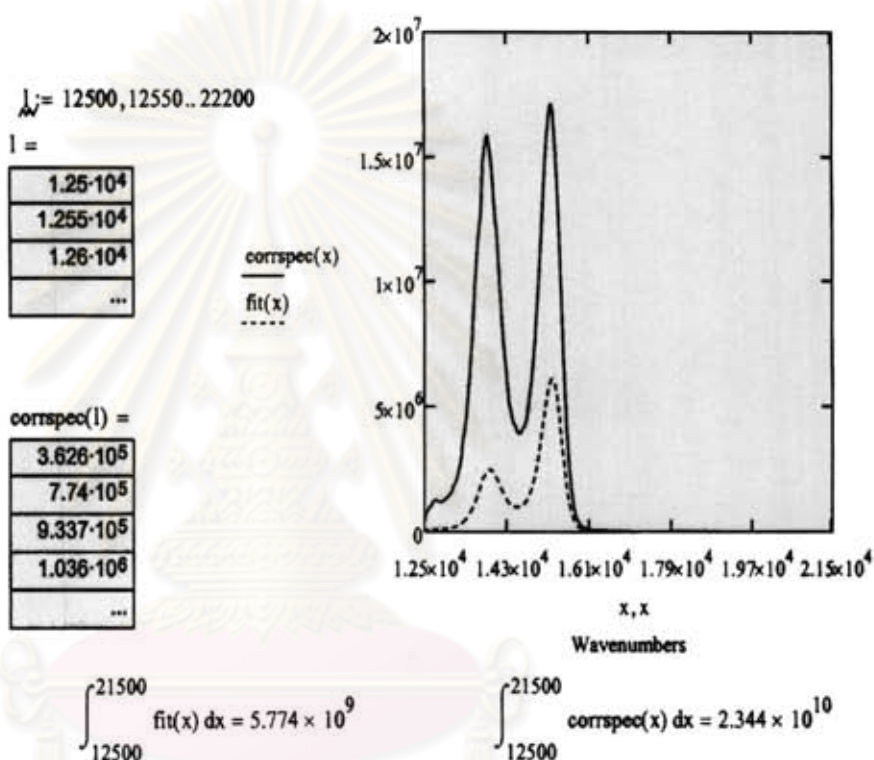
S := cspline(A, B)

Fitting function:

Fitting function:

corrfit(x) := interp(S, A, B, x)

`corrspec(x) := corrfit(x)·fit(x)`



Enter a matrix of X-Y data to be interpolated:

Enter spectral data for standard (TPP in toluene) after converting to wavenumbers, multiplying intensity by lambda squared DO NOT normalize intensities. Insert data from Excel -right key, paste table.

`stdata :=`

21000	50
20900	70
20800	...

Click on the **Input Table** above until you see the handles, and enlarge it to see the matrix **data** used in this example.

`stdata := csort(stdata, 0)`

`C := stdata <0>` `D := stdata <1>`

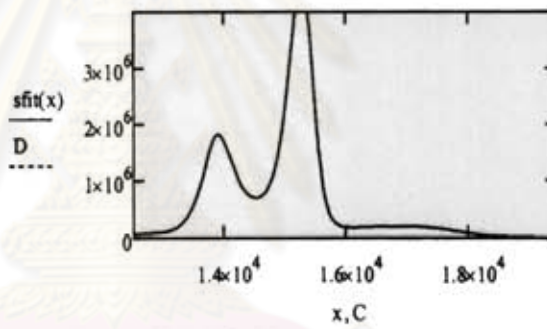
Spline coefficients:

`S := cspline(C, D)`

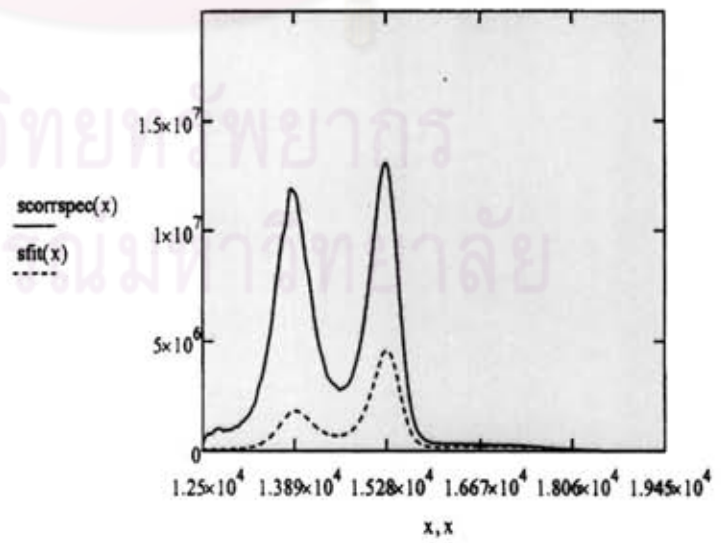
Fitting function:

`sfit(x) := interp(S, C, D, x)`

`sfit(18000) = 8.153 × 104`



`scorrspec(x) := corrfilt(x) · (sfit(x))`



Compound	Standard
$\int_{12500}^{21500} \text{corrspec}(x) dx = 2.344 \times 10^{10}$	$\int_{12500}^{21500} \text{sorrspec}(x) dx = 1.765 \times 10^{10}$

Area under corrected compound curve

$$D_c := \int_{12500}^{21500} \text{corrspec}(x) dx$$

$$D_c = 2.344 \times 10^{10}$$

Area under corrected standard curve

$$D_s := \int_{12500}^{21500} \text{sorrspec}(x) dx$$

$$D_s = 1.765 \times 10^{10}$$

	Compound	Standard
Absorbance at $\lambda(\text{ex})$	$A_c := 0.0559$	$A_s := 0.05389$
Index of refraction	CH ₂ Cl ₂	Toluene
	$n_c := 1.424$	$n_s := 1.496$
quantum yield of standard		$QY_s := 0.10$

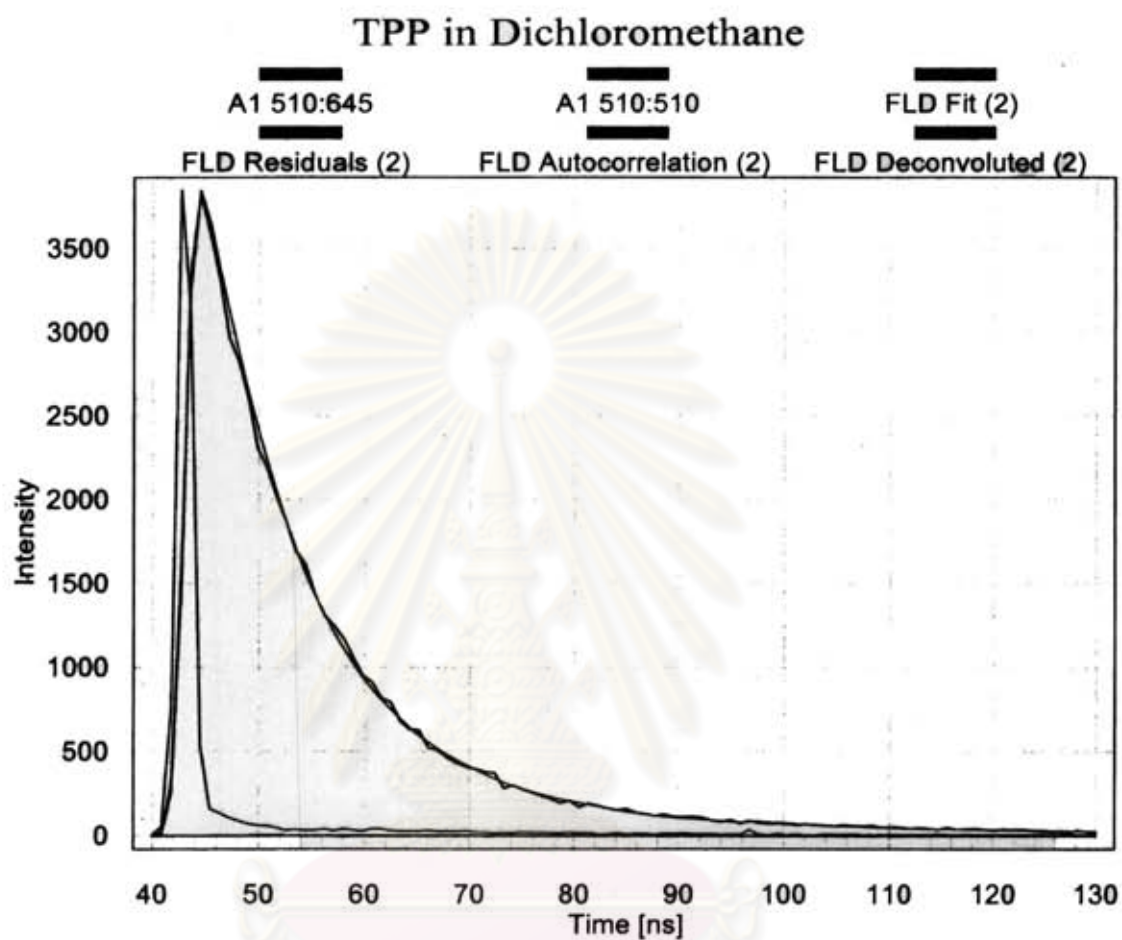
$$QY_c := QY_s \cdot \left(\frac{A_s}{A_c} \right) \cdot \left(n_c \frac{n_c}{n_s \cdot n_s} \right) \cdot \left(\frac{D_c}{D_s} \right)$$

$$QY_c = 0.116$$

ศูนย์วิทยทรัพยากร
จุฬาลงกรณ์มหาวิทยาลัย

APPENDIX G

Fluorescence lifetime determination



ศูนย์วิทยทรัพยากร
จุฬาลงกรณ์มหาวิทยาลัย

Analysis Function : TPP in CH₂Cl₂

***** one-to-four exponentials *****

***** Input Values *****

Decay curve: A1 510:645
IRF curve : A1 510:510

Start Time : 40
End Time : 130

Offset will be calculated
Shift fixed at 0

Pre-exp. 1 : 1
Lifetime 1 : 1

***** Statistics *****

Job done after 9 iterations in 0.047 sec.

Fitted curve : FLD Fit (2)
Residuals : FLD Residuals (2)
Autocorrelation : FLD Autocorrelation (2)
Deconvolved Fit : FLD Deconvoluted (2)

Chi2 : 1.399
Durbin Watson : 1.258
Z : -0.1129

Pre-exp. 1 : 0.625 ± 8.491e-003(100 ± 1.359%)
Lifetime 1 : **9.209** ± 7.345e-002

F1 : 1

Tau-av1 : 9.209
Tau-av2 : 9.209

Offset : -3.54
Shift : 0

APPENDEX H

Thermogravimetric analysis (TGA)

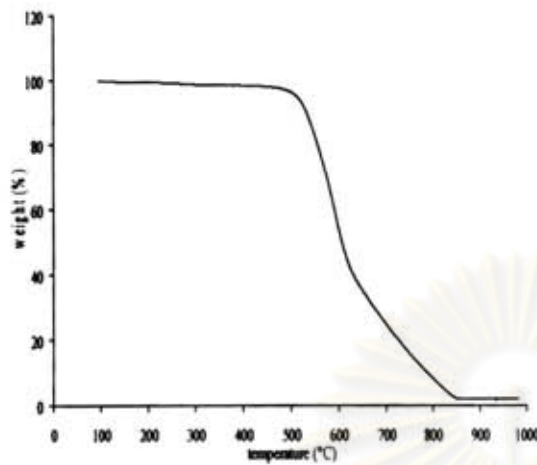


Figure H.1 TGA thermogram of polyimide PI0 in air

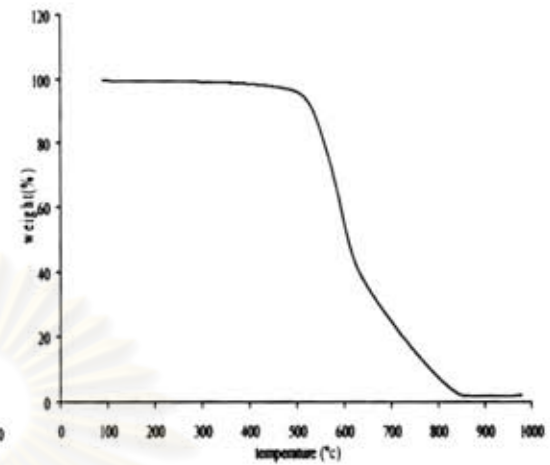


Figure H.2 TGA thermogram of polyimide PI-C1 in air

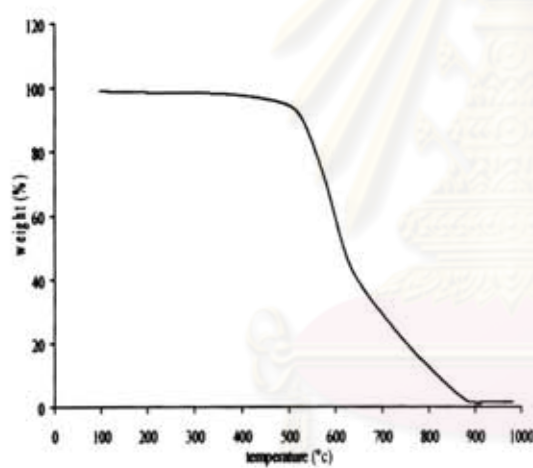


Figure H.3 TGA thermogram of polyimide PI-C2 in air

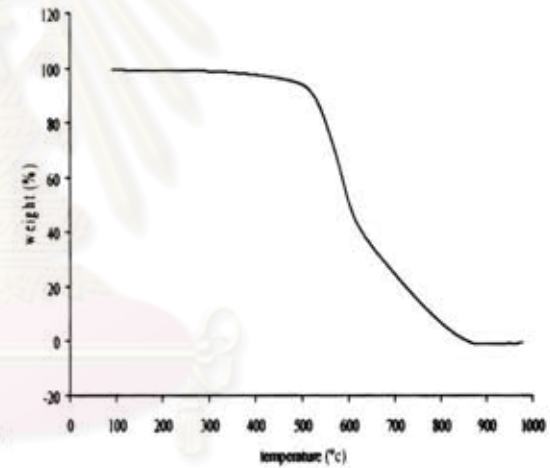


Figure H.4 TGA thermogram of polyimide PI-C3 in air

ศูนย์วิจัยทรัพยากร
จุฬาลงกรณ์มหาวิทยาลัย

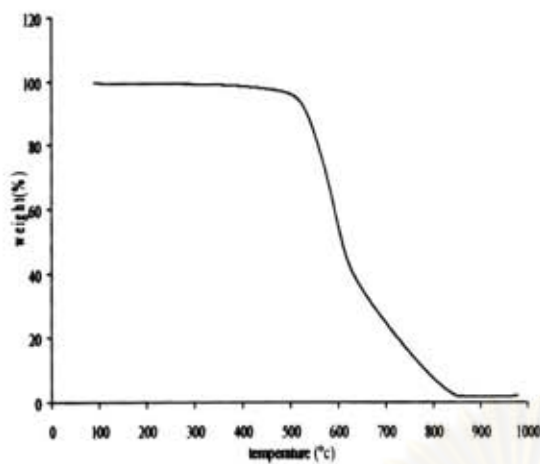


Figure H.5 TGA thermogram of polyimide PI-C4 in air

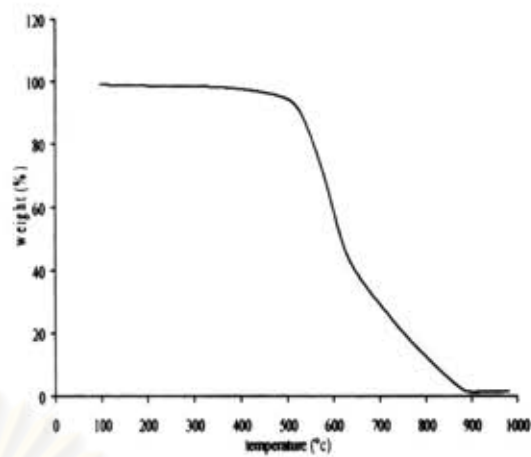


Figure H.6 TGA thermogram of polyimide PI-T1 in air

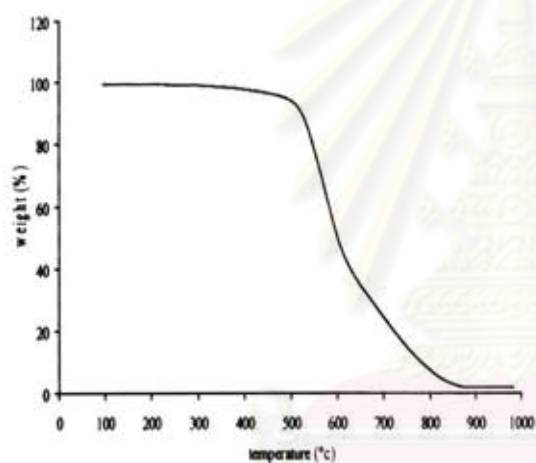


Figure H.7 TGA thermogram of polyimide PI-T2 in air

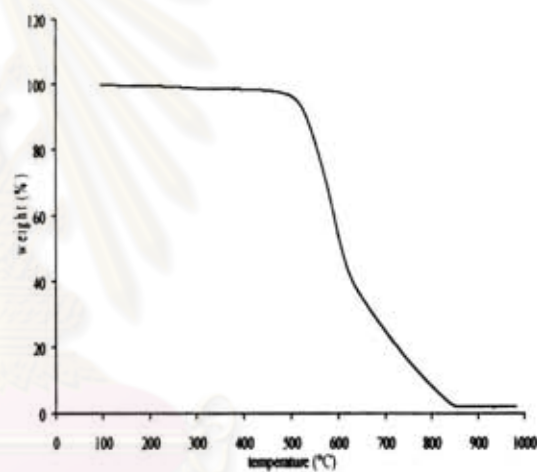


Figure H.8 TGA thermogram of polyimide PI-T3 in air

ศูนย์วิทยทรัพยากร
จุฬาลงกรณ์มหาวิทยาลัย

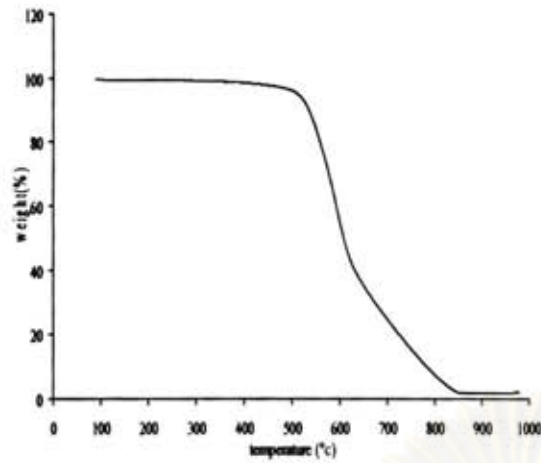


Figure H.9 TGA thermogram of polyimide PI-T4 in air

ศูนย์วิทยทรัพยากร
จุฬาลงกรณ์มหาวิทยาลัย

APPENDIX I

Intrinsic viscosity measurement

The intrinsic viscosity is determined experimentally by measurement of flow time of solvents (t_0) and a series of dilute polymer concentrations of known concentration (t_c) in a standard capillary viscosity. The specific viscosity is calculated from the equation.

$$\eta_{sp} = \frac{\eta_c - \eta_0}{\eta_0} = \frac{t_c - t_0}{t_0}$$

The intrinsic viscosity was obtained by plotting η_{sp}/C against Concentration and extrapolating to zero concentration

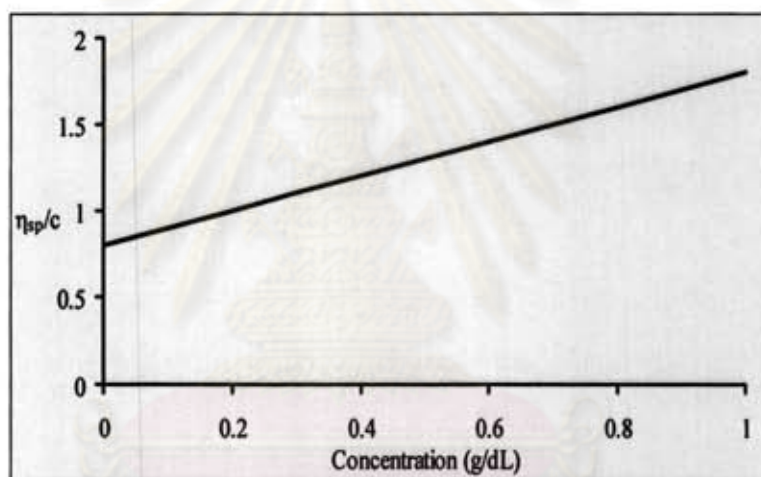


Figure I.1 Dilute solution viscometry: The plot of η_{sp}/c against concentration.

ศูนย์วิทยทรัพยากร
จุฬาลงกรณ์มหาวิทยาลัย

Table I. Average time of polyimide solutions traveling through the Ostwald viscometer

PI	Concentration ^a (g/dL)	Time(s)				η_{sp}^b	η_{sp}/C
		t_1	t_2	t_3	t_{ave}		
PI0	0.02	44.25	44.18	44.14	44.19	0.140	0.700
	0.04	50.32	50.40	50.45	50.39	0.300	0.750
	0.06	56.97	57.00	57.42	57.13	0.474	0.790
	0.08	65.30	65.22	65.29	65.27	0.684	0.855
	1.00	74.77	74.82	74.84	74.81	0.930	0.930
Series I PI-C1	0.02	48.84	48.75	48.81	48.80	0.259	1.295
	0.04	59.37	59.19	59.25	59.27	0.529	1.323
	0.06	70.31	70.29	70.33	70.31	0.814	1.357
	0.08	82.49	82.55	82.49	82.51	1.129	1.411
	1.00	94.88	94.90	95.10	94.96	1.450	1.450
PI-C2	0.02	48.00	48.04	48.14	48.06	0.240	1.200
	0.04	59.31	59.22	59.19	59.24	0.528	1.321
	0.06	71.10	71.11	71.06	71.09	0.834	1.390
	0.08	83.14	83.06	83.10	83.10	1.144	1.430
	1.00	94.90	95.01	94.97	94.96	1.450	1.450
PI-C3	0.02	46.44	46.51	46.34	46.43	0.198	0.990
	0.04	55.55	55.52	55.43	55.50	0.432	1.080
	0.06	65.00	65.11	65.01	65.04	0.768	1.130
	0.08	77.22	77.25	77.16	77.21	0.992	1.240
	1.00	89.50	89.49	89.33	89.54	1.310	1.310
PI-C4	0.02	44.99	45.03	44.86	44.96	0.160	0.800
	0.04	52.35	52.45	52.40	52.40	0.352	0.880
	0.06	61.49	61.51	61.65	61.55	0.588	0.980
	0.08	72.77	72.91	72.93	72.87	0.880	1.100
	1.00	86.80	86.75	86.91	86.82	1.240	1.240
Series II PI-T1	0.02	48.66	48.72	48.66	48.68	0.256	1.280
	0.04	59.23	59.33	59.25	59.27	0.529	1.323
	0.06	70.50	70.51	70.40	70.47	0.819	1.365
	0.08	82.63	82.69	82.60	82.64	1.132	1.415
	1.00	96.32	96.12	95.92	96.12	1.480	1.480
PI-T2	0.02	47.31	47.35	47.21	47.29	0.220	1.100
	0.04	57.61	57.72	57.74	57.69	0.488	1.221
	0.06	69.49	69.50	69.36	69.45	0.792	1.320
	0.08	82.55	82.50	82.39	82.48	1.128	1.410
	1.00	98.08	98.06	98.04	98.06	1.530	1.530
PI-T3	0.02	46.50	46.50	46.53	46.51	0.200	1.000
	0.04	55.70	55.83	55.90	55.81	0.440	1.100
	0.06	65.50	65.48	65.52	65.50	0.690	1.150
	0.08	77.18	77.26	77.19	77.21	0.992	1.240
	1.00	91.01	91.09	91.17	91.09	1.350	1.350
PI-T4	0.02	44.84	44.80	44.79	44.81	0.156	0.780
	0.04	52.27	52.30	52.30	52.29	0.348	0.870
	0.06	60.85	60.72	60.98	60.85	0.570	0.950
	0.08	69.53	69.56	69.29	69.46	0.792	0.990
	1.00	81.40	81.46	81.31	81.39	1.100	1.100
Series III PI-ZnCl	0.02	47.81	47.79	47.89	47.83	0.234	1.170
	0.04	58.09	58.06	57.85	58.00	0.496	1.241
	0.06	69.90	69.91	69.95	69.92	0.804	1.340
	0.08	83.10	83.03	83.17	83.10	1.144	1.430

PI-ZnC2	1.00	94.85	94.91	95.12	94.96	1.450	1.450
	0.02	46.50	46.49	46.54	46.51	0.200	1.000
	0.04	55.50	55.50	55.50	55.50	0.432	1.080
	0.06	65.72	65.69	65.81	65.74	0.696	1.160
	0.08	77.50	77.49	77.57	77.52	1.000	1.250
PI-ZnC3	1.00	93.04	93.10	92.92	93.02	1.400	1.400
	0.02	45.27	45.27	45.27	45.27	0.168	0.840
	0.04	52.55	52.51	52.62	52.56	0.356	0.890
	0.06	61.71	61.77	61.86	61.78	0.594	0.990
	0.08	71.30	71.29	71.34	71.31	0.840	1.050
PI-ZnC4	1.00	81.76	81.69	81.68	81.71	1.108	1.108
	0.02	44.79	44.81	44.59	44.73	0.154	0.770
	0.04	52.59	52.55	52.54	52.56	0.356	0.890
	0.06	63.81	63.85	63.98	63.88	0.648	1.080
	0.08	72.90	72.88	72.83	72.87	0.880	1.100
Series IV	1.00	86.75	86.80	86.91	86.82	1.240	1.240
	0.02	48.32	48.25	48.30	48.29	0.246	1.230
	0.04	58.85	58.88	59.00	58.91	0.520	1.300
	0.06	70.18	70.20	70.10	70.16	0.810	1.350
	0.08	82.23	82.19	82.09	82.17	1.120	1.400
PI-ZnT1	1.00	94.22	94.15	94.20	94.19	1.430	1.430
	0.02	46.45	46.48	46.60	46.51	0.200	1.000
	0.04	55.45	55.49	55.56	55.50	0.432	1.080
	0.06	66.73	66.74	63.75	65.74	0.696	1.160
	0.08	77.50	77.51	77.55	77.52	1.000	1.250
PI-ZnT2	1.00	93.01	93.09	92.96	93.02	1.400	1.400
	0.02	45.67	45.66	45.86	45.73	0.180	0.900
	0.04	53.04	53.08	52.94	53.02	0.368	0.920
	0.06	62.45	62.55	62.44	62.48	0.612	0.120
	0.08	71.34	71.40	71.22	71.32	0.840	1.050
PI-ZnT3	1.00	81.69	81.73	81.71	81.71	1.108	1.108
	0.02	45.45	45.49	45.56	45.50	0.174	0.870
	0.04	52.97	52.99	53.10	53.02	0.368	0.920
	0.06	62.04	61.98	62.01	62.01	0.600	1.000
	0.08	72.89	72.93	72.79	72.87	0.880	1.100
PI-ZnT4	1.00	85.35	85.25	85.21	85.27	1.200	1.200

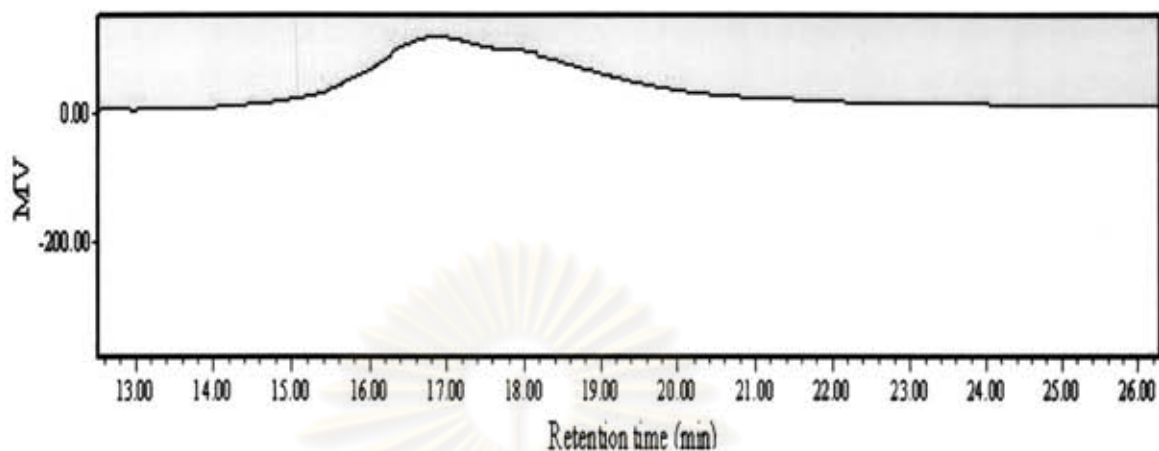
^a in DMAc and flow time were measured at 35±0.1°C

^b Calculated from equation I.1, where $t_0 = 38.76$

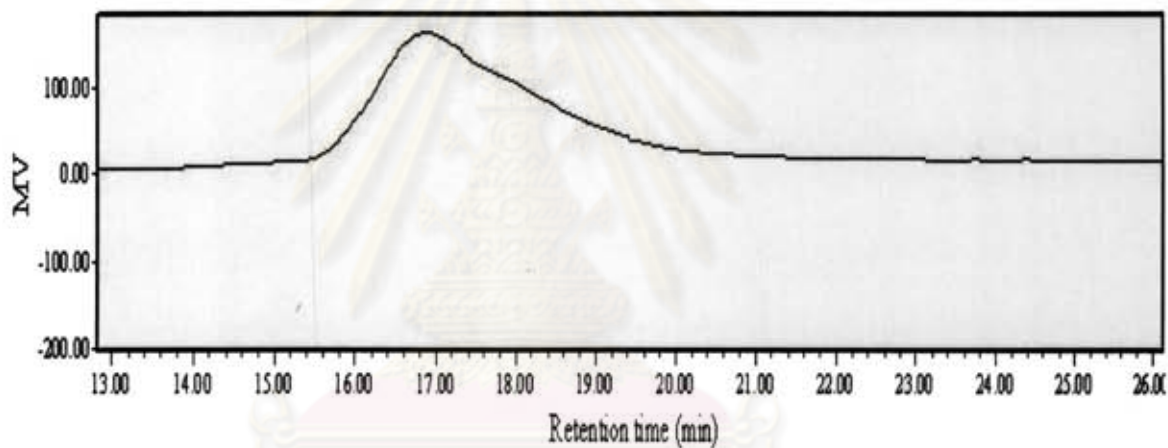
ศูนย์วิจัยทรัพยากร
จุฬาลงกรณ์มหาวิทยาลัย

APPENDIX J

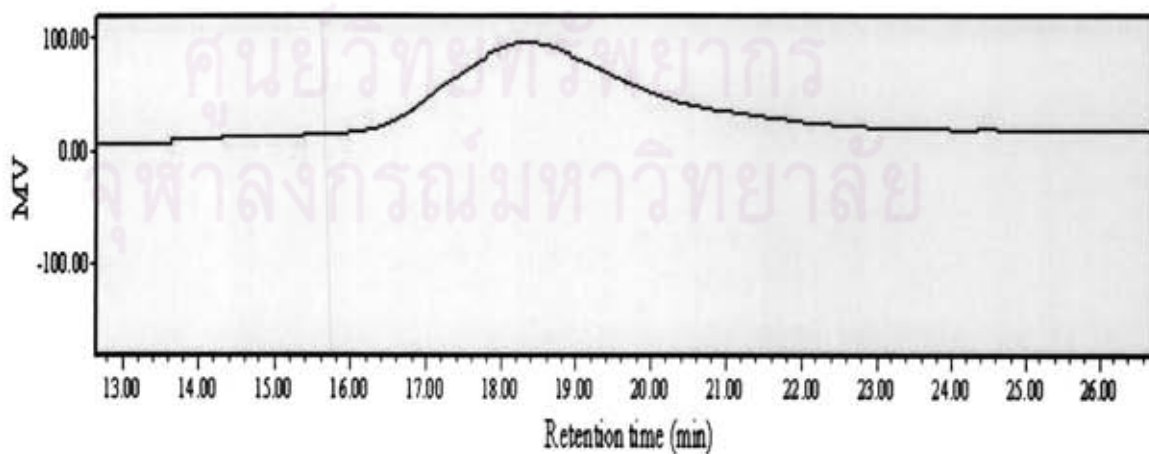
Molecular weight of polyimide determination



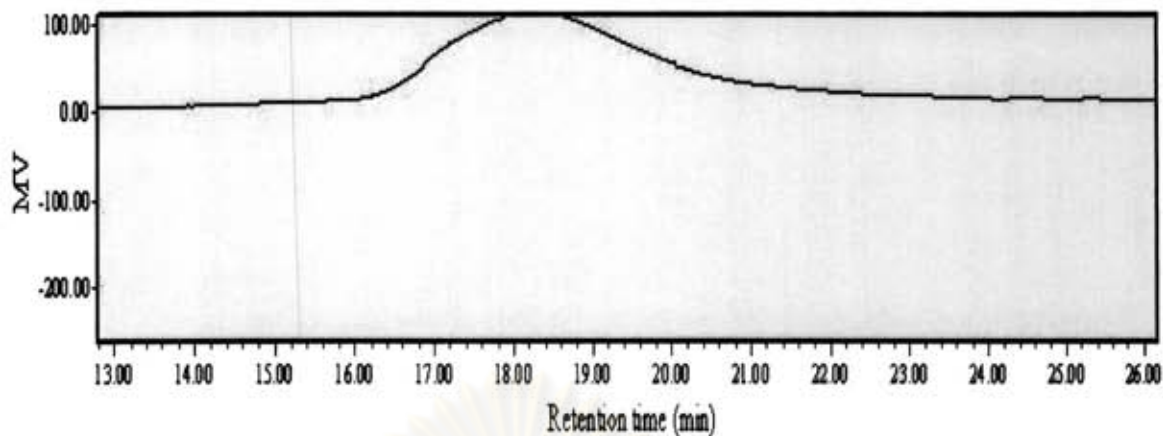
Picture J1. The chromatogram of polyimide without porphyrin (PI0)



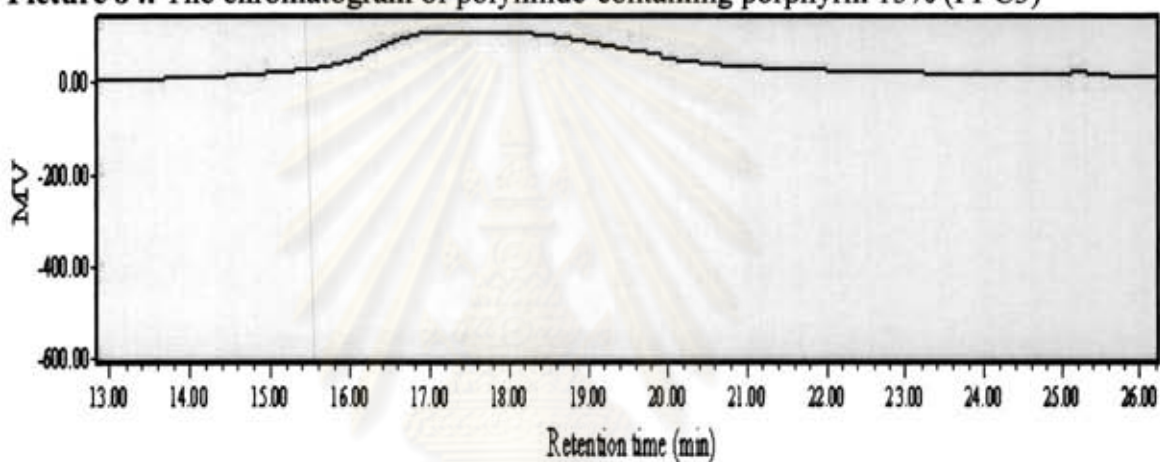
Picture J2. The chromatogram of polyimide-containing porphyrin 5% (PI-C1)



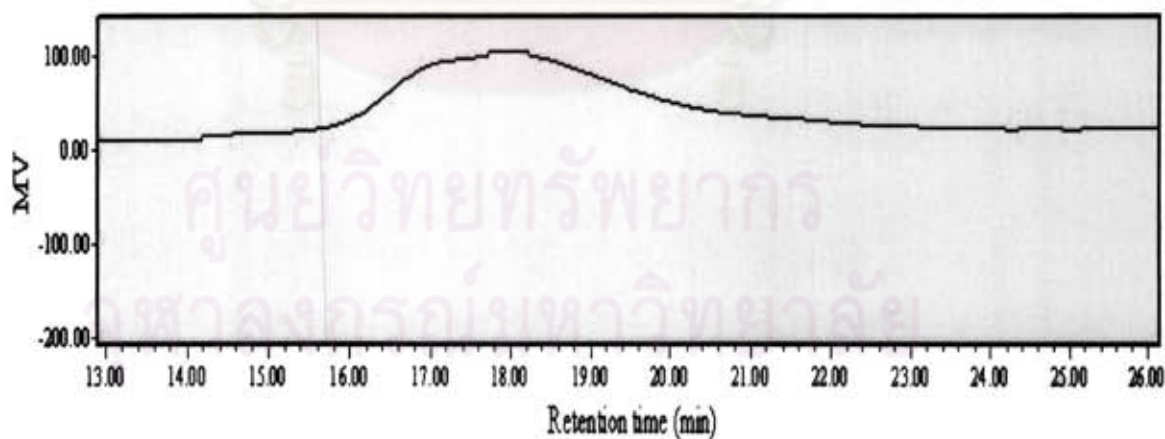
Picture J3. The chromatogram of polyimide-containing porphyrin 10% (PI-C2)



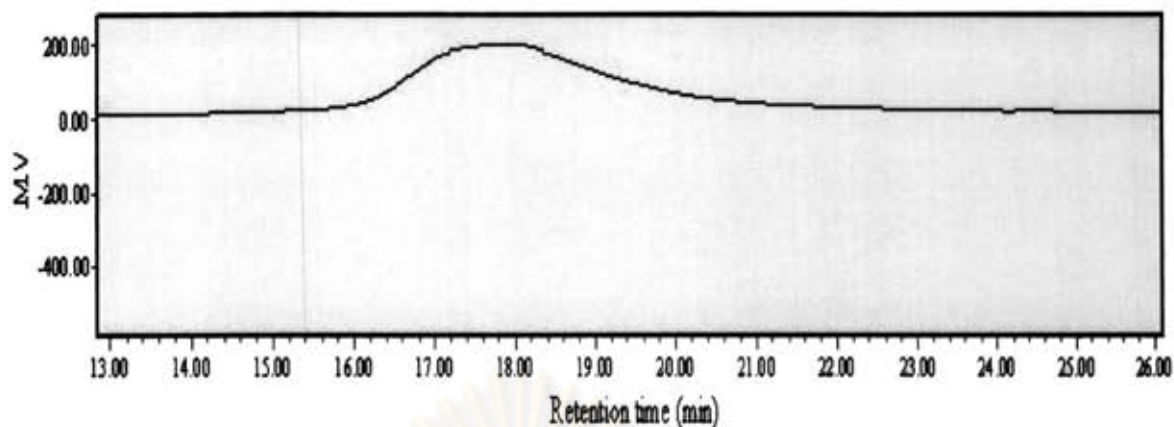
Picture J4. The chromatogram of polyimide-containing porphyrin 15% (PI-C3)



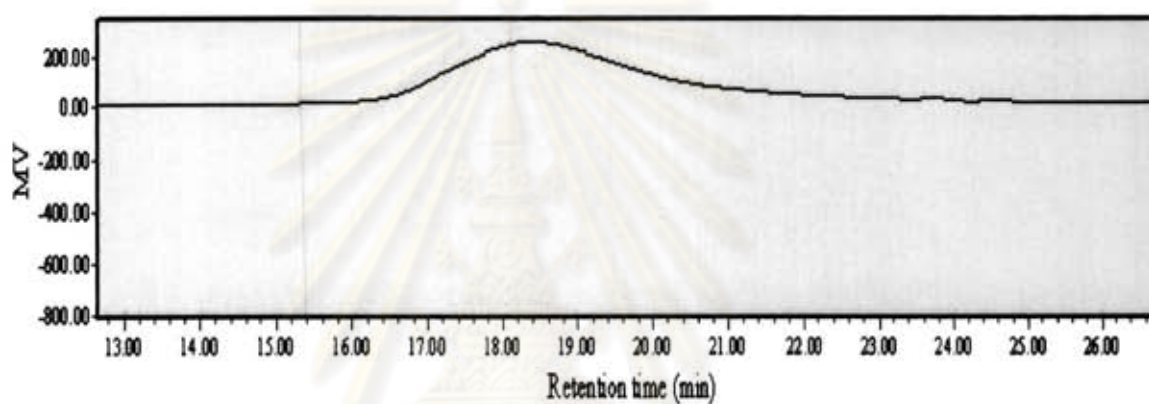
Picture J5. The chromatogram of polyimide-containing porphyrin 30% (PI-C4)



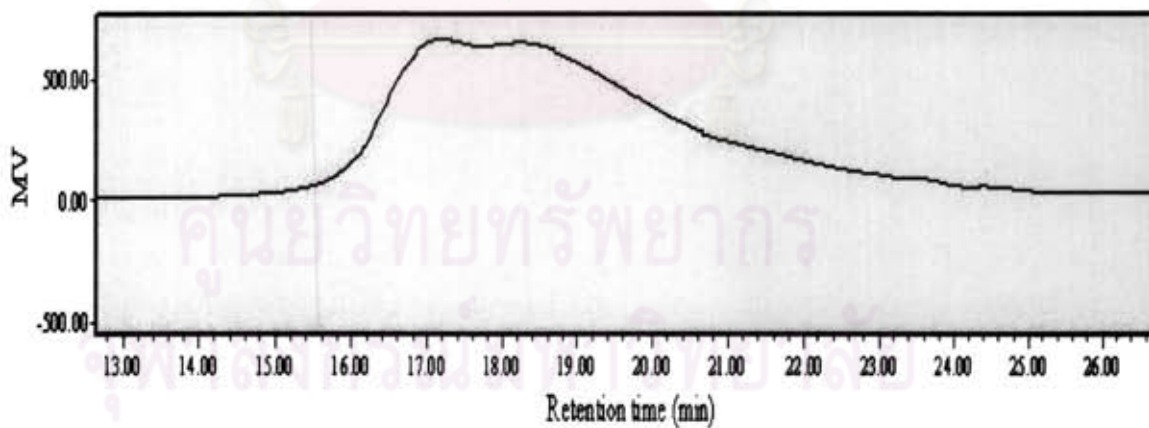
Picture J6. The chromatogram of polyimide-containing porphyrin 5% (PI-T1)



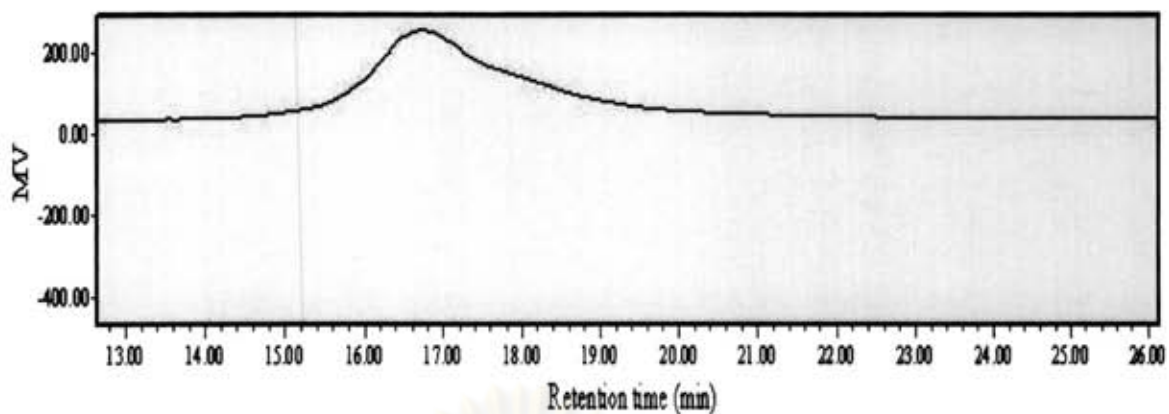
Picture J7. The chromatogram of polyimide-containing porphyrin 10% (PI-T2)



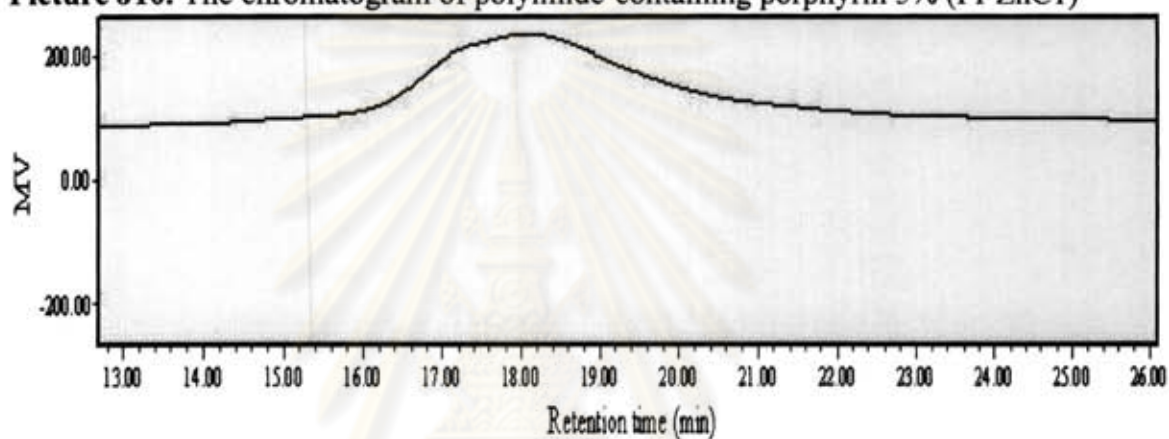
Picture J8. The chromatogram of polyimide-containing porphyrin 15% (PI-T3)



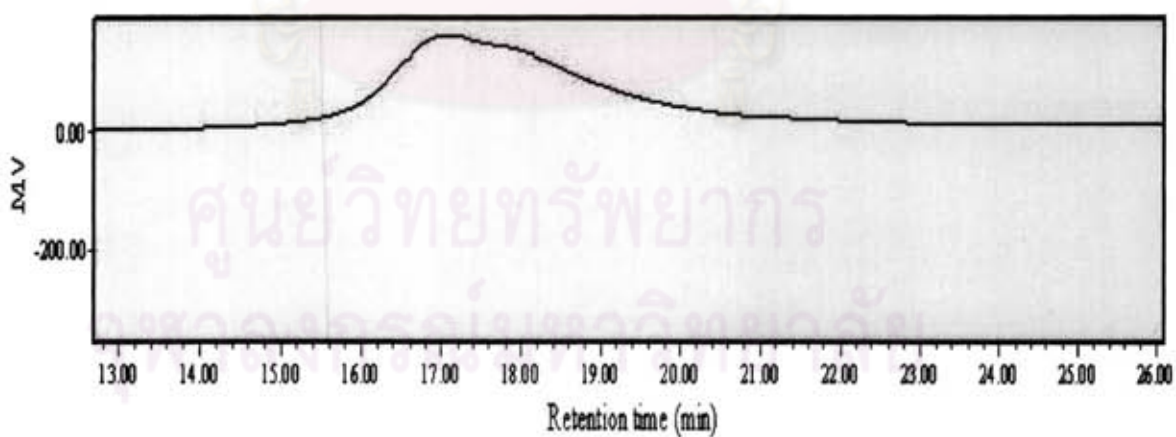
Picture J9. The chromatogram of polyimide-containing porphyrin 30% (PI-T4)



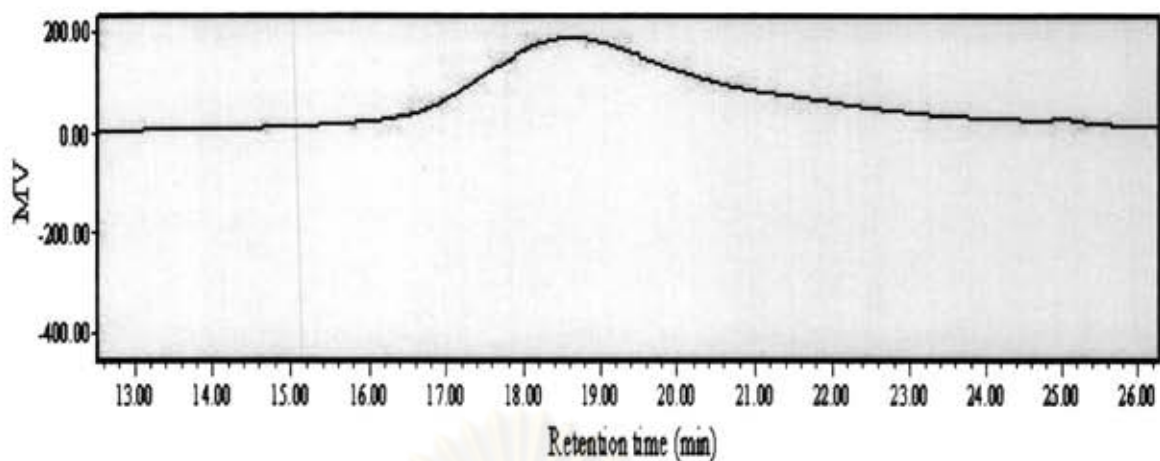
Picture J10. The chromatogram of polyimide-containing porphyrin 5% (PI-ZnC1)



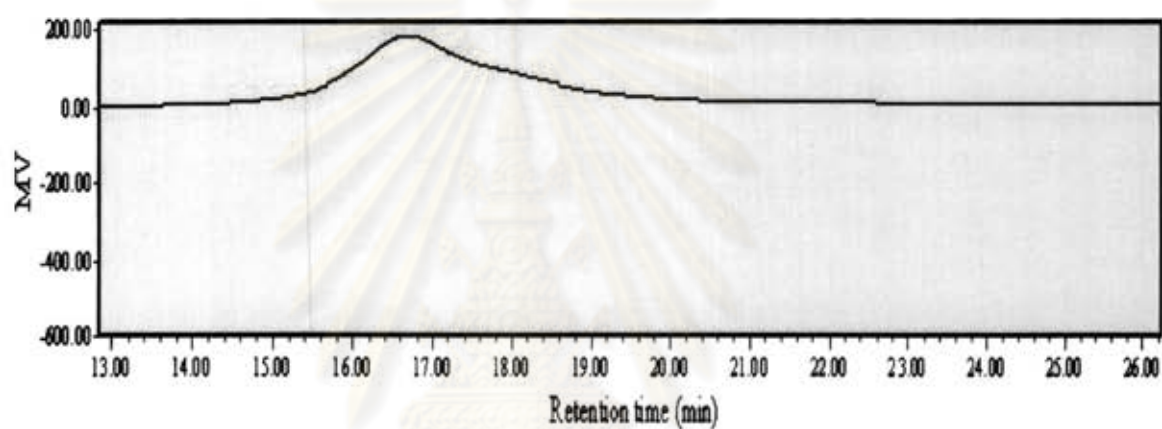
Picture J11. The chromatogram of polyimide-containing porphyrin 10% (PI-ZnC2)



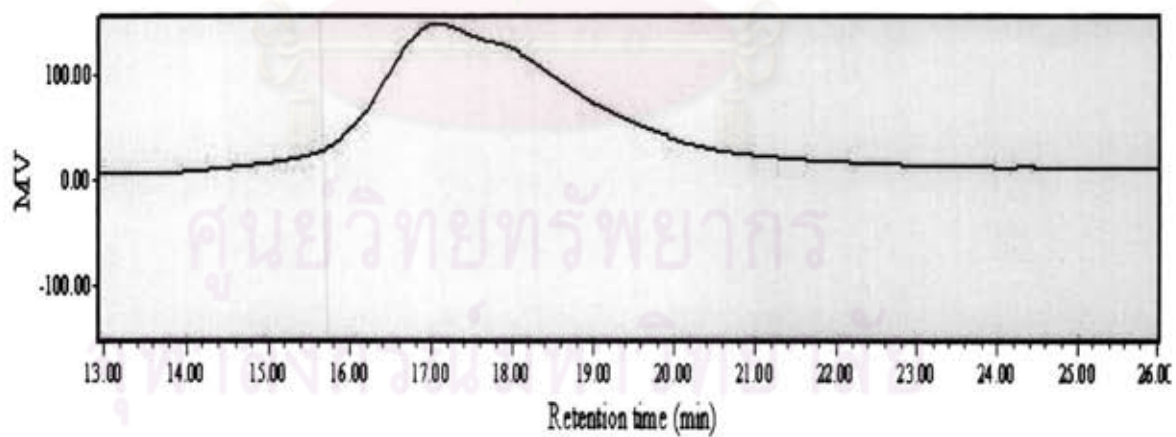
Picture J12. The chromatogram of polyimide-containing porphyrin 15% (PI-ZnC3)



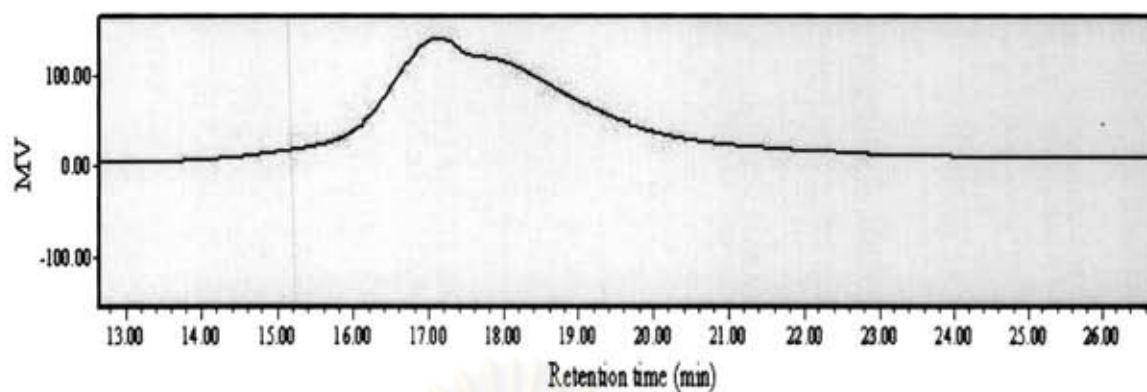
Picture J13. The chromatogram of polyimide-containing porphyrin 30% (PI-ZnC4)



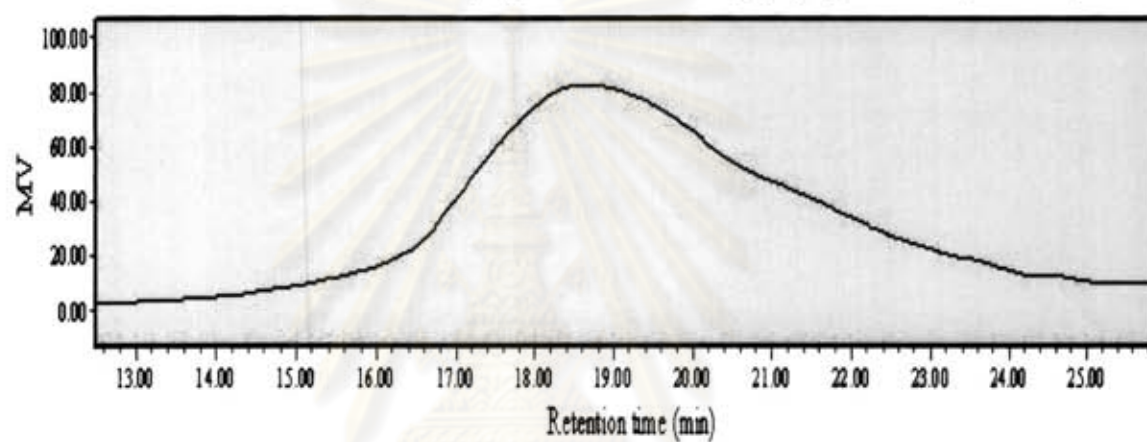
Picture J14. The chromatogram of polyimide-containing porphyrin 5% (PI-ZnT1)



Picture J15. The chromatogram of polyimide-containing porphyrin 10% (PI-ZnT2)



Picture J16. The chromatogram of polyimide-containing porphyrin 15% (PI-ZnT3)



Picture J17. The chromatogram of polyimide-containing porphyrin 30% (PI-ZnT4)

ศูนย์วิทยทรัพยากร
จุฬาลงกรณ์มหาวิทยาลัย

VITAE

Miss Sudkanueng Singto was born on September 24th, 1981 in Nakornratchasima Thailand. She graduated with a Bachelor Degree of Science (Chemistry) from Chulalongkorn University in 2005. In the same year, she was admitted to a master's degree of Science in Petrochemistry and Polymer Science, Faculty of Science, Chulalongkorn University and completed the program in 2008.



ศูนย์วิทยทรัพยากร
จุฬาลงกรณ์มหาวิทยาลัย